A HUMAN AIRWAY MODEL FOR

MYCOPLASMA PNEUMONIAE COLONIZATION

by

OLIVER ARNOLD PRINCE

(Under the Direction of DUNCAN CHARLES KRAUSE)

ABSTRACT

Mycoplasma pneumoniae is an important cause of acute and chronic respiratory disease, especially in school-aged children and young adults. To date, a suitable *in vitro* human model system for studying native mycoplasma interactions with the mucociliary defense has not been available nor has this aspect of infection been studied in detail. The current study employed normal human bronchial epithelial (NHBE) cells in air-liquid interface culture to examine the interaction(s) of *M. pneumoniae* with the mucociliary defense of differentiated airway epithelium. NHBE cells, when grown in air-liquid interface culture, form a pseudostratified, polarized epithelium, with tight junctions, mucus secretion, and ciliary function. The stepwise analysis of NHBE cell development and mycoplasma interactions are characterized utilizing immunohistochemistry and standard attachment assays. I have developed a model for acute and chronic exposure of *M. pneumoniae* to NHBE cells that details not only early localization events on the luminal surface but also mycoplasma transmigration of the paracellular surfaces and localization within the basolateral compartment, revealing a strong relationship between mycoplasma migration, desquamation and reorganization of the epithelium. This study is

the first and only report to describe a link between gliding mycoplasmas, early localization, and migration through basolateral surfaces followed by loss of ciliation, desquamation and subsequent reorganization of the epithelium. These findings are essential steps in elucidating *M. pneumoniae* pathogenesis, in that mycoplasmas primarily localize to the basolateral surfaces where they alter mucociliary clearance via initiation of airway reorganization, a hallmark of *M. pneumoniae* disease *in vivo*, potentially reflecting a mechanism for extrapulmonary spread.

INDEX WORDS: *Mycoplasma pneumoniae*, Airway, Acute, Chronic, Mucociliary

A HUMAN AIRWAY MODEL FOR *MYCOPLASMA PNEUMONIAE* COLONIZATION

by

OLIVER ARNOLD PRINCE

B.S., St. Francis College, 2002

M.S., Long Island University, 2006

A Dissertation Submitted to the Graduate Faculty of The University of Georgia in Partial Fulfillment of the Requirements for the Degree

DOCTOR OF PHILOSOPHY

ATHENS, GEORGIA

2014

A HUMAN AIRWAY MODEL FOR *MYCOPLASMA PNEUMONIAE* COLONIZATION

by

OLIVER ARNOLD PRINCE

Major Professor:	Duncan C. Krause
Committee:	Thomas M. Krunkosky
	Frederick D. Quinn
	Robert J. Maier

Electronic Version Approved:

Julie Coffield
Interim Dean of the Graduate School
The University of Georgia
December 2014

DEDICATION

This work is dedicated to Alinna, my loving wife, who has been there during the ups and downs. Thanks to my mother for raising a stubborn child who turned out to be a tenacious student. Thanks to my sister who was and is very supportive. Thanks to my absent father, who allowed me to figure it out on my own. That's quite a gift. Thanks to my uncles on both sides of the family that have offered support whenever I needed it. Let's not forget my main man Mitch Martin from Queens, NY. I would like to also thank the teachers of the New York City public school system. Thanks again, I am the sum total of your love, support and training.

ACKNOWLEDGEMENTS

I am very fortunate to have met and worked for Dr. Duncan C. Krause. Dr. Krause's mentorship has allowed me to develop transferable skills that extend beyond science. I was given enough space to make mistakes and I enjoyed making them. This process has made me a better person and scientist. Thank you.

I am grateful to have worked with Dr. Thomas M. Krunkosky. I have had more meetings with Dr. Krunkosky than any other faculty member outside of Dr. Krause. Because of Dr. Krunkosky, I feel like I have a dual degree in microbiology and tangent avoidance. Thank you.

I would like to thank both Dr. Robert J. Maier and Dr. Frederick D. Quinn. When I conducted experiments, interpreted data and wrote up the results I asked the question "What would non-mycoplasma researchers ask?" Thinking outside of the box is almost too cliché but an apt term when it comes to conducting research. I value both their perspective and input into my work. Thank you both.

I would also like to thank the entire Krause Lab both past and present. While our projects were different, the synergism and chemistry in the lab and the resultant meetings were great. I especially want to thank the undergraduates Lauren and Ali, whom I have had the pleasure of learning from, working with and training. Thank you.

I also would like to thank both Jamie and Barbara over at the University Of Georgia College of Veterinary Medicine Cytometry Core Facility. Thanks for the training and being available for questions. I spent a ton of hours in that cold room collecting data.

TABLE OF CONTENTS

Page

ACKNOWLEDGEMENTS.....v

LIST OF TABLES.....viii

LIST OF FIGURES.....ix

CHAPTER

1. INTRODUCTION.....#1
2. REVIEW OF THE LITERATURE.....#4

M. pneumoniae Overview.....#4

Virulence and Pathogenicity.....#12

M. pneumoniae Airway Disease.....#15

Conducting Airway Defense.....#18

3. MATERIALS AND METHODS.....#24

General Methods.....#24

4. RESULTS.....#33

Acute Exposure Study.....#33

Chronic Exposure Study.....#39

5. DISCUSSION.....#109

The *In Vitro M. pneumoniae*-NHBE Cell Model.....#109

Comparison of the *M. pneumoniae*-NHBE Cell Model to Animal Models #113

The Significance of *M. pneumoniae* Airway Infection.....#113

Future Work .....#114

6. REFERENCES ..... #118

LIST OF TABLES

Page

Table 1: Gliding and attachment data for strains used in acute study .....#31

Table 2: Gliding data for strains used in the chronic exposure study.....#32

LIST OF FIGURES

Page

Figure 1: Transwell chamber system and NHBE cell development .....#30

Figure 2: NHBE cell development .....#50

Figure 3: Colonization of NHBE cells at the indicated stages in development by wild-type (WT; Top) and mutant *M. pneumoniae* strains (Bottom) .....#52

Figure 4: Wild-type *M. pneumoniae* M129 colocalized with cilia on the apical surface of day 43 NHBE cells after 30 min .....#54

Figure 5: (A) Luminal view of mycoplasma localization and spreading patterns on day 43 NHBE cells as three-dimensional (3D) projections of regions from Fig. 4 at the indicated times postinfection .....#56

Figure 6: Quantification of mycoplasma fluorescence associated with ciliated cell density for the data set in Fig. 4C .....#58

Figure 7: Mycoplasma localization to non-ciliated cells was not enhanced upon mucus removal .....#60

Figure 8: Luminal view of wild-type *M. pneumoniae*-infected day 2 (Top) and day 10 (Bottom) NHBE cells at 240 min postinfection .....#62

Figure 9: MUC1 labeling in relation to mycoplasma localization on day 10 cells demonstrated no clear relationship .....#64

Figure 10: MUC4 labeling in relation to mycoplasma localization on day 10 cells demonstrated a localization pattern consistent with the observed reduction in attachment in Fig. 3.....#66

Figure 11: MUC4 polarity appeared to be inversely related with fluorescence intensity and mycoplasma colonization.....#68

Figure 12: Uninfected NHBE cells.....#70

Figure 13: Cross-sectional views of uninfected NHBE cells.....#72

Figure 14: Barrier function over 28 days postinfection.....#74

Figure 15: *M. pneumoniae* induced changes in cilia.....#76

Figure 16: Low-dose *M. pneumoniae*-infected NHBE cells at 4 h postinfection.....#78

Figure 17: Low-dose *M. pneumoniae*-infected NHBE cells at 7 days postinfection.....#80

Figure 18: Low-dose *M. pneumoniae*-infected NHBE cells at 28 days postinfection.....#82

Figure 19: High-dose *M. pneumoniae*-infected NHBE cells at 4 h postinfection.....#84

Figure 20: High-dose *M. pneumoniae*-infected NHBE cells at 7 days postinfection.....#86

Figure 21: High-dose *M. pneumoniae*-infected NHBE cells at 28 days postinfection....#88

Figure 22: *M. pneumoniae* attached to desquamated cells.....#90

Figure 23: Depth coding of actin in uninfected NHBE cells.....#92

Figure 24: Depth coding of actin reorganization of mycoplasma-infected NHBE cells (low-dose).....#94

Figure 25: Depth coding of actin reorganization of mycoplasma-infected NHBE cells (high-dose).....#96

Figure 26: Macroscopic impact of *M. pneumoniae* infection.....#98

Figure 27: E-cadherin localization in uninfected NHBE cells.....#100

Figure 28: E-cadherin localization in *M. pneumoniae* -infected NHBE cells .....#102

Figure 29: E-cadherin localization in low-dose *M. pneumoniae* infected NHBE at 28 days postinfection.....#104

Figure 30: E-cadherin localization in high-dose *M. pneumoniae* infected NHBE at 28 days postinfection .....#106

Figure 31: *M. pneumoniae* isolation .....#108

Figure 32: The *M. pneumoniae*-NHBE cell model.....#117

CHAPTER 1

INTRODUCTION

Mycoplasma pneumoniae is a primary pathogen of the conducting human airway. *M. pneumoniae* disease manifestations of the airway include acute and chronic pharyngitis, tracheobronchitis, bronchiolitis, croup and pneumonia, (1-3), with extrapulmonary involvement and asymptomatic carriage not uncommon (4-12). Additionally, *M. pneumoniae* has been associated with asthma and chronic airway disease (13-16). Early *M. pneumoniae* epidemiological studies indicate widespread dissemination (17). A lack of active and coordinated surveillance, along with the propensity for asymptomatic carriage, makes it difficult to gauge the true prevalence and impact of *M. pneumoniae* on human health. However, based on World Health Organization numbers, chronic respiratory disease as a global problem impacts $1/7^{th}$ of the world's population (18). *M. pneumoniae* bacterial infection likely adds to these numbers as a primary cause of airway disease that facilitate secondary infection (19, 20) and disease exacerbations (13, 21).

M. pneumoniae bacteria are described as preferentially adhering to the ciliated epithelium within the conducting airway (22-27). The principal structure involved, the terminal organelle, is responsible for attachment, gliding motility and cell division (28-31), and can best be defined as a polar, specialized membrane bound structure, studded with adhesins with redundant and specialized function(s). The terminal organelle has an

electron-dense core which is posited to drive the mechanism of gliding motility, which may involve protein phosphorylation (32, 33).

Elucidating the mechanism of *M. pneumoniae* infection and dissemination within the human host has been a challenging endeavor. Previous *in vivo* models have included *Sigmodon hispidus* (cotton rats), *Cricetulus auratus* (golden hamsters), *Mus musculus* (mice), while *in vitro* models have included human and hamster tissue culture as well animal and human cell lines (22, 26, 27, 34-37). The premise of such models is based on work by Eaton and coworkers, who used the development of airway lesions as their metric for the presence of the infectious agent (34). Based on recent reviews on *M. pneumoniae* airway pathogenesis (2, 38), *M. pneumoniae* bacteria are known to localize to the ciliated epithelium, via specific sialylated glycoprotein moieties (39-41), where they are suspected to initiate cell injury via peroxide formation and/or cytotoxins (42-45). Cell injury is thought to then facilitate an immune response that induces additional cell injury, which may or may not be localized (46-50) but mediated by cytokines (38). Radiographic data are consistent with this model in that bronchial wall thickening and interstitial infiltration are reported in humans (51-53). Recent work in mice suggests a relationship between lesion formation and mycoplasma motility (54). Despite these observations it is unclear how the extrapulmonary manifestation(s) of mycoplasmosis are established in the absence of frank pneumonitis or apparent resolution of disease, especially in the absence of cultivatable or detectable organism.

The topic of this dissertation is the development of a model of acute and chronic *M. pneumoniae* infection of the human airway using normal human bronchial epithelial (NHBE) cells. This model has the advantage of allowing examination of host-

mycoplasma interaction(s) in the air-liquid interface, with pseudostratified, primary, non-immortalized, human bronchial epithelial cells that produce mucus, ciliary beating and tight junction formation (55, 56), all of which contribute to an effective luminal barrier to infection (57, 58) and are discussed later. It is noteworthy, with respect to the NHBE cell model, that the airway infectious process begins at luminal surfaces, where the mucociliary defense is the primary barrier to infection (59). The mucociliary barrier protects the underlying cells, lamina propria (*in vivo*) and culture media (*in vitro*).

There are three objectives:

Objective 1: Develop a colonization model for acute exposure with *M. pneumoniae* in terminally developed NHBE cells exhibiting ciliary beating and mucus secretion.

Objective 2: Characterize the apical localization pattern of *M. pneumoniae* on the developing NHBE cell surface with specific focus on the relationship to structural components of the periciliary layer.

Objective 3: Develop a chronic exposure model of *M. pneumoniae* on terminally developed NHBE cells, specifically to determine the endpoint of colonization in this system.

CHAPTER 2

REVIEW OF THE LITERATURE

M. pneumoniae Overview

Seminal works. Initial isolation of the agent of primary atypical pneumonia (PAP; discussed later) was credited to Eaton and coworkers in 1938 (34). At the time, the infectious agent was referred to as a virus because of its intrinsic antibiotic resistance (beta-lactams and sulfonamide) and its filterability (< .45 μm) (34). Key contributing factors that facilitated Eaton's initial work included: cultivation of the agent in chick embryos, susceptible animal models, and antisera from suspected convalescing atypical pneumonia patients (34). The ability to sterilely inoculate and passage the infectious agent in chick embryos reduced the impact of contaminating bacteria from the sample, test animal and/or environment (34). This is noteworthy since it is unclear how these factors impacted their initial serological studies, which the authors indicated as being inconclusive (34). Studies from the direct inoculations of both hamster and cotton rat revealed infectious samples, one being De (derived from the human lung), capable of causing reproducible pulmonary lesions in test animals (34). The development of lung lesions in test animals, along with infiltrating white blood cells, were the principal observations used to determine the presence of the agent. Eaton and coworkers demonstrated that sample De, along with others, were capable of being passaged and maintained in chick embryos, where it could be used to inoculate test animals and produce pulmonary lesions (34). Importantly, neutralizing antibody from convalescing

rabbit (or human) serum but not pre-immune (or acute phase in humans) serum, blocked the presentation of lesions in experimentally infected animals (34). These data taken together demonstrated the isolation and maintenance of the Eaton agent in chicken embryos, as well the success in animal modeling of the pathognomonic lesions. Hereafter the "virus" was termed Eaton's agent.

Liu and coworkers used Eaton agent-specific hyper immune rabbit serum in conjunction with immunofluorescence microscopy in order to localize the Eaton's agent to the respiratory epithelium in chick embryos (60, 61). This was a significant step because prior to this there was no direct link between disease manifestation and the agent (17). Specifically, the combination of chick embryo infection and maintenance along with indirect fluorescein based detection, provided a specific test linking airway disease to Eaton's agent (62).

Marmion and Goodburn conducted both microscopic and susceptibility tests that not only demonstrated airway localization of Eaton's agent, but also inhibition of the pathognomonic airway lesions upon mycoplasma-specific chemical treatment (kanamycin sulphate or sodium aurothiomalate) (63, 64). The hamster model of lesion formation (34) was used to demonstrate that sodium aurothiomalate treatment reduced airway lesion and infiltration (63, 64). Using both modified Giemsa stain and indirect immunofluorescent labeling in chick embryos, the authors identified palisades of elementary bodies localized to the airway epithelium, whose presence could be reduced after chemotherapeutic treatment (63, 64). Similar observations were made for the grey lung "virus" of rats, which was also included in the study and is in fact a mycoplasma (63, 65).

Chanock and coworkers developed a solid agar based medium that allowed for the acellular cultivation and visualization of the characteristic fried egg morphology associated with the genus *Mycoplasma* (66, 67). The key components for mycoplasma bacterial growth were shown to be serum (horse) and yeast extract, without which Eaton's agent did not grow (66). The authors further demonstrated the ability to detect the agent on solid medium by using immunofluorescence with hyperimmune rabbit serum or human convalescent serum, but not human acute phase serum (66). Overall, there was general agreement between the ability to label Eaton's agent on supplemented agar, similar to early chick embryo maintenance culture (34, 60, 61, 66).

Taxonomy. Eaton's agent at one time was considered to be a virus due to its filterability, and then an L-form (no cell wall) due to resistance to beta-lactams and sensitivity to tetracycline (34, 63-65). There was some controversy with regard to the distinction between spontaneously generating L-forms, which were recognized as being pleomorphic, and mycoplasma (68-70), but were shown to be distinct based on DNA-DNA hybridization (71).

The genus *Mycoplasma* is grouped within the phylum *Tenericutes* (Latin: tender skin), members of which characteristically lack the ability to synthesize peptidoglycan (67). The closely related, low G+C, *Firmicutes* (Latin: strong skin), which includes clostridia and lactobacilli, are believed to be their predecessors (72, 73). The genus *Mycoplasma* is comprised of pleomorphic, mostly non-motile, chemo-organotrophic, filterable (<.45 μm) agents that require a host for survival (74). Some also possess a specialized terminal organelle (discussed later) and are capable of gliding motility (67, 74). Most mycoplasmas can effectively be cultured acellularly with media supplemented

with serum (lipids and sterols) and/or yeast extract (various cofactors and nucleobases) (66, 75, 76). It is important to note that the majority of mycoplasmas have not been cultivated and that new technologies involving 16S rRNA sequencing are being employed to demonstrate the existence of such organisms. However, stringent taxonomic standards are employed to distinguish and confirm the existence of novel organisms (77). *Mycoplasma*, species, have a dynamic host range including fish, cattle, goats, birds, cats, dogs, insects, plants, seals and monkeys, in addition to humans (74). The relationship can vary by host and includes pathogenic, opportunistic and commensal associations (74). *M. pneumoniae* is an exclusive pathogen of humans and it's adaptation to the conducting airway is the focus of this dissertation.

Terminal organelle. The *M. pneumoniae* terminal organelle is a membrane bound, protein studded structure that most resembles the head and crown of a bowling pin (78). It is essential for cell polarity, structure, attachment, gliding motility and cell division (28, 30, 31). The complexity and maturation of the terminal organelle, will not be the foucs of this introduction (79, 80), but rather the focus will be on specific surface-exposed proteins which have been demonstrated to have host specific targets and where available, assayed in an animal/tissue/cell culture system. Studies on attachment to erythrocytes and their clinical relevance have been discussed (2, 81). The *M. pneumoniae* interaction with host cell targets is defined by a characteristic polarity that essentially characterizes the microorganism (22, 24, 27, 80, 82) . What is important here is that the terminal organelle is essential for *M. pneumoniae* survival, and that proteins associated with attachment and gliding principally localize to this structure, in particular P1 and P30 (29-31, 83).

Cytoskeleton. The length of the core is 220 -300 nm with a width of 40 - 80 nm (84, 85). Removal of the *M. pneumoniae* membrane by Triton X-100 treatment (84, 85) reveals a complex structure that defines the bowling pin-like morphology. The underlying structure of the terminal organelle is an actin-like structure that forms a terminal button with extended fibrils that terminate into a second, somewhat larger, ring-like, negatively staining region (84, 85). Residing between the terminal button and the ring-like region is lucent space (84, 85), which houses the electron-dense core. Additional *M. pneumoniae* fibrils were observed by Göbel and coworkers in the cell body distal to the ring-like structure, but it is unclear if this was a dividing mycoplasma cell or not, which could explain the appearance of the third negatively staining region (85).

P1. Hu and coworkers identified P1 as a surface-exposed, trypsin-sensitive adhesin associated with attachment to hamster tracheal rings (22). The authors demonstrated that erythromycin treatment of wild-type *M. pneumoniae*, following trypsin treatment, blocked P1 recovery consistent with the loss of attachment after trypsin treatment (22).

Baseman and coworkers identified P1 as a 165 kDa protein primarily localized to the tip of the terminal organelle (86). Importantly, the authors demonstrated that while virulent and avirulent *M. pneumoniae* present with equivalent P1 levels on polyacrylamide gels, the localization patterns are quite distinct (86). Only the virulent, attachment capable, wild-type *M. pneumoniae* exhibited the characteristics polar tip P1 localization (86).

P1 antibody was previously shown to block cytadherence, and to localize to the terminal organelle tip (29, 87-90). Additionally, Gerstenecker and Jacobs identified three

regions within mature P1 (1 N-terminal domain and 2 C-terminal domains, D1,D2) that interact 3-dimensionally to facilitate mycoplasma attachment to sheep erythrocytes (87). It is likely that these same regions perform a similar role for gliding motile *M. pneumoniae*. P1 has been shown to be differentially phosphorylated, which may play a role in protein conformation, attachment and gliding motility (32, 33).

Seto and coworkers demonstrated that antibody directed against P1 caused gliding motile mycoplasmas to detach from coverglass, while non-gliding mycoplasmas were not significantly impacted (29). The authors also reported that the relative mycoplasma gliding velocity decreased with increasing P1 antibody concentration, further strengthening the link between P1 and *M. pneumoniae* gliding motility (29).

The isolation of *M. pneumoniae* strains deficient in P1 and accessory proteins has been very useful in elucidating P1 function. Mutants III-4 and IV-22 are *M. pneumoniae* M129B25C isolates recovered from a hemadsorption screen that identified colonies that failed to bind to erythrocytes (91). The roman numerals were assigned based on the absence of specific terminal organelle proteins (HMW1,HMW2,HMW3,A,B,C,P1), with an additional numbered designation referring to the colony picked (91). III-4 is the fourth hemabsorbance-negative isolate lacking proteins A,B and C, which is the result of a frameshift mutation in *MPN142* (91, 92). Similarly, IV-22 is the 22nd hemabsorbance-negative isolate lacking proteins A, B, C and P1, which is the result of a frameshift mutation in *MPN141* (91, 92). The significance of these isolates resides in their use in the identification of the P1-B-C complex and how it functions in conferring attachment and polarity to the *M. pneumoniae* cell. Waldo and coworkers demonstrate that complementation of IV-22 with *MPN141* (P1) and *MPN142* (B/C) restore wild-type

protein levels of P1, B/C (92). Similarly, complementation of III-4 restore B/C, however, complementation of IV-22 with *MPN142* (B/C) did not result in P1 expression and yielded barely detectable B/C (92). What is interesting is that genomic *MPN142* in IV-22 is identical to wild-type (92). These findings, in addition to the paraformaldehyde crosslinking studies of Layh-Schmitt and coworkers, indicate that P1 and B/C are part of a transcriptionally and translationally linked and codependent complex (83, 92).

P30. P30 was first identified by Baseman and coworkers as a 32-kilodalton protein associated with hemadsorption (93). P30 is localized to the tip of the terminal organelle (28, 30) and is essential for attachment to host cells and gliding motility (30, 31, 94, 95). Analysis of the deduced amino acid sequence of P30 revealed homology with P1, specifically with regard to the abundance of proline repeats within the cell surface exposed C-terminal region (96, 97). The N-terminus of P30 houses two hydrophilic regions that sandwich the transmembrane domain (97). A protease inaccessible domain (II) exists just upstream of the C-terminal proline rich region (domain III) but downstream of the transmembrane domain (94, 97). Chang and coworkers demonstrated the importance of these domains, in particular, extracellular domain III, where deletions resulted in deleterious effects on hemadsorption, gliding and P30 stability (94). Interestingly, deletions within domain (I) severely reduced attachment and gliding motility but not P30 stability to the same degree as domain (III) (94). Similar results were reported when the same group examined the signal peptide associated with the N-terminus of P30 (95). Importantly, cross reactivity of antibodies directed against P30 with fibrinogen, keratin and myosin has been demonstrated (97), and thus autoimmunity may contribute to some extrapulmonary manifestations of disease.

P200. P200 is a terminal organelle protein localized to the very tip of the *M. pneumoniae* cell body, just distal to the electron dense core, as indicated by Jordan and coworkers (98). Its structure includes several N- and C- terminal aspartate- and proline-rich regions which flank two internally located glutamate- and proline- rich regions, collectively referred to as acidic proline rich repeats (98). It is unclear if and how these regions contribute to the overall function of the P200 protein or other proteins that may be in close proximity (98). The focus of the study was to identify the location of P200 and characterize a P200 mutant in terms of adherence, motility and overall cell morphology. A wild-type *M. pneumoniae* strain possessing two insertions, Tn*4001* in *MPN452* (HMW3) and IS256 in *MPN567* (P200) underwent a transposon excision that restored *MPN452* (HMW3) but not *MPN567* (P200). The lack of P200 did not appear to impact attachment to erythrocytes or the A549 cell line (98). However, differences were observed when attachment to NHBE cells was assayed. Briefly, the NHBE cell system allows study of *M. pneumoniae* interactions in the air-liquid interface that directly parallels what occurs *in vivo* (covered later). The essential difference here is that the mycoplasmas have to deal with cilia and mucus within the NHBE cell system. What can be gleaned from the NHBE attachment data is that there is a reduction in attachment in the P200 mutant when compared to wild-type. This correlates with the >60% reduction in gliding velocity of the mutant. In agreement with this, complementation of the P200 mutation resulted in restoration of attachment and gliding velocities to wild-type (98).

Additional proteins. Kannan and coworkers determined that the protein product of *MPN372* is capable of interaction with human surfactant protein A (hSP-A) (99). Human surfactants are known for their opsonic capabilities as well as the ability to reduce

surface tension in the lung (100, 101). The MPN372 product was accessible to trypsin treatment, and hSP-A binding activity was enhanced in the presence of calcium but not zinc or magnesium, suggesting further a distinct interaction (99). Interestingly, the authors observed N-terminal homology between the putative adhesin and the S1 subunit of *Bordetella pertussis* toxin (99). Dallo and coworkers have described an additional interaction between fibronectin (component of the extracellular matrix) and mycoplasmal proteins (102). However, it is unclear how either of these proteins or their interactions impact disease or disease progression *in vivo*. For example, early images of *M. pneumoniae* interactions demonstrate organisms perpendicular to the plane of infection (26, 27, 103), consistent with the polar nature of P1 and P30 but not with the proteins suggested by Kannan (104) and Dallo (102). Also, it would be challenging to distinguish the roles of such proteins from P1 and P30, which the literature supports as primary movers in terminal organelle function (previous section).

Virulence and Pathogenicity

Attachment and gliding motility. Early work by Lipman and coworkers suggested colony morphology and the inability to attach (to glass or eukaryotic cells) as markers for virulence (45, 105). Attachment assays by Powell and coworkers employing radiolabeled mycoplasmas demonstrated that *M. pneumoniae* M129 B172 (non-adherent to glass) lacked fitness for cytadherence when tested in animal tracheal sections (24). Similarly, Krause and coworkers demonstrated an important link between loss of specific terminal organelle proteins, failure to persist and reduced respiratory pathology (91).

Mycoplasma gliding motility requires attachment to surfaces to be functional (106, 107). Early work by Leith and coworkers (108), along with recent work (54, 98),

indicate that attachment and gliding motility are separable characteristics when it comes to virulence. Szczepanek and coworkers linked poor gliding ability to reduced lung lesions and airway clearance in mice (54). Taken together, adherence is a necessary but not sufficient indicator for virulence. The intimate relationship between attachment and gliding motility prohibits a definitive statement on which is more important. For example, attachment may be important for delivery of certain enzymes or toxins to epithelial targets.

Peroxide formation. Peroxide production by *M. pneumoniae* is less controversial. In fact, reactive oxygen species have been shown to directly impact the barrier function and cytoskeletal organization of the airway (109, 110). In the 1960s Somerson and coworkers conducted simple but important experiments on the putative *M. pneumoniae* hemolysin (42). While they did not identify a specific protein, lipid or pathway by which peroxide was generated, they did show that the end product could cause cell injury, and that this process was capable of being inhibited in a titratable manner. The assay employed catalase and/or peroxidase as an inhibitor of erythrocyte lysis. Specifically, catalase activity would remove the mycoplasma-produced peroxide, thereby blocking hemolysis. As little as 400 catalase units was capable of limiting hemolysis, while heat inactivated catalase had no effect on hemolysis (42). The addition of the catalase inhibitor 3-amino-1,2,4- triazole (AT) allowed hemolysis to occur in the presence of catalase, and in a few cases enhanced hemolysis in the absence of catalase (42). Interestingly, the authors pointed out that the inhibitory effect of AT requires the formation of a catalase-peroxide complex (42), further suggesting peroxide as the hemolysin. A mechanism for mycoplasma induced peroxide formation involves glycerol

metabolism, where the production of hydrogen peroxide is formed as a product of dihydroxyacetone phosphate formation (111) .

Lipoprotein. Pattern recognition receptors (PRR) of innate immunity recognize pathogen-associated cell wall components, nucleotide, glycoproteins and glycolipid patterns, which then facilitate pro-inflammatory signaling and subsequent clearance (112). *M. pneumoniae* di- and tri-acylated lipoproteins have been implicated in the activation of Toll-like PRR (113-115). Chronic *M. pneumoniae* infection is likely to result in prolonged pro-inflammatory signaling with concomitant white blood cell infiltration and airway injury. It is noteworthy that this response is likely to occur for whole cell *M. pneumoniae* and its lysed cellular components.

Community Acquired Respiratory Distress Syndrome toxin. Kannan and coworkers identified the *MPN372* product as Community Acquired Respiratory Distress Syndrome (CARDS) toxin based on homology with the S1 subunit of *Bordetella pertussis* toxin (43). It is unclear if the toxin is secreted or if it is solely responsible for the reported toxicity. Recent efforts have been directed with associating CARDS toxin with chronic pulmonary disease (116, 117). The toxin is reported to cause cell injury in immortalized human cell lines and baboon tracheal organ culture (43).

Intracellular localization of *M. pneumoniae.* With the emergence of macrolide resistance, extrapulmonary manifestations, and long-term shedding and recovery of organisms, an epithelial niche for mycoplasmas has been highly sought after (118, 119). While no direct clinical evidence of intracellular localization has been observed, *in vitro* evidence of *M. pneumoniae* intracellular localization is available (120-123). The methods used to examine the internalization of mycoplasmas have been quite diverse. Baseman

and coworkers employed cell sorting and double fluorescent labeling (lipid specific $DilC_{18}$ and Fluorescein) techniques (120) while Dallo and coworkers utilize the transformed Hep-2 cell line (121), which are HeLa cell derivatives (124) and not derived from the larynx as reported previously (125). In the model proposed by Meseguer and coworkers, the authors used a human cell line derived from the human liver (Hep-G2) and a mouse neuroblastoma cell line derived from the brain (N2-A) (122). In contrast to the previous studies, the authors used clinical isolate *M. pneumoniae* RYC15989 recovered from a patient with pericarditis (122), which would be expected to be invasive considering the isolation site. Yavlovich and coworkers used an enrichment method that would select for internalized mycoplasma by using 400 µg/ml of gentamicin for 2 hours (123). Extracellular mycoplasmas would be killed, while those within the host epithelium would be protected. This method was employed previously by Andreev and coworkers showing invasion of HeLa cells by *Mycoplasma penetrans* (126). The observations made by the authors in this section can best be described as model specific. The common thread among these works is that they utilize a cell culture system that more likely reflects an injured airway, whereby, the monolayer is in a state of repair, migration, and low polarity (127). Thus, these observations become relevant during chronic disease states, where the epithelium is more sensitive to colonizing bacteria, and intracellular localization may set up the next round of infections. A similar model-specific outcome has been described for *Pseudomonas aeruginosa* infections (128, 129).

M. pneumoniae Airway Disease

Primary atypical pneumonia (PAP). In 1942 a detailed study of 100 cases of non-fatal PAP was conducted by Meakins (53). The majority of cases reported slow onset

disease with mild to moderate presentation of symptoms, which include cough, general malaise, headache, chills, fever, and general aches (53). The characteristic dry cough became productive with convalescence and correlated with bronchial lung infiltration observed on X-ray (51-53). Prolonged convalescence was also reported, taking as long as 47 days (53). It is noteworthy that of the 100 cases, 32 were treated with sulfonamides, which had no effect on the course of disease (53). Mycoplasmas are intrinsically resistant to sulfonamides and beta-lactams antibiotics (74). Additionally, Meakins' work demonstrated a relationship between the widespread nature of the cases and the slow onset of disease (53), which is in agreement with Chanock (130). Penicillin or sulfonamide resistance, slow onset of disease and failure to culture bacteria were the initial descriptors of PAP.

A prisoner volunteer study on the progression of PAP was conducted by Chanock and coworkers (62). Fifty-two men were infected via the nasal and oral route and monitored serologically and symptomatically (62). Noteworthy is the demonstration of PAP disease symptoms in the test population and the ability to detect Eaton agent-specific antibody via fluorescence (62). The authors did not report complete isolation of Eaton's agent despite observable airway disease symptoms and positive serology (62), which is a pattern that persists and helps explain the focus on non-culture based techniques to this day (131-134). This study also added to the mounting evidence indicating the unreliability of the indirect cold agglutinin serological test for Eaton's agent in PAP (62, 135). This indirect test assays for antibody titers that causes clumping of erythrocytes when refrigerated *in vitro* and is not specific for *M. pneumoniae* (135).

Chronic airway disease. Asthma is potentially a fatal chronic airway disease characterized by wheezing, airway constriction, abnormal mucus production, eosinophil infiltration and airway reorganization (57, 58, 136, 137). It is well known that *M. pneumoniae* airway disease is usually non-fatal and so it is unclear if mycoplasma airway disease results in asthma or an asthma-like spectrum. Additionally, it is unclear what the case may be for cystic fibrosis or chronic obstructive pulmonary disease, where poor mucus clearance results in high bacterial burden (138-140).

Hardy and coworkers investigated chronic mycoplasma airway disease using a murine model (118, 141). In the initial chronic exposure work, BALB/c mice received intranasal inoculation of *M. pneumoniae* bacteria in broth and were held for extended periods up to 530 days (118). The ability to culture and detect *M. pneumoniae* bacteria from bronchial alveolar lavage decreased over the course of the experiments (118). Characteristic histopathology associated with chronic infection was observed at 530 days, the severity of which was lessened if the immunoglobulin G titers were increased (118). Seven of nine BALB/c mice at 530 days postinfection presented with peribronchial and perivascular infiltrates, with negative cultures (118). PCR as a detection method was of limited value (118). The lack of detection does not suggest that the *M. pneumoniae* bacteria are not present (see previous section). This is not entirely surprising when you revisit the early work of Meakins, who reported the extended stay recovery of a few months with cases of PAP (53). A later study by Hardy and coworkers demonstrated reduced histopathology associated with a 10-day treatment with telithromycin (MIC $\leq$0.001μg/mL) of chronically infected BALB/c mice at 530 days postinfection (141). Taken together, for human infection, these studies indicate that while direct observation

of *M. pneumoniae* in clinical cases (or current available models) remains elusive, the brunt of the impact will be felt by the subset of cases that may be predisposed to chronic infection (118). The nature of the chronicity may result in an asthma-like spectrum in humans, as demonstrated by Hardy (118, 141). Additionally, the existence of this population will keep *M. pneumoniae* persistent in the community, making eradication impossible. Improved model systems would be a step in the right direction, providing a better understanding of the missing link between acute and chronic disease.

Conducting Airway Defense

The mucociliary apparatus. The mucociliary apparatus is the primary airway defense of the conducting airways (59). It is a complex three layer system that includes the gel layer mucus, periciliary layer and polarized epithelium. Each layer provides an additive barrier that together restricts pathogen colonization. Airway mucus captures and dilutes substances for transport via coordinated ciliary beating. Healthy airway mucus is 95% water, with the remainder consisting of sulfated glycoproteins, lipid, antibody, surfactants and innate defense proteins. The thickness and viscosity of gel layer mucus is regulated via degree of sulfation of polymeric mucins and hydration of the gel-layer, which is in part regulated by the periciliary layer. The barrier forming epithelium of the conducting airway is supported by junctional protein arrays that give the epithelium its apical and basal polarity, as well as regulating ion and fluid flow to the periciliary layer.

Gel-forming and tethered mucins. Mucins make up the principal glycoprotein component of the mucociliary defense. Mucins serve as both gel-forming (MUC5AC, MUC5B) and tethered (MUC1, MUC4) polymers involved in barrier formation. For gel-forming mucins (MUC5AC, MUC5B), crosslinking via N- and C- terminal cysteine

residues yields a branched fully extended macromolecular mesh that characterizes the spinnability of gel layer mucus (discussed later). Tethered mucins found in the periciliary layer are localized to the luminal surface of epithelia and are often used as markers of polarization and development (142, 143), and have been shown to have a role in cell signaling (144). MUC1 and MUC4 are associated with the microvilli and cilia, respectively, and extend perpendicular to their surfaces forming a meshwork that restricts access to the underlying epithelium (145). Mucins characteristically possess a mucin domain consisting of a variable number of tandem repeats, where serine and threonine are targeted for O-glycosylation by transglycosylases. The variable size of mucins is directly associated with the size of the mucin domain and level of glycosylation. It has been suggested that the net negative charge of the airway, provided mainly by glycosylated mucins, is responsible for clearance of bacteria (146). It is noteworthy that *M. pneumoniae* has been known to interact with various oligosaccharide residues, especially sialic acids, found on airway epithelium (40, 41) and it has been proposed that differential oligosaccharides may affect motility (147). This is by no means an extensive coverage of the field of mucin biology, see (146, 148) for reviews on secreted and tethered mucins, respectively. Taken together mucins account for a major portion of the rheological properties of the airway, due mainly to the O-glycosylation of the mucin domains.

Airway mucus properties. The gel-layer of airway mucus is referred to as having viscoelastic properties or those of a non-Newtonian fluid (149, 150). For Newtonian fluids, there is a linear relationship between shear stress and shear rate, the quotient of which is termed viscosity (149, 150). Shear stress is the force applied to a specific area while shear rate is the velocity gradient (149). For airway mucus, this

means that functional mucus resists motion and deformation while also being able to flow with enough elasticity such that it does not fall apart or tear (149, 150). Transport-capable mucus must have load bearing capacity and spinnability, which is the ability to draw mucus into long beads (149, 150). These properties allow mucus movement as a continuous blanket and permit diffusion of select molecules involved in innate defense (150-154).

Periciliary layer. Cilia are located within the periciliary layer (PCL) and are tasked with propelling the overlying gel-layer mucus. The motile cilia of the ciliated epithelium of the human airway are 5-7 μm in length, which spans the PCL (58). Cilia are membrane bound protrusions of a cytosolic arrangement of microtubules that are anchored to basal bodies, which are then anchored to filamentous actin via ciliary adhesion complexes (155). This association gives support and coordination to the cilia stroke in order to propel the overlying mucous blanket, which is coordinated with mucus secretion (156, 157). Ciliary beat frequencies range from 10-14 Hz (158), which when combined with the rheological properties of healthy mucus facilitate movement of the contiguous mucous blanket.

The secondary barrier residing beneath gel-layer mucus is referred to as the periciliary layer (PCL). Button and coworkers have described the periciliary layer as having a brush-like quality as opposed to liquid phase (145). In this "gel-on-brush model," as ciliary beating ensues the gel layer mucus compresses the PCL, which brings the gel layer mucous in close proximity to the underlying epithelial cells (145). Within the PCL, tethered mucins and associated mucopolysaccharides form a barrier that not only regulates gel layer mucous rheology, through hydration, but also prevents the gel

layer mucus from interacting with the underlying epithelial cells (145). This same barrier was demonstrated to limit the penetration of 40 nm fluorescent beads in much the same way that gel layer mucus fails to make contact with the underlying epithelium (145). When ciliary beating was inhibited by pretreatment with 1% isoflurane, the PCL barrier was not only maintained but also appeared to increase in thickness (145). In summary, the PCL acts as secondary barrier to colonization by limiting the penetration of the overlying gel layer mucous.

The epithelial barrier. The third physical barrier in the airway centers on functional cell junctions associated with epithelial cells. The protein complexes associated with anchoring and tight junctions are responsible for: regulating paracellular transport and concentration gradients, while also fencing in lipids that give the epithelium its characteristic polarity (159-162). Useful markers of cell polarity are the cadherins, integrins, occludins, claudins, and junction adhesion molecules, which are linked either to actin or intermediate filaments of the cytoskeleton.

The barrier function can be assayed via trans epithelial electrical resistance (TEER). An intact epithelial barrier will have electrical resistance reported in Ω-cm^2. As indicated by Ohm's law, V=IR, where V= voltage, I=current, R=resistance. A reduction in resistance indicates an increase in current at constant voltage, which suggests a change in barrier function. Claude and coworkers have demonstrated a relationship between electrical resistance and complexity at the tight junction (163, 164). TEER measurements have been used in conjunction with immunohistochemistry for the junctional proteins to indicate a loss of barrier function (165-168). An alternative to TEER is the use of

fluorescent molecules to assay for paracellular permeability, where paracellular transport can be visualized and quantified via fluorescence units (169).

Normal human bronchial epithelium (NHBE) culture. Human bronchial epithelial cells in air- liquid interface culture offer a favorable alternative to submerged cell culture models. Gray and coworkers demonstrated that serially passaged bronchial epithelial cells cultured in air-liquid interface present with cilia, mucus secretion and a functional barrier measured via electrical resistance (55). The authors detected lysozyme, lactoferrin and secretory leukocyte protease inhibitor (SLPI), which are antimicrobial peptides characteristically associated with the mucociliary defense (55). Two important observations were made by the authors. The first was that 5×10^{-8} M retinoic acid (RA) supplementation with 0.5 ng/ml epidermal growth factor (EGF) was associated with a non-necrotic normal appearing columnar epithelium in contrast to 25 ng/ml EGF (55). This is an important observation because when determining cytological pathology induced by organisms it is essential to consider the conditions in which the assay is taking place. The second, was that successive serial passages resulted in reduced electrical resistance and reduced numbers of ciliated cells (55), both of which are components of a functional mucociliary barrier (58, 145, 159, 170).

NHBE culture model for *M. pneumoniae* studies. The first *M. pneumoniae in vitro* air-liquid interface culture study was conducted by Krunkosky and coworkers (171). In contrast to previous models, this study demonstrated a stable and testable barrier function (TEER, Zona occludin-1, ciliary beating, mucus secretion) that a colonizing mycoplasma would encounter during normal infection, which parallels *in vivo* conditions in the human airway (171). Another key distinction is the recognition that host-pathogen

interactions occur in the lumen of the airway, sequestered from the lamina propria (*in vivo*) or culture media (*in vitro*). An important initial observation was that mycoplasmas rapidly colonized ciliated epithelium in as little as 2 minutes, and that the localization increased with time (171). This observation becomes more striking when viewed in the same plane as non-ciliated cells, which appeared devoid of detectable mycoplasmas (171). The authors also demonstrated increased mRNA levels for of adhesion molecules associated with inflammatory localization (56, 171, 172). Taken together, the *in vitro* air-liquid interface studies conducted with NHBE cells offer the best available model to study host-pathogen interactions at the mucociliary barrier.

CHAPTER 3

MATERIAL AND METHODS

General Methods

Mycoplasma strains. Wild-type *M. pneumoniae* M129 (17^{th} broth passage) (105), S1 (43, 99) P01 (173) ; P30 mutants II-3, II-7, and II-3 revertant (30, 31, 97) and II-3 P30 complement (30, 94, 95); P200 mutant (98); prpC mutant (33).

Gliding measurement. *M. pneumoniae* gliding phenotypes were confirmed as described (30) but with modifications. Briefly, mycoplasmas were grown overnight at 37^0C in chambered slides (Nunc Nalgene, Naperville, IL) in modified SP-4 medium (no phenol red; + 3% gelatin, pH 7.2). The spent medium was then removed and replaced with fresh pre-warmed modified SP-4 medium. Mycoplasma bacteria were viewed by using a Leica DM IL inverted microscope (Leica Microsystems, Buffalo Grove, IL) with digital CCD camera (Hamamastsu Photonics K.K., Hamamatsu-City, Japan) and analyzed using Openlab version 5.5.0 (Perkin Elmer, MA). A minimum of 20 uninterrupted frames at a constant time interval, were analyzed along a collision-free path for $\geq$ 100 individual cells per strain for gliding velocity. For the chronic exposure study a minimum of 50 individual cells were measured. This software allows for movement tracking with time stamp capability for calculating distance traveled over time. Gliding frequency was determined by counting the number of motile cells per field and dividing by the total number of cells in the same field (n= approximately 2100 cells per strain).

The mutant II-3 is non-motile (30) and was not measured but confirmed visually. Gliding data for the acute and chronic exposure experiments are listed (tables 1& 2, respectively)

NHBE cell culture. NHBE cells are primary airway cells from the bronchial epithelium, cultured as described (56, 171). Briefly, expanded NHBE cells (Lonza, USA) were seeded onto collagen coated transwell inserts (Costar, Cambridge, MA) and grown to near confluency in submerged culture in 1:1 bronchial epithelial cell growth medium: Dulbecco's Modified Eagles medium with high glucose (BEGM:DMEM-H; Lonza) supplemented with Single-Quot (Lonza) components: 0.5 ng/ml human recombinant epidermal growth factor, 0.5 µg/ml hydrocortisone, 5 µg/ml insulin, 10 µg/ml transferrin, 0.5units/ml epinephrine, 6.5 ng/ml triiodothyronine, 50 µg/ml gentamicin, 50 ng/ml amphotericin B, and 65 ng/ml bovine pituitary extract, as well as 5×10^{-8} M all-trans retinoic acid (Sigma-Aldrich, St. Louis, MO). The culture was maintained in a humidified atmosphere with 5% CO_2 at 37^0C. The apical medium was then removed and the epithelium fed only basally from this point forward. As indicated in figure 1, the number of days in development was designated relative to initiation of air-liquid interface (ALI) culture, corresponding to day 0. For the chronic exposure study PneumaCult-ALI Medium (Stem Cell Technologies, Canada) was used to facilitate terminal differentiation within 30 days, instead 50 using the previous method (56). NHBE cultures were switched to antibiotic free media at least 3 days before infection for all studies.

Mycoplasma growth and radiolabeling. Mycoplasmas were grown at 37^0C in SP-4 medium (75) until the phenol red pH indicator turned orange. Antibiotics were included as appropriate for certain mutants (33). For radiolabeling studies, mycoplasmas were cultured in the presence of 100 µCi (methyl- ^{3}H) thymidine (6.7 Ci/mmol;

PerkinElmer) harvested and collected by centrifugation and washed 3× in fresh SP-4 medium as described (174). Mycoplasmas were suspended in 1.8 ml SP-4 medium, incubated at 37^0C for 10 min, syringe-passaged 10× with a 25-gauge needle, and centrifuged at 123 × *g* for 5 min at 25^0C to remove large clumps. The resulting supernatant was used for NHBE cell infection. Infections were initiated with 10^{10} colony-forming units (CFU) of radiolabeled mycoplasmas in 150 µl SP-4 medium (7.6×10^5-3.2×10^6 CFU/CPM). Mycoplasma CFU were measured as described (175). Cytadherence assays were carried out over a three-day period for each time point due to the time required for sample processing. Assays were repeated twice, and the two highest and lowest results from 12 data points per sample were omitted before calculating means and confidence intervals.

Mycoplasma infection and labeling. For the acute exposure studies, NHBE cells were washed apically with Hank's Balanced Salt Solution (HBSS; Sigma-Adlrich) 4 h prior to infection and incubated at 37^0C in a humidified atmosphere with 5% CO_2 to allow mucus accumulation to a depth approximating that in the human airway (58). Unlabeled mycoplasmas at 10^6 CFU in 150 µl SP-4 broth were added to the apical surface. For chronic exposure studies, 10^6 or 10^9 color change units (CCU) (176) in 100 µl HBSS, was used to infected NHBE cells in parallel. During the infection, NHBE cells were normally fed (antibiotic free medium) every 3 days from the basal medium compartment and washed with 200 µl HBSS. At the appropriate timepoint, for both acute and chronic exposure, the inoculum was removed by gentle suction and cells were washed with HBSS, fixed with PBS + 7.4% formalin (v/v) for 1 h at room temperature and blocked with 10% goat serum (Sigma-Adlrich) in PBS. Blocked specimens were

probed for *M. pneumoniae* by using rabbit antisera raised against whole organisms (1:250 for immunofluorescence) (86), followed by goat anti-rabbit Cy3 (1:250; Invitrogen, Eugene, OR). Actin localized to tight junctions was identified by using phalloidin-647 (1:40; Invitrogen). Beta-tubulin in cilia was detected with conjugated fluorescein isothiocyanate (FITC) anti-tubulin antibody (1:250; Abcam Inc., Cambridge, MA). Additional tight junction markers also were screened using anti-zona occluden-1 (1:250; Invitrogen) and anti- E-cadherin (1:250; Abcam Inc.). Antibody directed at the tethered mucins (MUC1 and MUC4) were used as cell polarity markers (1:250; Abcam Inc.) with conjugated-FITC goat anti-mouse used as secondary (1:200; Invitrogen) and nuclei were stained using DAPI (Sigma-Aldrich). An alternative nuclear stain was used for *M. pneumoniae* infected desquamated epithelium, NucBlue Live Cell Stain (Life Technologies, Grand Island, NY). Immunohistochemistry (periodic acid-schiff stain, hematoxylin and eosin) was conducted as described (56, 177).

Mycoplasma growth experiments. Assessment of mycoplasma growth in infected transwells and the associated basal chambers were measured using color change units (CCU) (176). Briefly, infected airway cells were moved to a new chamber, washed with 200 µl HBSS followed by incubation with 200 µl of trypsin- EDTA (Sigma-Aldrich) for 15 min at room temperature. Two hundred microliters of SP-4 medium was added and then the surface was scraped with a P1000 to remove any attached cells from the transwell. The suspension was syringe passaged 10 × using a 25 gauge needle and then replicate aliquots were taken and serially diluted. The basal chamber was assessed similarly but did not require trypsin treatment. Assessment of *M. pneumoniae* associated

with the luminal supernatant was conducted using days to color change of the SP-4 medium.

Microscopic analysis. For the acute exposure study, images were captured and Z-stacks constructed using either a Zeiss LSM 510 META (Carl Zeiss, Thornwood, NY) or Nikon A1R (Nikon Instruments Inc., Melville, NY) confocal microscope, with subsequent image analysis using ImageJ (National Institutes of Health, Bethesda, MD; (178). To quantify mycoplasma colonization levels with ciliated NHBE cells, regions of interest (ROI) having approximately 200 NHBE cells were identified and categorized based on density of ciliated cells: <20%, 21-80%, and 81-100%. The *M. pneumoniae* bacterial numbers associated with each ROI were measured by fluorescence intensity above the background control. Confidence intervals or standard deviations were reported as indicated. For the chronic exposure study, baseline fluorescence was established using uninfected controls at 4 h to assess all samples (infected and uninfected). Microscopic images are representative data from a minimum of three independent experiments (acute and chronic exposure).

Airway barrier function. Trans epithelial electrical resistance (TEER) was measured as an indicator of barrier function using the Epithelial Voltohmmeter (World Precision Instruments, Inc. Sarasota, FL) (179). Briefly, the epithelial apical surface was washed once with HBSS to remove secreted mucus, 200 or 500-µl (for 0.33cm^2 or 1.12 cm^2 corning transwells, respectively) volume of fresh HBSS was added to the apical surface and electrical resistance was measured per the manufacturer's instructions. Following the manufacturer's instructions, the baseline measurement was defined as the TEER of uncoated transwell inserts without NHBE cells ($\leq 200\ \Omega\text{-}cm^2$).

Fig. 1. Transwell chamber system and NHBE cell development. From left to right: airway cells on transwell inserts (black) are fed from the basal compartment (red) of the system and terminally differentiate from squamous-like (day 2) to pseudostratified epithelium (day 40) secreting mucus (blue) and ciliary beating (black lines). Not drawn to scale.

Transwell chamber system

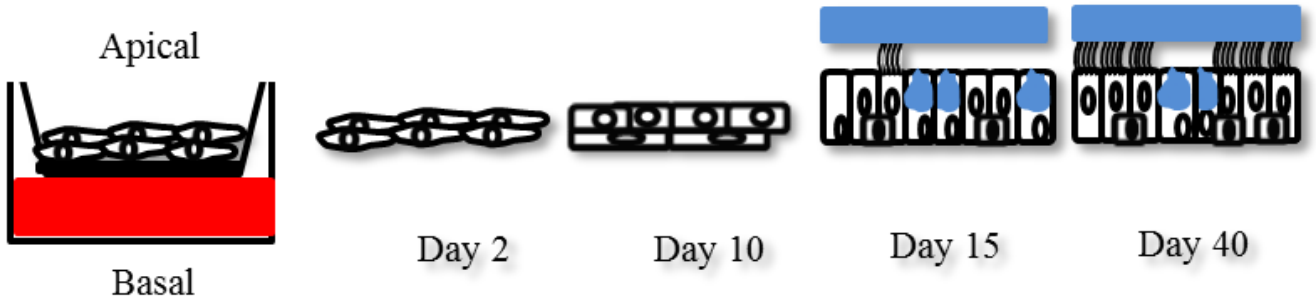

Table 1 Gliding and attachment data for strains used in the acute study.

Strain	Hemadsorption (% wild-type)	Gliding motility		Reference
		Velocity (μm/sec)[a]	Frequency[a]	
Wild-type M129	100	0.378 ± 0.023	27% ± 5.3	(30, 31)
II-3	5	0	0	(30, 31)
II-7	35	0.021 ± 0.028	9% ± 1.2	(30, 31)
II-3 Complement	100	0.358 ± 0.024	28% ± 4.96	(30, 31)
II-3 Revertant	60	0.012 ± 0.002	10% ± 1.9	(30, 31)
P200	90	0.167 ± 0.019	9% ± 1.4	(98)
prpC	70	0.403 ± 0.019	53% ± 8.6	(33)

[a] Reported as the mean and 95% confidence interval.

Table 2. Gliding data for strains used in the chronic exposure study.

Strain	Gliding motility (μm/sec)[a]	Reference
Wild-type M129	0.3028 ± 0.148	(105)
Wild-type PO1	0.294 ± 0.114	(173)
Wild-type S1	0.1805 ± 0.086	(43, 99)

[a] Reported as the mean and standard deviation.

CHAPTER 4

RESULTS

Acute Exposure Study

The purpose of the acute exposure study was to examine the role of mycoplasma gliding motility during colonization of terminally differentiated NHBE cells expressing a mucociliary defense. Developing NHBE cells were infected with gliding, reduced-gliding or non-gliding mycoplasmas to determine relative numbers of colonization and localization. Examination of underdeveloped NHBE cells yielded greater resolution as to how gliding mycoplasmas interact with the fully differentiated epithelium**.** In addition, mycoplasmas likely encounter underdeveloped airway (basal) cells as a result of normal epithelial turnover (180, 181), and the mycoplasma burden of the "unprotected" epithelium has not been previously examined.

Airway cell development. The development of normal human bronchial epithelium was monitored visually by immunohistochemical staining and TEER (Fig. 2). At day 2-4 ALI (air-liquid interface) epithelial cells were squamous-like morphologically with cells as large as 30 μm in diameter. The cell layer appeared fully confluent, with no evidence of culture medium from the basal compartment in the apical chamber. Actin labeling demonstrated organized tight junctions over > 90% of the transwell surface, and analysis by confocal microscopy indicated that the monolayer was as thin as 10 μm in some regions (data not shown). These observations were consistent with the near-baseline TEER ($\leq$ 200 Ω-cm^2) measured at this point (Fig. 2). PAS staining was positive, but

secreted mucus was not observed on the apical surface. In summary, day 2-4 airway cells characteristically presented as underdeveloped epithelium with no detectable cilia or mucus secretion. These early developmental cells collectively are referred to as day 2 airway cells.

Day 10-12 airway cells exhibited a cobblestone morphology, with large squamous-like cells less numerous. Actin labeling was localized to cell borders in all areas of the transwells. PAS staining was positive, but mucus secretion was not typically observed, and ciliated cells accounted for less than 1 % of the apically exposed cells (data not shown). In summary, day 10-12 airway cells were more polarized, as indicated by an increase in TEER, but lacked mucus production and ciliation was rare. These intermediate developmental cells collectively are referred to as day 10 airway cells.

Day 15-17 airway cells demonstrated cobblestone morphology similar to day 10 airway cells but with fewer squamous-like cells. Fluorescence microscopy indicated the presence of more ciliated cells than with day 10 airway cells, but their presence accounted for < 5% of the surface area. PAS staining was positive, and mucus production was clearly visible. Secreted mucus at the apical surface exhibited no evidence of the phenol red indicator from the basal compartment, and TEER was higher at this stage, indicating further cell polarization and adequate barrier function. These mucus-producing, intermediate-development cells are collectively as day 15 airway cells.

Day 43-45 airway cells exhibited robust mucus production and ciliated cell presence, although ciliated cells were unevenly distributed in the transwells. In some regions populations of ciliated cells were observed in large areas of near confluence, while other areas had only sparse ciliation. Ciliary beating and directional movement of

mucus was observed by using fluorescent microspheres (0.05, 2.0 and 9.9 μm; data not shown). The epithelium had largely a cobblestone appearance, but some ciliated cells appeared to be narrower or larger than the 10-15-μm range observed for most cells. In summary, day 43-45 airway cells characteristically exhibited abundant mucus secretion and substantial ciliation. These airway cells are referred to as terminally differentiated day 43 airway cells.

Primary airway cell development and *M. pneumoniae* adherence. Attachment of radiolabeled mycoplasmas to airway epithelium was measured at different stages of development (Fig. 3). The highest adherence for all strains was observed with day 2 airway cells and dropped 3-5-fold with day 10 airway cells, correlating with epithelial cell polarization but not appearance of mucociliary function. Wild-type adherence was comparable for day 10 and 15 airway cells but then dropped again significantly with day 43 airway cells. As expected, non-adherent mutant II-3 exhibited the lowest levels of adherence at all stages of NHBE cell development. Mutants II-7 and II-3R exhibited adherence to erythrocytes at 35% and 60% of wild-type, respectively, but very low gliding velocities ((30); Table 1) and colonized NHBE cells at day 10 and beyond at levels comparable to the baseline levels for mutant II-3. The P200 mutant adhered at a wild-type level with day 2 airway cells but at levels below wild-type for airway cells at later points in development (Fig. 2). We previously showed that complementation of this mutant with the recombinant wild-type allele for P200 in *trans* restores NHBE cell colonization to wild-type levels (22), but it also cannot be ruled out that revertants in the mutant population contribute to the adherence observed both here and previously (22). In

contrast to the P200 mutant, the hyper-motile *prpC* mutant attached at lower levels than wild-type with day 2, 10, and 15 cells but at wild-type levels with day 43 cells (Fig. 3).

Initial mycoplasma interactions on differentiated NHBE cells. *M. pneumoniae* localization was assessed on day 43 cells at 2, 30 and 240 min postinfection. Figure 4A illustrates the typical interaction of *M. pneumoniae* with ciliated cells after 30 min. Organisms resided in the same plane as the cilia, and note that the DAPI stain corresponded to mycoplasmas on the apical surface, while NHBE cell nuclei were beneath the scanning area and not in view. Detection was inconsistent at 2 min and appeared to be very sparse. Colonization patterns became more apparent but changed little between 30 min and 240 min postinfection (Fig. 4C). At all time points wild-type *M. pneumoniae* largely localized to ciliated cells, and colonization favored regions of the epithelium with dense clusters of ciliated cells versus sparsely ciliated regions (Figs. 4, 5 and 6). The overall density of mycoplasma fluorescence associated with ciliated cells increased with incubation time. This pattern was likewise observed with the intermediate-gliding P200 mutant, but with reduced overall mycoplasma fluorescence density (Fig. 5). As expected, mycoplasma fluorescence was low and often barely detected for mutants II-3R and II-3 and largely failed to correlate with cilia density (data not shown and Fig. 4, respectively).

In order to evaluate further the relationship between mycoplasma colonization and ciliated cell density, the data from figure 4B were analyzed for each strain and time point according to the extent of ciliation, which was categorized as low, medium, or high (<20% , 20-80%, and >80% ciliated cells, respectively; Fig. 6). Colonization was not consistently quantifiable at 2 min, but at 30 min mycoplasma fluorescence increased with

ciliated cell density, and at 240 min mycoplasma fluorescence associated with medium and high ciliated cell densities had increased approximately 2.5-fold. Significant association of wild-type mycoplasmas with areas of low ciliated-cell density was not noted until 240 min and was >3-fold higher than that for the P200 mutant. Interestingly, while spreading from ciliated cell foci may account for colonization of non-ciliated cells, at no time was an equal distribution of *M. pneumoniae* bacteria on ciliated and non-ciliated cells (Fig. 4 & 5). Furthermore, removal of the gel-layer mucus by washing day-43 airway cells with Hank's Balanced Salt Solution or dithiothreitol (10mM) did not appear to enhance colonization of non-ciliated cells by wild-type *M. pneumoniae* or negatively impact localization to cilia (Fig. 7).

Spatial and temporal colonization patterns. Mycoplasma localization on underdeveloped epithelium of the conducting airway has not been described. The stepwise development of NHBE cells and the previously described attachment assays (Fig. 3) suggested that localization patterns were likely to be similarly striking. Mycoplasmas may not always encounter fully differentiated epithelium *in vivo*. Examination of the localization patterns on NHBE cells lacking all or part of the mucociliary defense was expected to give a snap shot to likely patterns that may occur.

Confocal analysis of day 2 cells infected with wild-type *M. pneumoniae* revealed mycoplasmas in numerous, near-confluent consolidations separated by areas of much lower colonization density, but otherwise with no apparent pattern to the mycoplasma distribution (Fig. 8, top panel). Mycoplasma colonization of day 10 cells was less consolidated and more diffuse, consistent with the reduced adherence observed in binding assays with radiolabeled mycoplasmas. Mycoplasmas appeared randomly localized in

areas of diffuse colonization, except that highest mycoplasma densities where often noted along NHBE cell perimeters colocalized with actin (Fig. 8, bottom panel, arrows; data not shown). The colonization pattern for day 15 cells was similar to that for day 10 cells, with consistent mycoplasma colocalization with actin staining at cellular junctions (data not shown). Thus for day 2, 10, and 15 airway cells the data suggested a relationship between reduction in attachment levels and emergence of a localization pattern. Consistent with this observation, anti-mucin labeling of day 10 cells, which accounted for over 90% of the apical surface, revealed distinct patterns for MUC1 and MUC 4 (Figs. 9 & 10). MUC1 labeling demonstrated no clear discernable patterns with regard to mycoplasma localization, which was generally diffuse with some areas suggestive of an association with MUC1-negative cells (Fig. 9, panels A & B) while there was also evidence of colocalization with MUC1-positive cells (Fig. 9, panel C). A stronger colocalization pattern was observed with respect to MUC4-positive cells, with mycoplasma localization between MUC4-positive cells (Fig. 10), suggestive of a barrier (Fig.10). A closer look at the mycoplasma interactions with MUC4-positive cells suggested a packing of mycoplasmas localized to the non-labeling region (Fig. 11). The luminal and cross-sectional views in Fig. 11 are designed to give a complete picture of the region of interest. The guide bar (gold) within the luminal view indicates the region observed in the cross-sectional view; both images should be considered together. The luminal views in Fig. 11 illustrate accumulations of mycoplasmas that begin in non-labeling regions. In all cases, mycoplasma density was greater at the non-labelling cell periphery. This was observed even in apparent cases of mycoplasmas covering particular epithelial cells (Fig. 11, panel B compare views). Comparison of the luminal view and

cross-sectional views suggest a relationship between the cobblestone-like morphology of organized epithelium and the fluorescence intensity associated with MUC4-positive cells (Fig.11, panel A). The MUC4 labeling in the cross-sectional view of panel A was of low fluorescence intensity and localized to a narrow region of the epithelium (arrows). In contrast, comparison of the luminal and cross-sectional views of panel B suggest a relationship between the larger, squamous-like epithelium and the high fluorescence and wider band of MUC4 labeling (arrows).

Chronic Exposure Study

A major hurdle from the previous experiments was time. On average it took > 40 days in culture to achieve terminal NHBE cell differentiation to, reproducibly, >70 % ciliated cell population representative of the conducting airway (182). In order to characterize the long-term interactions between *M. pneumoniae* and NHBE cells a growth medium was used that allowed the cells to terminally differentiate within 30 days in culture. TEER measurements (1413 ± 232 Ω-cm^2) appeared indistinguishable from the previous culture system for day 43 cells (Fig. 2). For the uninfected samples, ciliated cell density appeared to increase over the course of the experiment (Figs.12 &13, compare top and bottom panels), but there were no other detectable differences (Fig. 13, compare A & B). All experiments were started at day 15 air-liquid interface. The uninfected controls were treated with Hank's balanced salt solution (HBSS) for 4 h in parallel with the infected samples. For the controls, 4 h and 28 days refer to post-HBSS treatment and are synonymous with days of culture. As a result, the total time in air-liquid interface culture is 43 days.

Confocal microscopy was used extensively in this section to indicate localized expression changes via fluorescence. In practice, baseline fluorescence was established using uninfected controls at 4 h to assess all samples (infected and uninfected). This is why more cilia appeared brighter at 28 days versus 4 h (Fig. 12, compare top and bottom). This was a useful tool because, as described later, *M. pneumoniae*-epithelial interactions appeared to alter the structural nature of the epithelium which was observed as difference in fluorescence intensity and localization. Unless otherwise stated, the 28 days uninfected control will be used for comparison to infected samples.

Loss of barrier function and airway reorganization. NHBE cell barrier function changed over time in relation to inoculum (Fig. 14). For the high-dose *M. pneumoniae*-infected samples, TEER increased to 139% and 126% at 7 and 14 days postinfection, respectively. Comparatively, for the low-dose *M. pneumoniae*-infected samples, TEER was 103% and 116 % for the same time points (Fig. 14). The elevated electrical resistance for both samples was unexpected, while the reduction at 28 days postinfection was significantly less than control ($P<0.01$). The TEER measurements paralleled differences in inoculum size between samples, indicating the measurements were the result of the infection and not variation within the NHBE cell model. Note that despite the decrease in TEER there was no evidence of basal compartment-airway media (see Fig. 1) on the luminal surface at any point during the course of the experiments. Three timepoints were examined for immunohistochemistry based on the TEER results and were used for further analysis (4 h, 7 and 28 days postinfection).

Confocal microscopy of *M. pneumoniae*-infected samples indicated structural changes in cilia and actin based on fluorescence (Fig. 15). Low-dose *M. pneumoniae*

infection appeared to result in poor cilia detection as indicated by reduced fluorescence from 4 h to 28 days postinfection (Fig. 15, top panels). By 28 days postinfection, actin labeling also exhibited reduced fluorescence intensity as well as wave-like architecture (Fig. 15, overhead view). Interestingly, the detected cilia were observed lining the invaginations of the wave-like monolayer (Fig. 15, compare top panels). High-dose *M. pneumoniae* infection yielded drastic structural changes in cilia and actin (Fig. 15, bottom panels). Cilia were detectable at 4 h postinfection but appeared to increase in fluorescence intensity and lose some detail in specific areas of the monolayer by 7 days postinfection (Fig. 15, compare bottom panels). The high-dose infected samples, characteristically, presented with patches of intense cilia labeling and actin reorganization at 7 and 28 days postinfection (Fig. 15, bottom). At 28 days postinfection, *M. pneumoniae* bacteria were observed in heavily infected regions, where they appeared to surround the involved epithelium. These heavily infected regions were closely associated with the reorganizing cilia and actin.

The low-dose *M. pneumoniae* samples at 4 h postinfection appeared similar to the control (Fig. 16). Cilia and actin exhibited a distinct polar nature and were readily detectable (Fig. 16, box 3 and 5, respectively). Rare evidence of mycoplasma invasion was observed (Fig. 16, panels A & C, box 4). By 7 days postinfection, detection of cilia was inconsistent, showing evidence of variable fluorescence intensity (Fig. 17, compare A to B & C). Actin labeling revealed a wave-like pattern, which was difficult to distinguish from the control (Fig. 17, compare box 5). Evidence of mycoplasma invasion was observed more often than at 4 h (Fig. 17, box 4). At 28 days postinfection, cilia detection was low to poor (Fig. 18, box 2). Actin appeared to be more wave-like with

monolayer invaginations 10-20 μm deep (Fig. 18, box 5). This was consistent with the reduced TEER (Fig. 14). Mycoplasmas were detected primarily on the luminal surface, which was unexpected (Fig. 18, box 4).

The high-dose *M. pneumoniae* samples exhibited evidence of invasion at 4 h postinfection (Fig. 19). Variable cilia distribution also was observed with areas of intense fluorescence that appeared to surround the involved epithelium (Fig. 19, panel C). Mycoplasma aggregates were observed colocalizing with regions of irregular actin and cilia labeling (Fig. 19, boxes 3 & 5). In all cases, the actin in *M. pneumoniae*-infected epithelium appeared to lose its polarity localized to the involved region. At 7 days postinfection, *M. pneumoniae* bacteria were observed on the luminal surface (Fig. 20), which consistently appeared wave-like with deep, shallow and wide invaginations (Fig. 20, box 5). *M. pneumoniae* bacteria were observed at the bottom of these invaginations (Fig. 20, panel B), at the peaks associated with cilia (Fig. 20, panel A) or at the peaks associated with regions with poor cilia labeling (Fig. 20, panels B & C). Intense areas of cilia labeling were observed in specific regions that extended ~10 μm into the monolayer (Fig. 20, panels B&C). It is unclear why the TEER appeared higher than control for the 7 day infection, but the main observable NHBE cell difference between *M. pneumoniae* doses was the intense cilia fluorescence and the associated wave pattern of the actin. It is likely that, for the low-dose *M. pneumoniae* samples, the change in barrier function was more subtle and not sensitive to TEER measurements. At 28 days postinfection, *M. pneumoniae* bacteria were observed invading and surrounding the epithelium to a high degree (Fig. 21). Cilia fluorescence intensity appeared greatest when colocalized with epithelium heavily infected with *M. pneumoniae*. The invaded epithelium extended to

variable depths within the monolayer and may be responsible for the observed wave pattern (Fig. 21, box 5). Additionally, the actin network appeared to loop-out the mycoplasma infected regions, as suggested by the lack of actin labeling above the invaginations (Fig. 21, box 5).

Desquamation of the epithelium and actin reorganization. The wave pattern associated with the luminal surface actin (Figs. 17 - 21) suggested that some *M. pneumoniae* bacteria may be lost to desquamation of the epithelium. This might account for the elevated TEER at 7 days postinfection for the high-dose *M. pneumoniae* samples (Fig. 14) since a heavily infected monolayer may be loaded with enough mycoplasmas within the basolateral surface to affect the TEER. It is likely that the mycoplasma infected epithelium became uncoupled from the monolayer and was removed via the HBSS wash. This observation is consistent with the looping-out of certain sections of the epithelium (Fig. 21). The apical washings were examined for evidence of mycoplasma and observed morphology consistent with mycoplasma on epithelial cells (Fig. 22). *M. pneumoniae* bacteria were observed prominently at the cell periphery, with few areas of consolidation, very similar to Figs. 8 & 11. These mycoplasmas were viable, and were cultivatable within 4 days or less, suggesting a high infection burden (data not shown). Note that the fluorescence of the eukaryotic nuclei was different in intensity and morphology (Fig. 22, yellow arrowhead). Groups of *M. pneumoniae*-infected desquamated cells appeared individually or in sheets consisting of as many as 50 cells.

Actin localization within uninfected epithelium had a distinct polarity associated with luminal ciliated cells (Figs. 12 - 13). Depth coding of the actin network in uninfected samples demonstrated actin labeling associated with the luminal surface (Fig.

23). Low- and high-dose *M. pneumoniae* samples exhibited actin reorganization consistent with a loss in luminal polarity (Figs. 24 & 25). Actin reorganization extended 40 to 60 μm into the basolateral surface (compare Figs. 23 - 25). Note that there appeared to be no limitation in depth into the monolayer the infection extended (20 - 40 μm). In fact, it appeared that *M. pneumoniae* invasion depth and epithelial desquamation were directly related (Figs. 15, bottom panel, 24 & 25). Low-dose *M. pneumoniae* samples appeared to cover a more diffuse region that did not extend as deep into the monolayer (Figs. 18 & 24), which may explain the indistinguishable TEER at 7 days postinfection (Fig. 14). In contrast, the high-dose *M. pneumoniae* samples appeared to concentrate in regions of variable size and extend deeper into the monolayer (Figs. 15, 21 & 25).

Macroscopic impact of mycoplasma infection. The macroscopic impact of mycoplasma infection on the NHBE cell system was readily observable under low-power microscopy, with or without immunohistochemistry (Fig. 26 and data not shown). The luminal view of Fig. 26 shows the most commonly observed manifestation of *M. pneumoniae* chronic infection (Fig, 26, compare top and bottom). It is noteworthy that the NHBE cell monolayer invaginations are lined with ciliated cells extending >40 μm in length on the luminal surface (Fig. 26, arrows) and depth consistent with the actin reorganization (Fig. 25). The variable intensity of the cilia associated with the monolayer invaginations are likely an indication of return of ciliation within these specific regions, whereby high fluorescence would be an indicator of ciliated cell abundance (Fig. 26, arrowheads). The wave pattern in Fig. 26 was observed as early as 7 days postinfection (data not shown) and prominent to some degree in all mycoplasma-infected samples by

28 days postinfection, independent of inoculum size and wild-type *M. pneumoniae* strain (data not shown) Evidence of vacuolation was not observed.

E-cadherin localization in *M. pneumoniae* infected NHBE cells. *M. pneumoniae* localization to the cell junctions was consistently observed throughout the course of this study. Epithelial tight and adherens junctions characteristically localize to the luminal and basolateral surfaces, respectively, and made convenient markers (see previous section). Elucidating the possible mechanism of mycoplasma invasion is beyond the scope of this dissertation. The combination of mycoplasma localization and the potential for a possible mechanism of invasion was expected to be assayable via TEER (Fig. 14) and expression of cell junctional components (via fluorescence) of the NHBE cell barrier.

ZO-1 labeling and localization was inconsistent and difficult to interpret for both infected and uninfected samples (data not shown). There was evidence of variable expression, such that ZO-1 was more detectable within mycoplasma infected regions of interest while being barely detectable in the uninfected controls (data not shown). Due to the limited number of samples available for experimentation E-cadherin was used for this experiment. E-cadherin was consistently detectable, localized primarily to the upper 10 μm of the monolayer (Fig. 27). The baseline fluorescence was set based on the uninfected 4 h control (Fig. 27, top) and was observed to be consistent at 28 days (Fig. 27, bottom). The uninfected controls demonstrated near uniform E-cadherin detection with little variation in fluorescence intensity (Fig 27, compare overhead and cross-sectional views). Note that this is in contrast to the increase in fluorescence associated with cilia over the same period (Figs. 12 & 13).

At 28 days postinfection E-cadherin labeling was highly variable in fluorescence and localization (Fig. 28). The presence of luminal *M. pneumoniae* bacteria appeared to correlate with high E-cadherin fluorescence (Fig.28, yellow arrowheads). In contrast, regions heavily infected with *M. pneumoniae* demonstrated low to barely detectable E-cadherin (Fig 28, white arrowheads). The overhead views in Fig. 28 point to the overall differences in inoculum size with regard to infection. The high-dose *M. pneumoniae* regions appeared to have deeper wave-like monolayer invaginations, which made the regions of interest appear more like islands with intense E-cadherin detection (Fig 28, bottom panels). In contrast, the low-dose *M. pneumoniae* sample demonstrated isolated regions of intense E-cadherin detection adjacent to regions of low or non-detectable E-cadherin (Fig 28, top panel). The localized E-cadherin labeling pattern and the correlation with *M. pneumoniae* localization and desquamation suggested that the impact of the infectious process is localized and not global.

Closer examination of the low-dose *M. pneumoniae*-infected samples further demonstrated a distinct relationship between luminal mycoplasma localization and E-cadherin labeling (Fig. 29). *M. pneumoniae* bacteria appeared localized to the luminal surface (Fig 29, box 4). What is striking is that in panel A, fewer *M. pneumoniae* bacteria were observed in conjunction with diffuse E-cadherin detection (Fig 29, box 3). In contrast, panels B & C demonstrated highly fluorescent E-cadherin labeling with evidence of increased luminal *M. pneumoniae* (Fig 29, box 4). This pattern was maintained for the high-dose *M. pneumoniae* samples, which exhibited a higher infection burden (Fig. 30, box 4) and increased monolayer invaginations, as suggested by the actin labeling (Fig. 30, box 5). Fig. 30 panel C, demonstrates abnormal E-cadherin detection

that extended > 10 μm into the monolayer. These observations are consistent with reorganizing cilia and actin and as wells as the observed differences in barrier function (TEER).

***M. pneumoniae* isolation.** Isolation of *M. pneumoniae* bacteria from the transwell and basal media compartments was examined in order to determine viability. This is an important distinction because viable, metabolically, active mycoplasmas are necessary for dissemination. Growth was assessed using serially diluted samples from three regions: the luminal supernatant, transwell and basal compartments. The luminal supernatant was expected to represent mycoplasmas associated with desquamated epithelium. An early attempt to conduct serial dilutions from the supernatant was challenging due to the associated gel-layer mucus (data not shown). As an alternative, samples were monitored over 10 days in the presence of SP-4 medium for color change (pH), which was observed in as little as 4 days (data not shown). Rarely, were samples negative from the supernatant.

Isolation of mycoplasmas directly from the transwell was expected to represent viability of attached and basolaterally localized bacteria. This was a necessary oversimplification. As part of the experimental design trypsin was added to the NHBE cell luminal surface in order to remove the NHBE cells from the transwell so that the inoculum could be homogenized and serially diluted. The effect of the trypsin treatment on *M. pneumoniae* was assessed and lysis was observed after 5 min of treatment (data not shown). A 15 min trypsin treatment offered the best NHBE cell removal and likely reduced the cultivable *M. pneumoniae* bacteria reported in Fig. 31 (transwell). The transwell measurements from Fig. 31 represent isolation mycoplasmas from the trypsin

treated epithelium. Despite the trypsin treatment, isolation of *M. pneumoniae* bacteria from the transwell increased over time. It is noteworthy that the infection inoculum needed to be increased for the chronic exposure studies. Preliminary experiments at lower inoculum sizes resulted in no recovery of mycoplasmas from the transwell until 7 days postinfection (data not shown). This also made interpretation of TEER measurements as well as IHC studies challenging. For example, the preliminary TEER and airway cell architecture data were difficult to distinguish from the uninfected controls (data not shown). This did not indicate that the *M. pneumoniae* infection had no impact, but rather that the impact was beyond the resolution of the tools employed. There were two choices: increase the inoculum size or add longer time points.

M. pneumoniae cells that bypass the mucociliary defense were expected to be isolated from the basal media compartment (Fig. 31). Three of eight basal compartments were quantitatively assayed for growth while the other 5 were observed over 10 days for indications of color change (pH) and viewed microscopically for *M. pneumoniae* bacteria (Fig. 31 and data not shown). The basal compartments changed color in as little as 6 days. True negative samples were observed in the uninfected control at 4 h and 28 days of culture, which was expected. In all iterations of these experiments, *M. pneumoniae* bacterial recovery from the transwell preceded recovery from the basal compartment (Fig. 31). However, recovery of *M. pneumoniae* bacteria from the transwell did not always result in recovery of mycoplasmas from the basal media compartment, but this was primarily observed at the lower inoculum sizes and early timepoints 4 h and 2 days postinfection (data not shown).

Fig. 2. NHBE cell development. (Top) Representative images of actin labeling as described, illustrating an epithelium in the process of organizing into a pseudostratified monolayer at the indicated time points in ALI culture. Bar, 15 µm. (Bottom) Features of differentiating NHBE cells. N = 12 for TEER and n = 20 for cell diameters, with standard deviations indicated; -, absent; + to +++, rare to prominent; NT, Not tested.

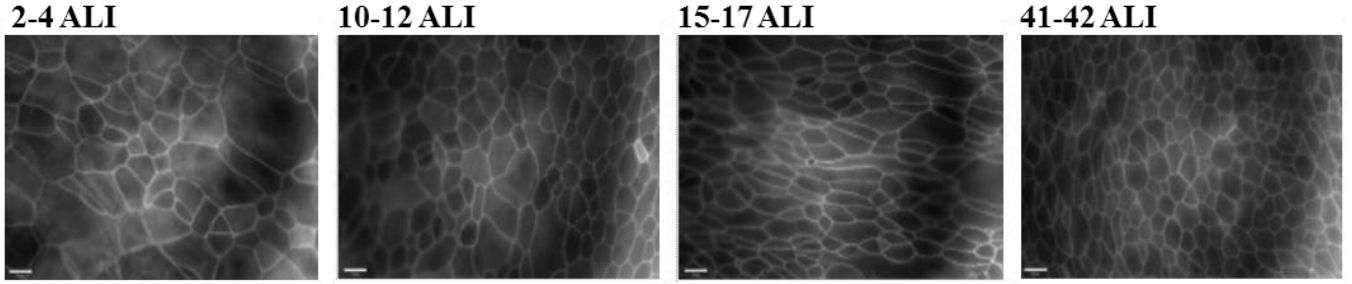

Days in ALI	Tight Junction	Cilia	PAS	Mucus	TEER (Ωcm^2)	Cell Diameter (µm)
2-4	+	-	+++	-	230 ± 10	24.9 ± 10.3
10-12	+++	+	+++	-	697 ± 165	14.6 ± 5.90
15-17	+++	++	+++	+++	1006 ± 27	18.2 ± 9.08
43-45	+++	+++	NT	+++	1339 ± 242	9.94 ± 2.60

Fig. 3. Colonization of NHBE cells at the indicated stages in development by wild-type (Top) and mutant *M. pneumoniae* strains (Bottom). For wild-type attachment (Top), comparisons were made to day 2 airway cells. For mutant *M. pneumoniae* strains (Bottom) comparisons were made relative to WT for that timepoint. NHBE cells were infected with radiolabeled mycoplasmas on the luminal surface and incubated 240 min as described. Each bar represents the mean and 95% confidence interval for 8 data points from 3 independent experiments. *, P = <0.05; #, P<0.10; NS, not significant.

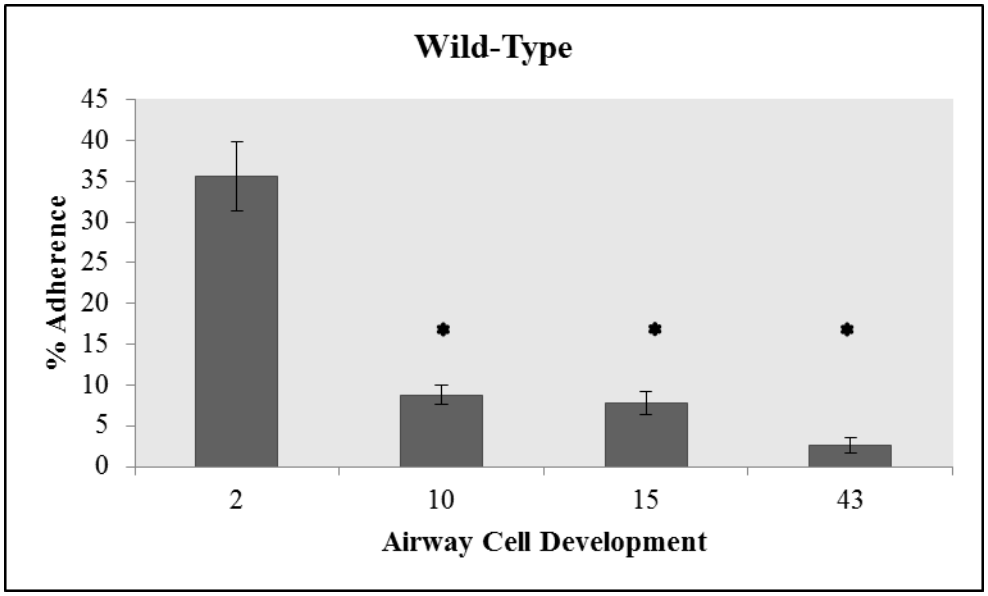
Wild-Type
% Adherence
45
40
35
30
25
20
15
10
5
0
2
10
15
43
Airway Cell Development

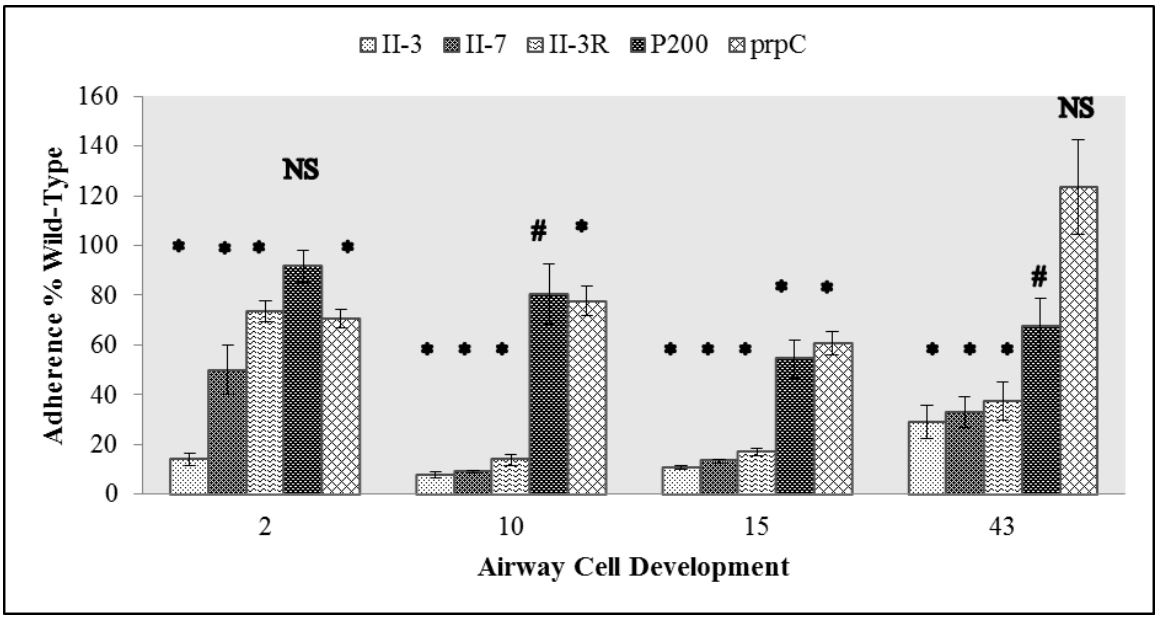
II-3
II-7
II-3R
P200
prpC
Adherence % Wild-Type
160
140
120
100
80
60
40
20
0
NS
NS
#
#
2
10
15
43
Airway Cell Development

Fig. 4. Wild-type *M. pneumoniae* M129 colocalized with cilia on the apical surface of day 43 NHBE cells after 30 min. (A) Blue, DAPI; green, cilia; red, mycoplasmas; purple, mycoplasmas costaining with DAPI. Bars = 10 μm. The DAPI staining corresponds to mycoplasmas on the NHBE cell surface. (B) Day 43 NHBE cells at 2, 30, or 240 min postinfection with the indicated *M. pneumoniae* strains. Random fields with high ciliated-cell density were selected. Green, cilia; red, mycoplasmas; yellow, mycoplasmas colocalized with ciliated cells. Bars = 20 μm. (C) Quantification of wild-type and mutant mycoplasma colonization in arbitrary fluorescence units at the indicated time points for 6,700 to 9,200 NHBE cells per strain per time point, presented with 95% confidence intervals. For each time point, a background control was subtracted, and comparisons were made to II-3 (negative control). *, $P < 0.05$; #, $P<0.10$; NS, not significant relative to the negative control.

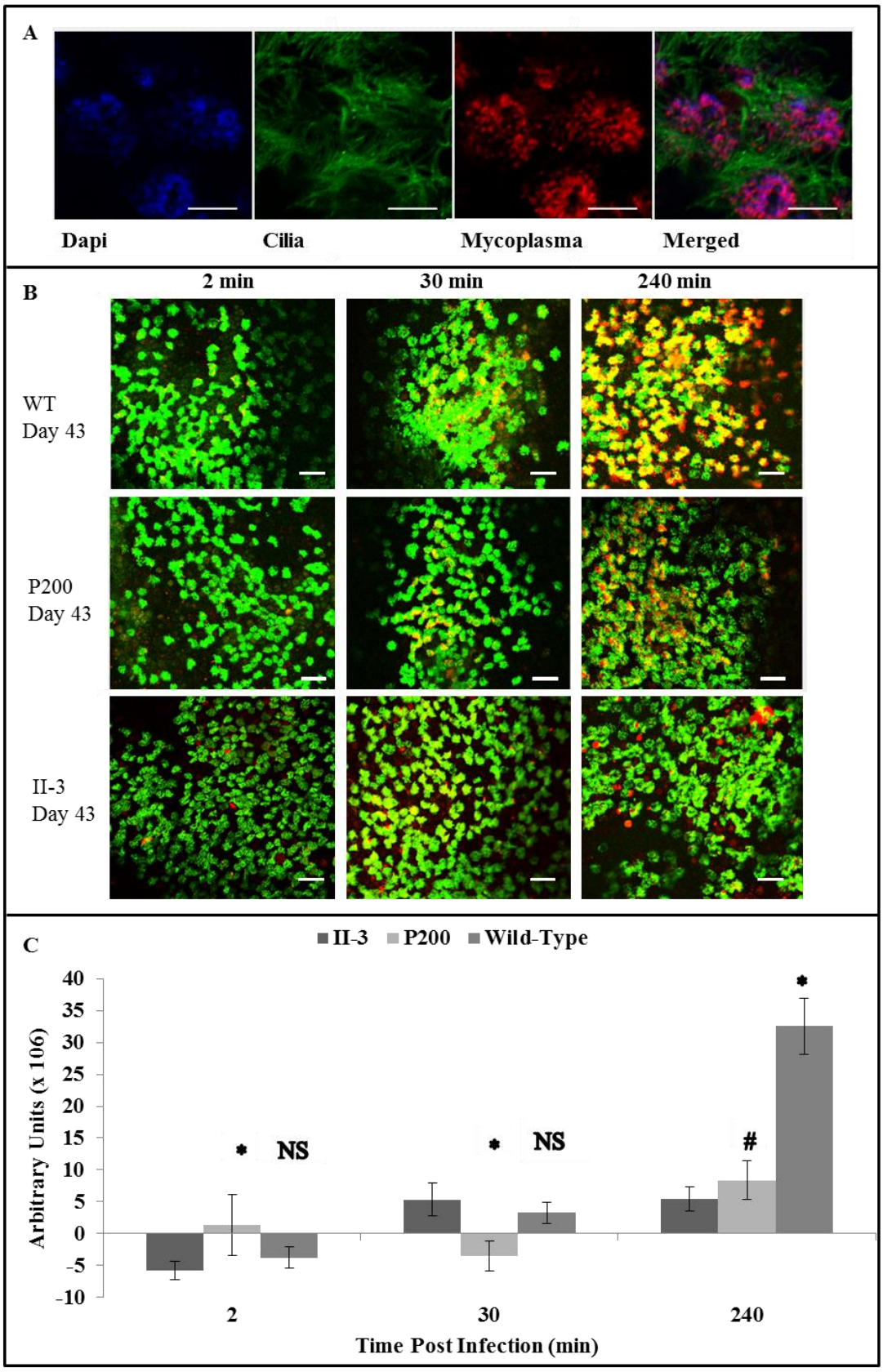
A
Dapi
Cilia
Mycoplasma
Merged
B
2 min
30 min
240 min
WT
Day 43
P200
Day 43
II-3
Day 43
C
II-3
P200
Wild-Type
Arbitrary Units (x 106)
40
35
30
25
20
15
10
5
0
-5
-10
*
NS
*
NS
#
*
2
30
240
Time Post Infection (min)

Fig. 5. (A) Luminal view of mycoplasma localization and spreading patterns on day 43 NHBE cells as three-dimensional (3D) projections of regions from Fig. 4 at the indicated times postinfection. Likely mycoplasma spreading (yellow arrows) was observed for the wild type but was more limited for the P200 mutant, which correlates with localization to ciliated cells (white arrows). Bar = 10 μm. Purple, mycoplasmas; green, cilia; blue, DAPI. (B) Cross-sectional view of mycoplasmas interacting with ciliated (white circles) and nonciliated (yellow circle) cells. Bars = 10 μm. Red, mycoplasmas; green, cilia; yellow, mycoplasmas colocalized with cilia; purple, actin; pink, mycoplasmas colocalized with actin; blue, DAPI.

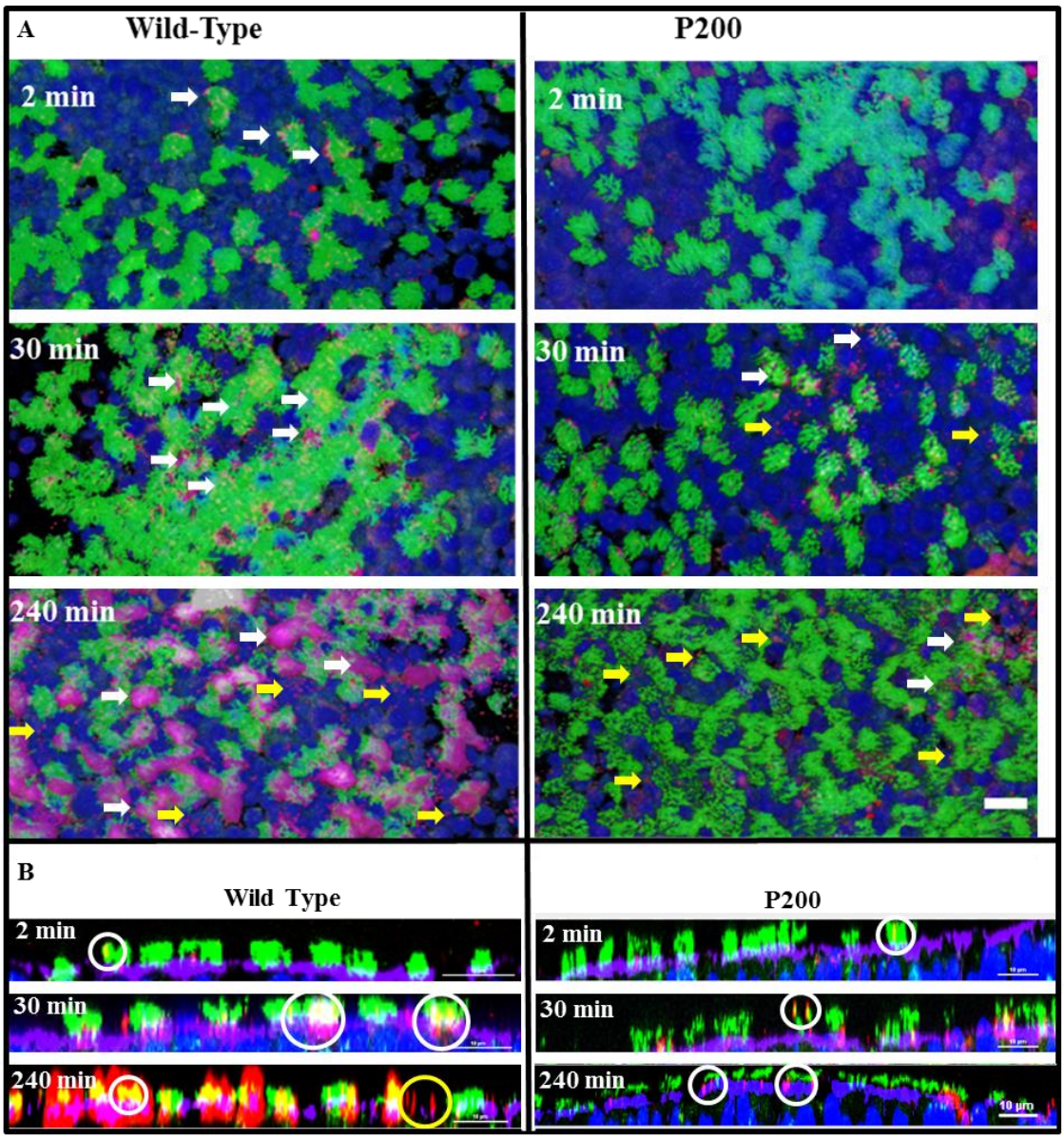
A
Wild-Type
P200
2 min
2 min
30 min
30 min
240 min
240 min
B
Wild Type
P200
2 min
2 min
30 min
30 min
240 min
240 min

Fig. 6. Quantification of mycoplasma fluorescence associated with ciliated cell density for the data set in Fig. 4C. 6,700 to 9,200 NHBE cells per strain per time point were analyzed. The data are reported as means, and the error bars reflect the standard deviations. II-3 was omitted, since it failed to colonize NHBE cells.

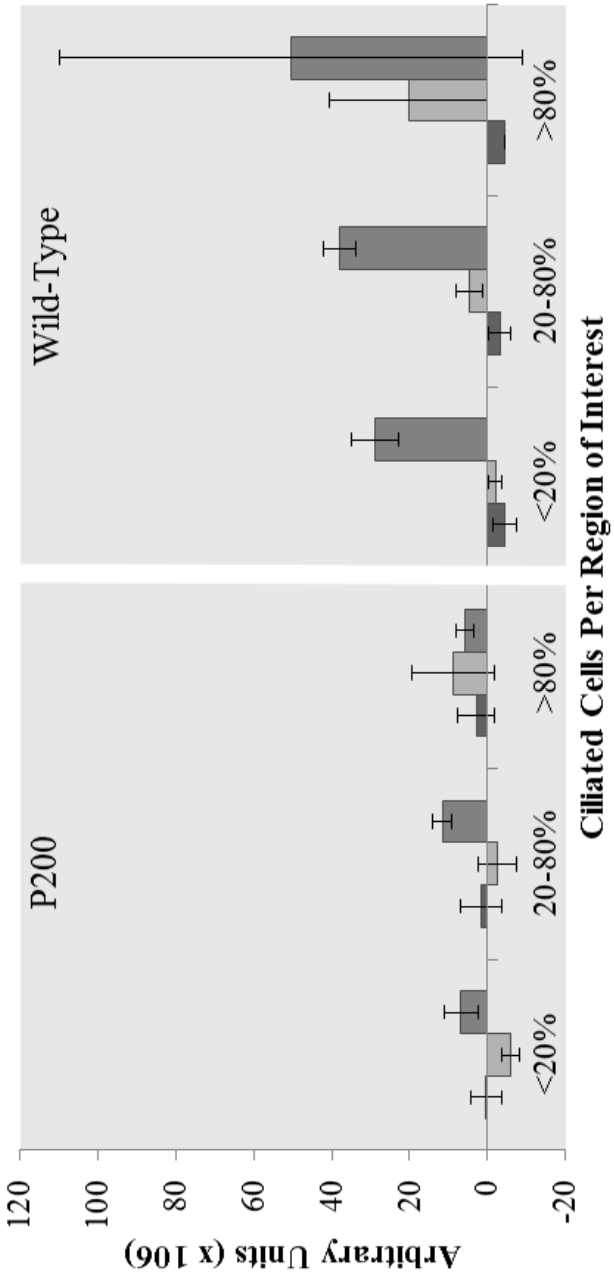
2 min
30 min
240 min
P200
Wild-Type
Arbitrary Units (x 106)
120
100
80
60
40
20
0
-20
<20%
20-80%
>80%
Ciliated Cells Per Region of Interest

Fig. 7. Mycoplasma localization to non-ciliated cells was not enhanced upon mucus removal. NHBE cells were pretreated with HBSS or 10mM DTT for 5-min followed by 10 additional HBSS washes and then immediately infected with wild-type *M. pneumoniae* M129 for 240 min. The control sample had mucus accumulation followed by infection with mycoplasma for 240 min. The control (A), HBSS (B) and DTT (C) samples in all panels shown demonstrated mycoplasma localization to cilia but only minimal enhancement of localization to non-ciliated cells (yellow arrowheads). Panels show cilia, mycoplasma and actin, respectively. Bars = 20 μm.

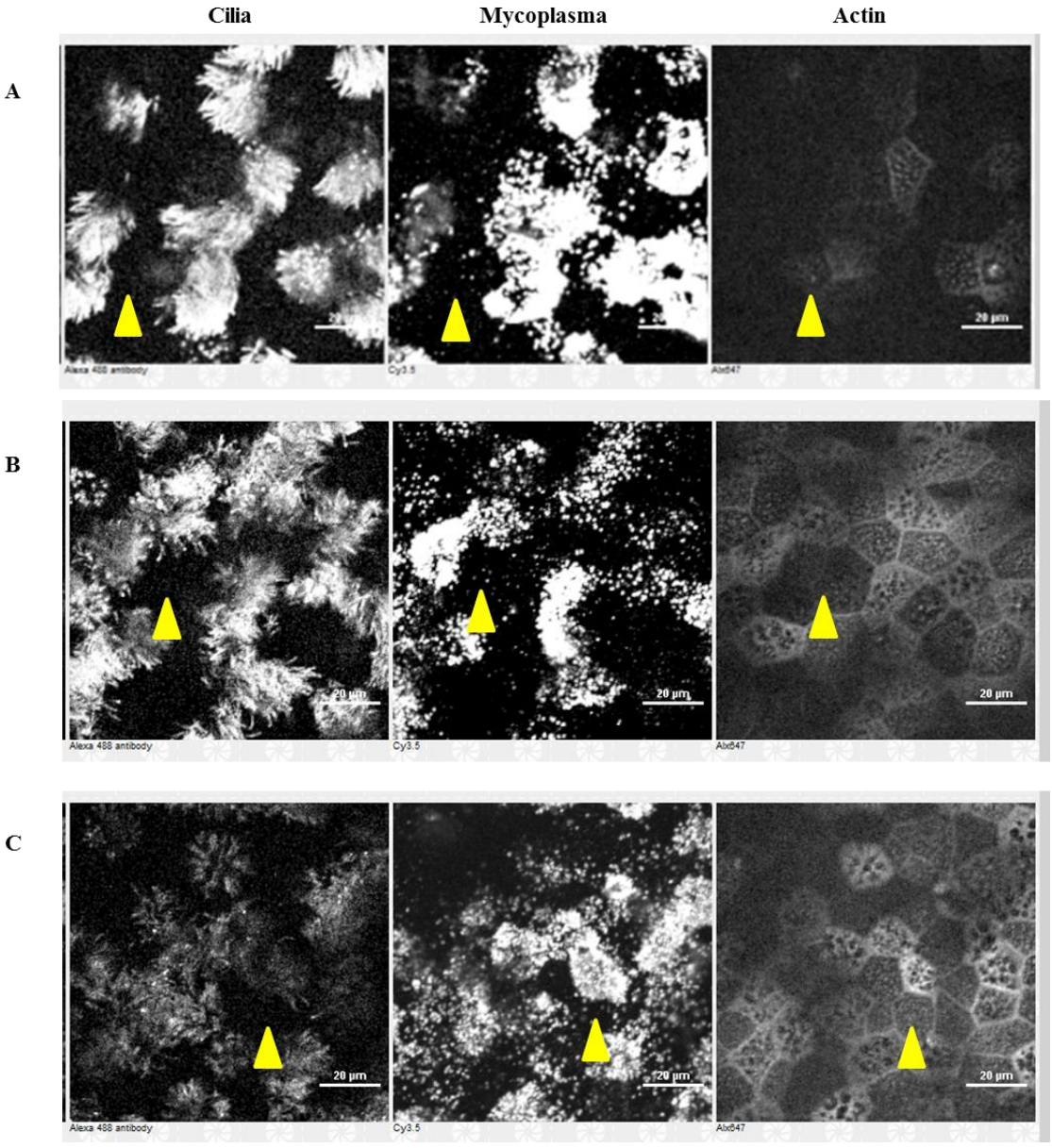
Cilia
Mycoplasma
Actin
A
B
C
20 µm
Alexa 488 antibody
Cy3.5
Alx647

Fig. 8. Luminal view of wild-type *M. pneumoniae*-infected day 2 (Top) and day 10 (Bottom) NHBE cells at 240 min postinfection. Representative images show Cy3-labeled wild-type mycoplasmas (red) illustrating near-confluent (day 2) and less dense and more diffuse (day 10) localization patterns. The uninfected control images show nuclear DAPI (blue) and Cy3 background staining (red). The arrows indicate mycoplasma localization to cell perimeters. Bars = 20 μm.

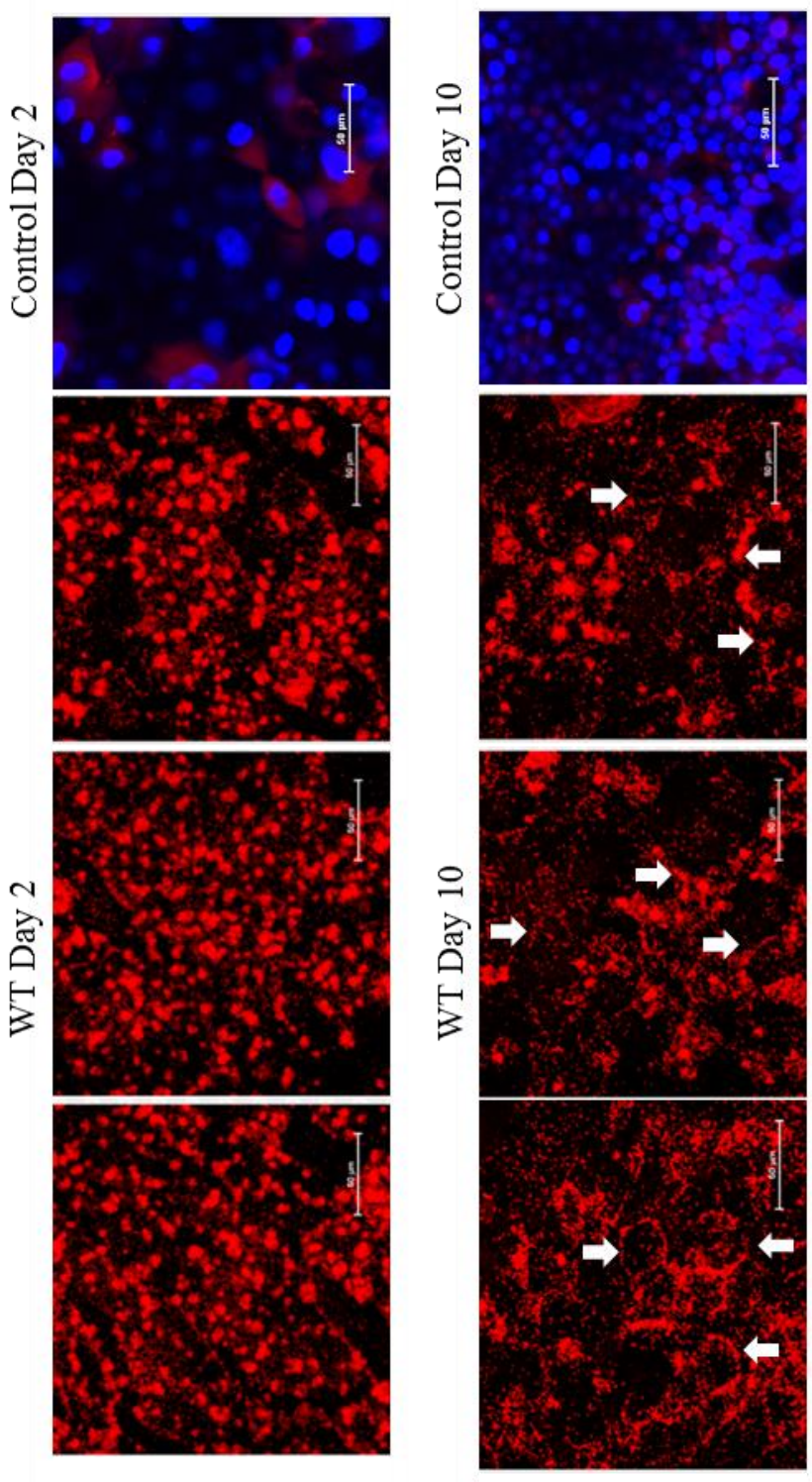
Control Day 2
WT Day 2
Control Day 10
WT Day 10

Fig. 9. MUC1 labeling in relation to mycoplasma localization on day 10 cells demonstrated no clear relationship. Shown are 3 separate regions of interest where the absence or presence of MUC1 positive cells showed no distinct localization pattern in relation to mycoplasma (A-C). Merged: DAPI, blue; MUC1, green; mycoplasma, red. Bar = 20 μm.

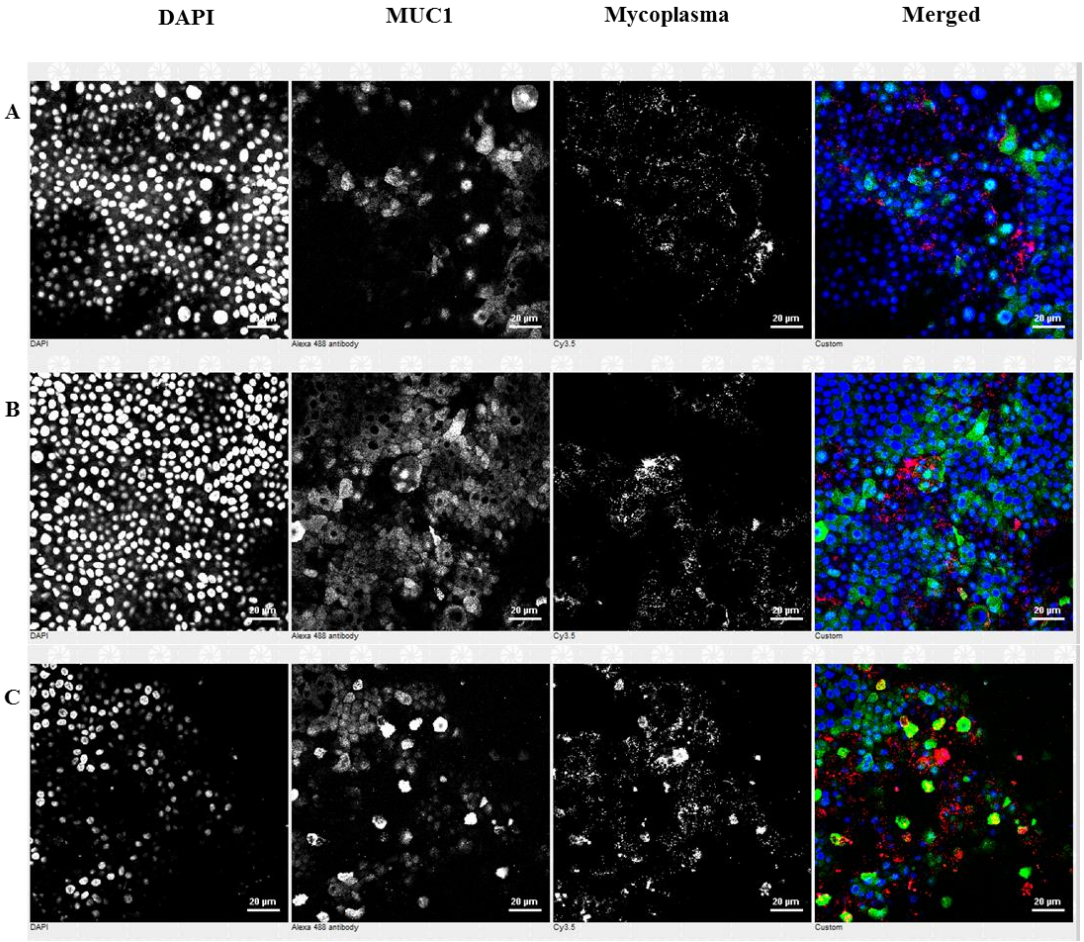
DAPI
MUC1
Mycoplasma
Merged
A
B
C
20 µm
DAPI
Alexa 488 antibody
Cy3.5
Custom

Fig. 10. MUC4 labeling in relation to mycoplasma localization on day 10 cells demonstrated a localization pattern consistent with the observed reduction in attachment in Fig. 3. Shown are 3 separate regions of interest where mycoplasma localization correlates with the absence of MUC4 (A-C) Note that aggregates of mycoplasma are more prominent between MUC4 labelled cells (compare to Fig. 9). Merged: DAPI, blue; MUC1, green; mycoplasma, red. Bar = 20 μm.

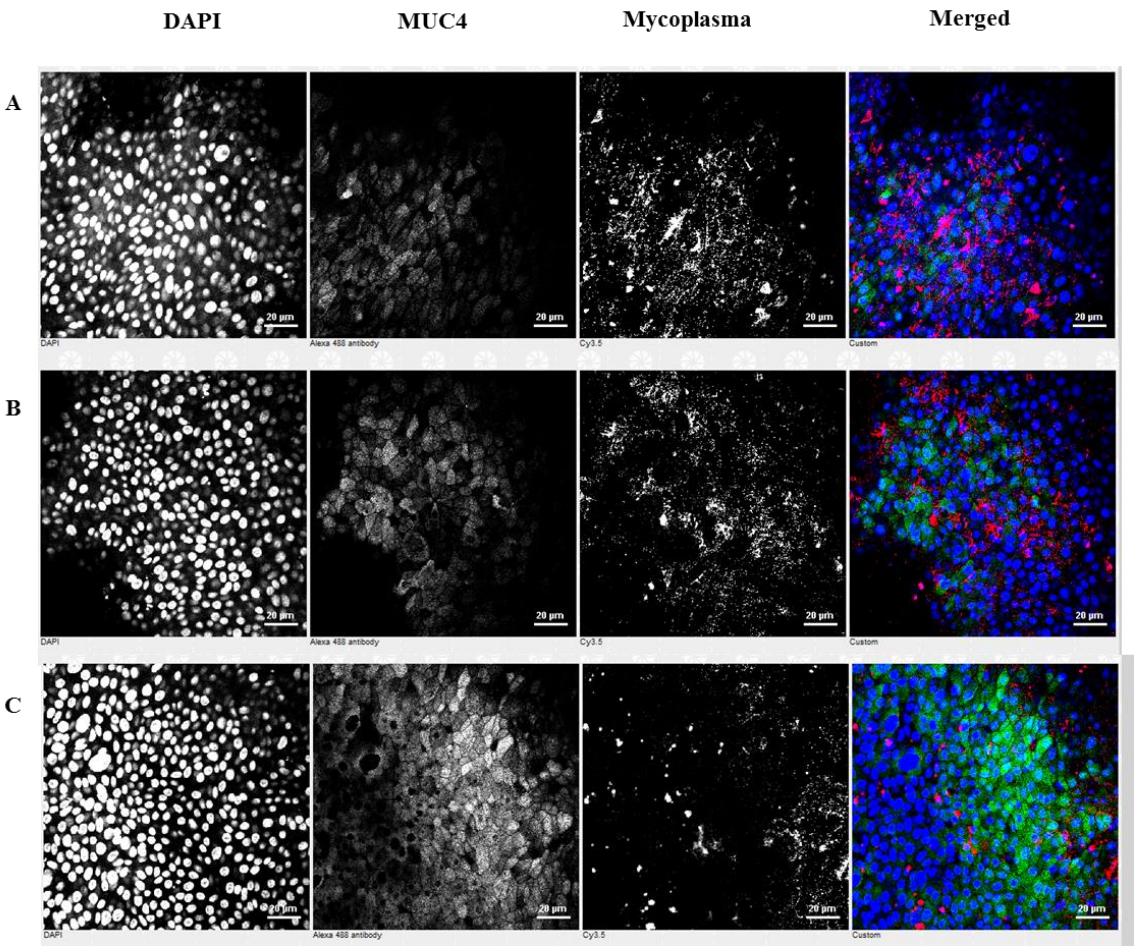
DAPI
MUC4
Mycoplasma
Merged
A
B
C
20 µm
DAPI
Alexa 488 antibody
Cy3.5
Custom

Fig. 11. MUC4 polarity appeared to be inversely related with fluorescence intensity and mycoplasma colonization. Shown are luminal and cross-sectional views of MUC4 labeled day 10 cells from Fig. 10 demonstrating a relationship between fluorescence intensity of MUC4 labeling and polarity (arrows). (**A**) MUC4 labeling appears to be defined to a narrow region on the apical surface with reduced fluorescence intensity. (**B**) MUC4 fluorescence was elevated and more diffuse. Note that the epithelium in the top panel appears more uniform (cobblestone-like) in contrast to the bottom panel (squamous-like). DAPI, blue; MUC4, green; mycoplasma, red; guide bar, gold. Bars = 10 μm.

A

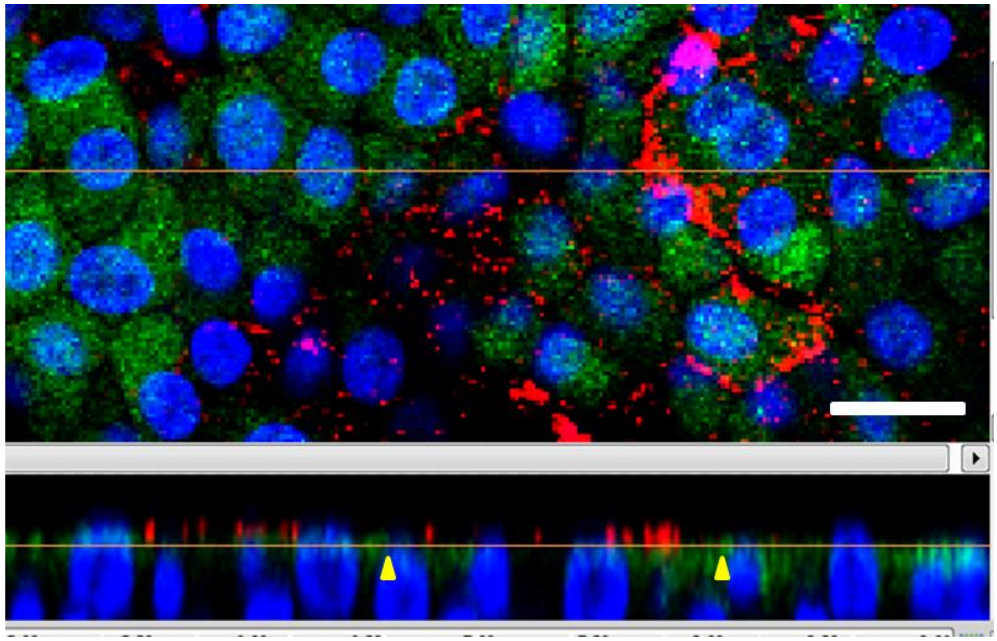

B

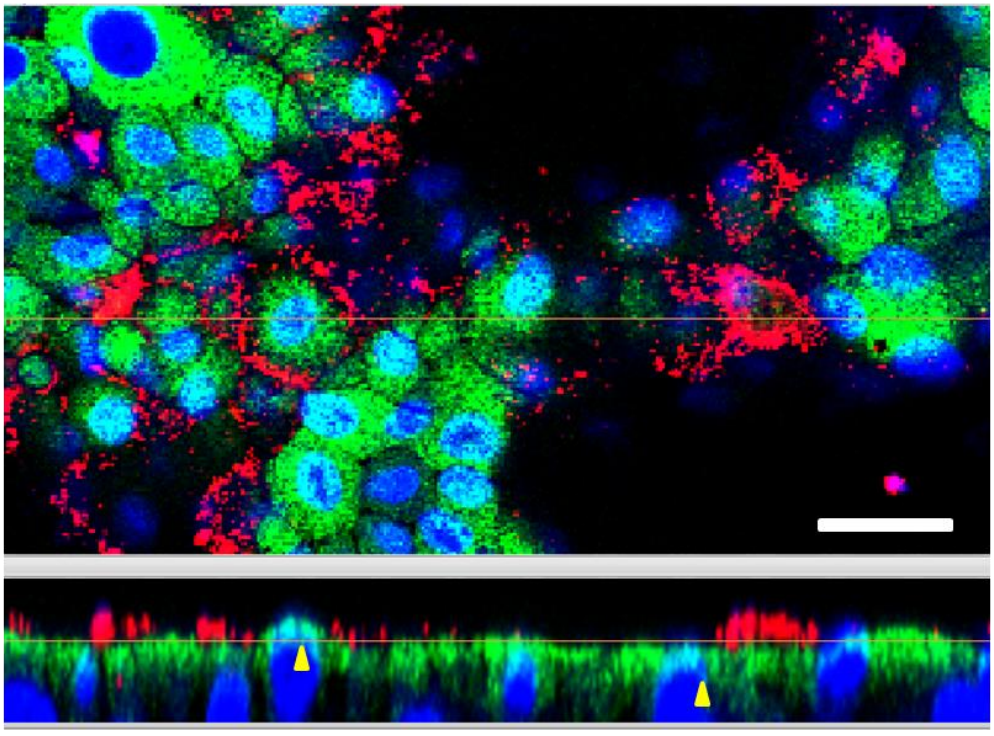

Fig. 12. Uninfected NHBE cells. Uninfected controls at 4 h (Top) and 28 days (Bottom) of culture showing the typical pseudostratified layer of conducting airway cells. Both overhead and cross-sectional views (guide bar) of the region of interest are shown. Over time, the amount of cilia increased as indicated by the fluorescence intensity (Top vs Bottom panels). Cilia, green; actin, purple; DAPI, blue; background, red. Bar = 20 μm.

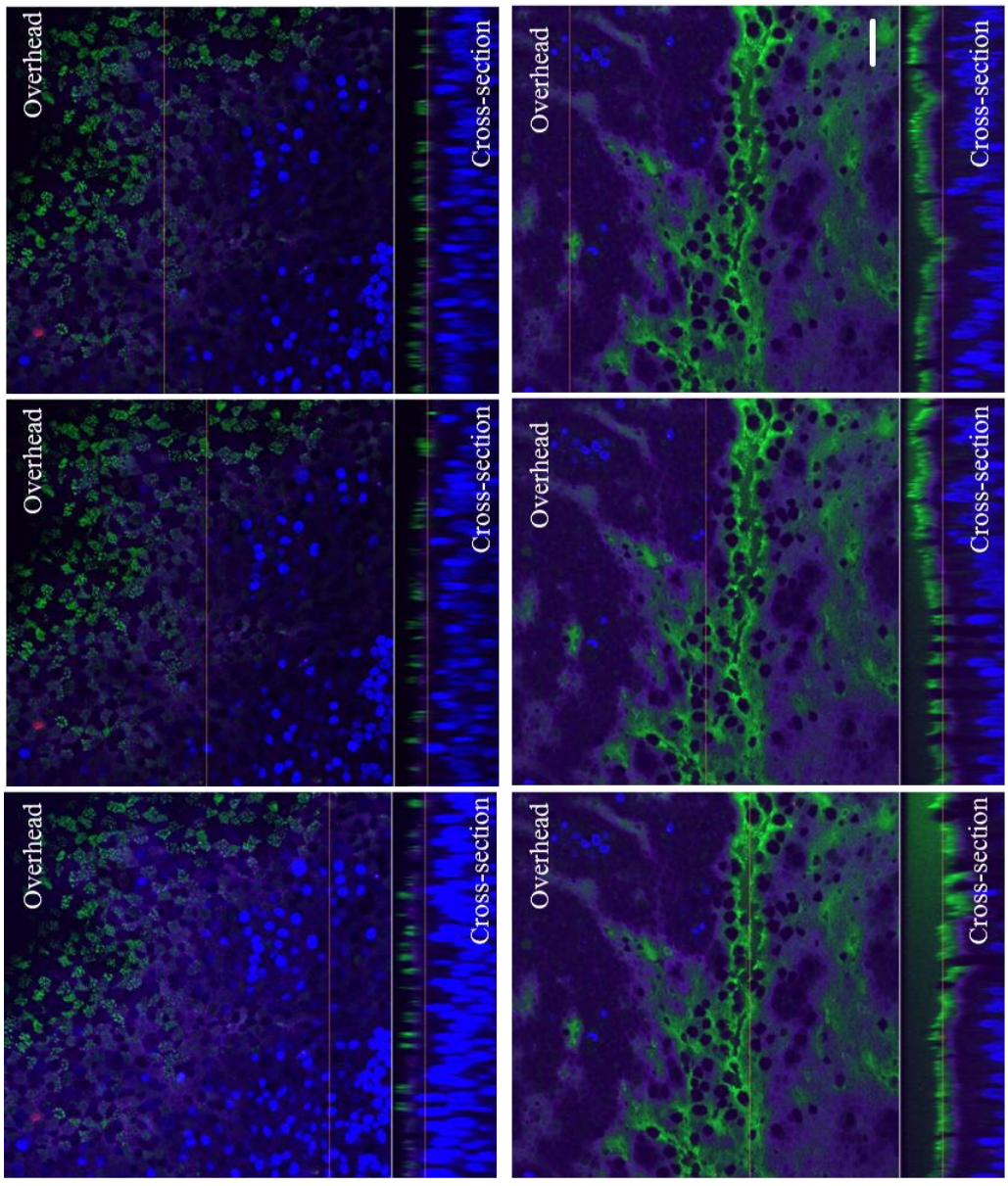
Overhead
Cross-section
Overhead
Cross-section
Overhead
Cross-section
4 h
Overhead
Cross-section
Overhead
Cross-section
Overhead
Cross-section
28 days

Fig. 13. Cross-sectional views of uninfected NHBE cells. Uninfected controls at 4 h (A) and 28 days (B) of culture showing the typical pseudostratified layer of conducting airway cells. Note that over time the amount of cilia increases, which also increases the fluorescence intensity. Merged (cilia, green; actin, purple; DAPI, blue; background, red) (1); DAPI (2); cilia (3); background (4); and actin (5) Bar = 40 μm.

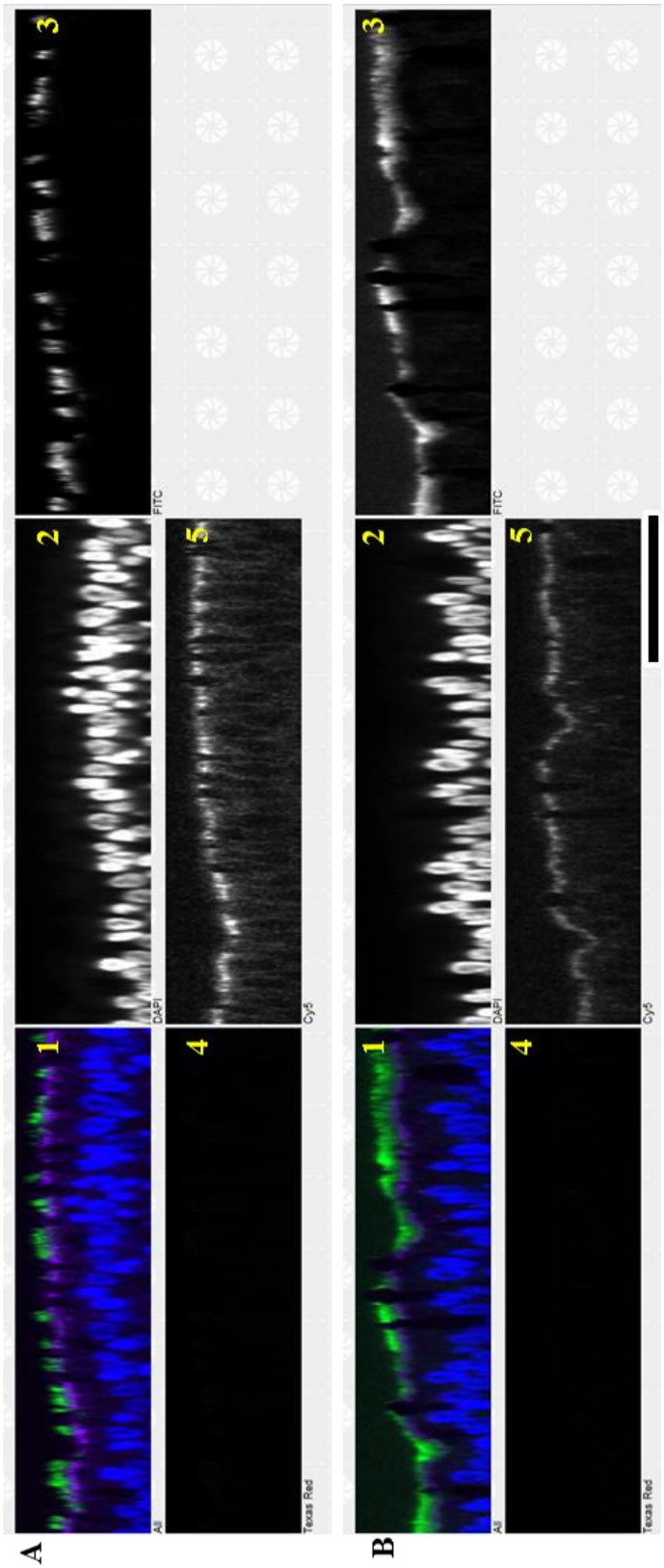
A
B
1
2
3
4
5
All
DAPI
FITC
Texas Red
Cy5

Fig. 14. Barrier function over 28 days postinfection. TEER measurements of mycoplasma infected NHBE cells (LOW, 10^6 CCU; HIGH, 10^9CCU) over time are shown as percent of uninfected control. Each bar represents the mean and 95% confidence interval for 8 data points . *, P <0.01; N, not significant. Color change units (CCU/100 μl).

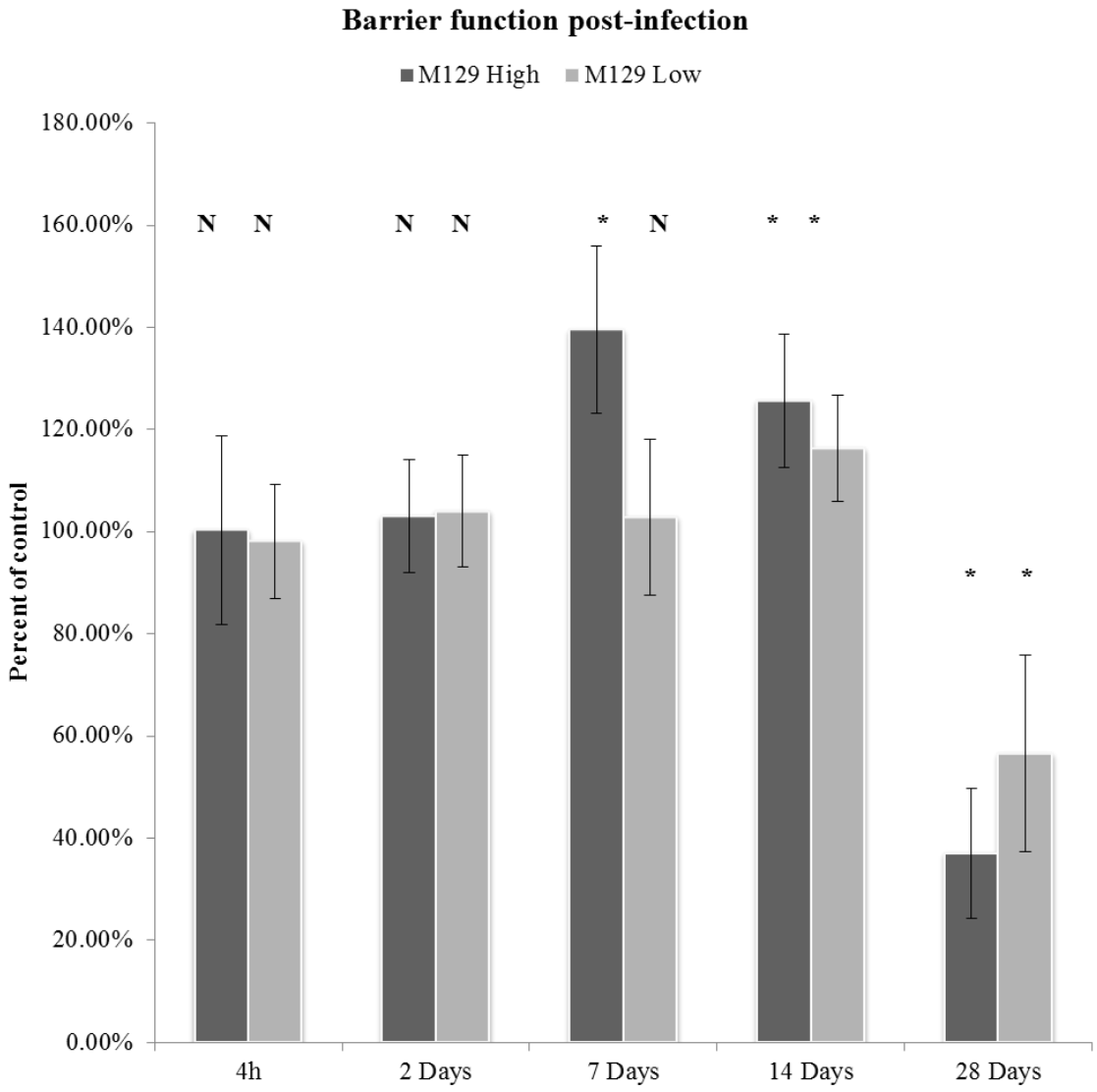
Barrier function post-infection
M129 High
M129 Low
Percent of control
180.00%
160.00%
140.00%
120.00%
100.00%
80.00%
60.00%
40.00%
20.00%
0.00%
N N N N * N * *
* *
4h
2 Days
7 Days
14 Days
28 Days

Fig. 15. *M. pneumoniae* induced changes in cilia. Mycoplasma (LOW=10^6CCU, Top; HIGH=10^9CCU, Bottom) infected NHBE at 4 hours, 7 and 28 days postinfection. (Top) Low-dose mycoplasma infection resulted in poor cilia detection and a wave-like pattern in the actin network by 28 days postinfection. (Bottom) High-dose mycoplasma infection resulted loss of cilia detection by 7 days postinfection and evidence of cilia reorganization involving large regions of interest by 28 days postinfection (bright green). Both overhead and cross-sectional views of the region of interest are shown (guide bar). Controls over the same period appeared normal (Fig. 12). Cilia, green; actin, purple; DAPI, blue; mycoplasma, red. Color change units (CCU/100 μl). Bar = 20 μm.

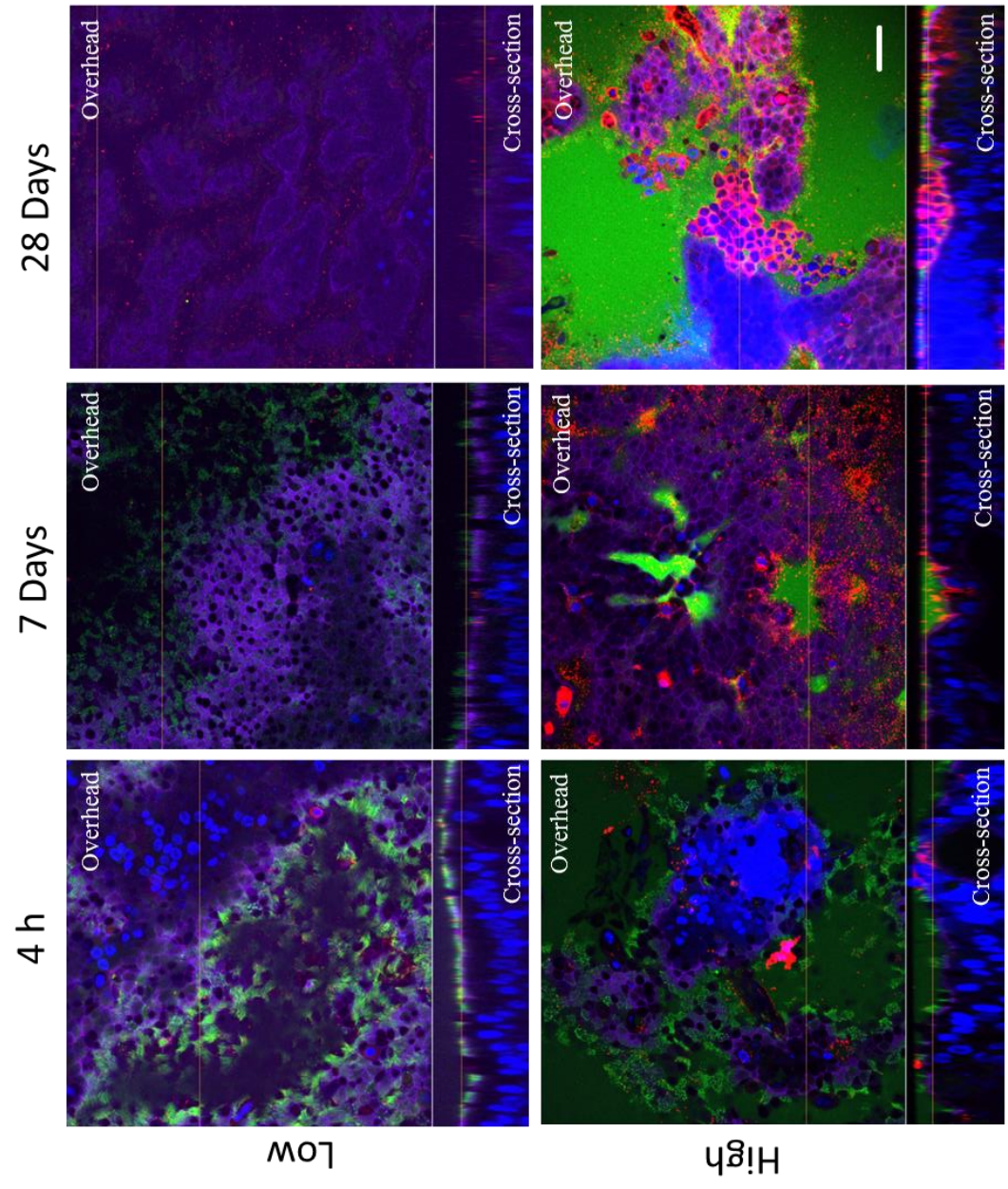
4 h
7 Days
28 Days
Low
High
Overhead
Cross-section

Fig. 16. Low-dose *M. pneumoniae* infected-NHBE cells at 4 h postinfection. Mycoplasma dose 10^6 CCU. (A-C) Cross-sections of merged (cilia, green; actin, purple; DAPI, blue; mycoplasma, red) (1), DAPI (2), cilia (3), mycoplasma (4) and actin (5) appeared indistinguishable from control (D). Color change units (CCU/100 μl). Bar = 40 μm.

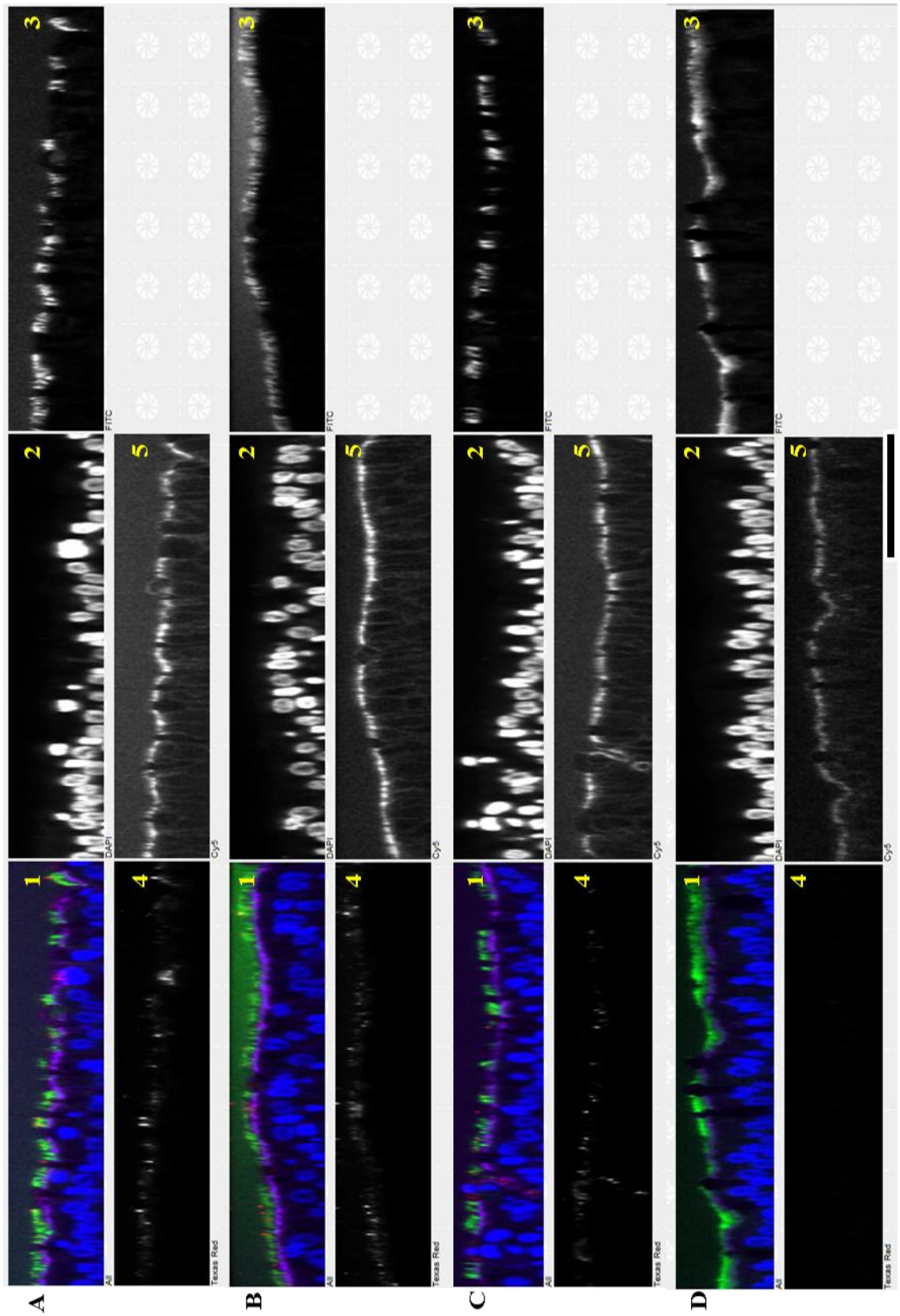
A
B
C
D
1
2
3
4
5
All
DAPI
FITC
Texas Red
Cy5

Fig. 17. Low-dose *M. pneumoniae* infected NHBE cells at 7 days postinfection. Mycoplasma dose 10^6 CCU. (A-C) Cross-sections of merged (cilia, green; actin, purple; DAPI, blue; mycoplasma, red)(1), DAPI (2), cilia (3), mycoplasma (4) and actin (5) demonstrated evidence of mycoplasma localized in the basolateral compartment (panel 4). Poor cilia detection (panel 3) was also observed. Control (D). Color change units (CCU/100 μl). Bar = 40 μm.

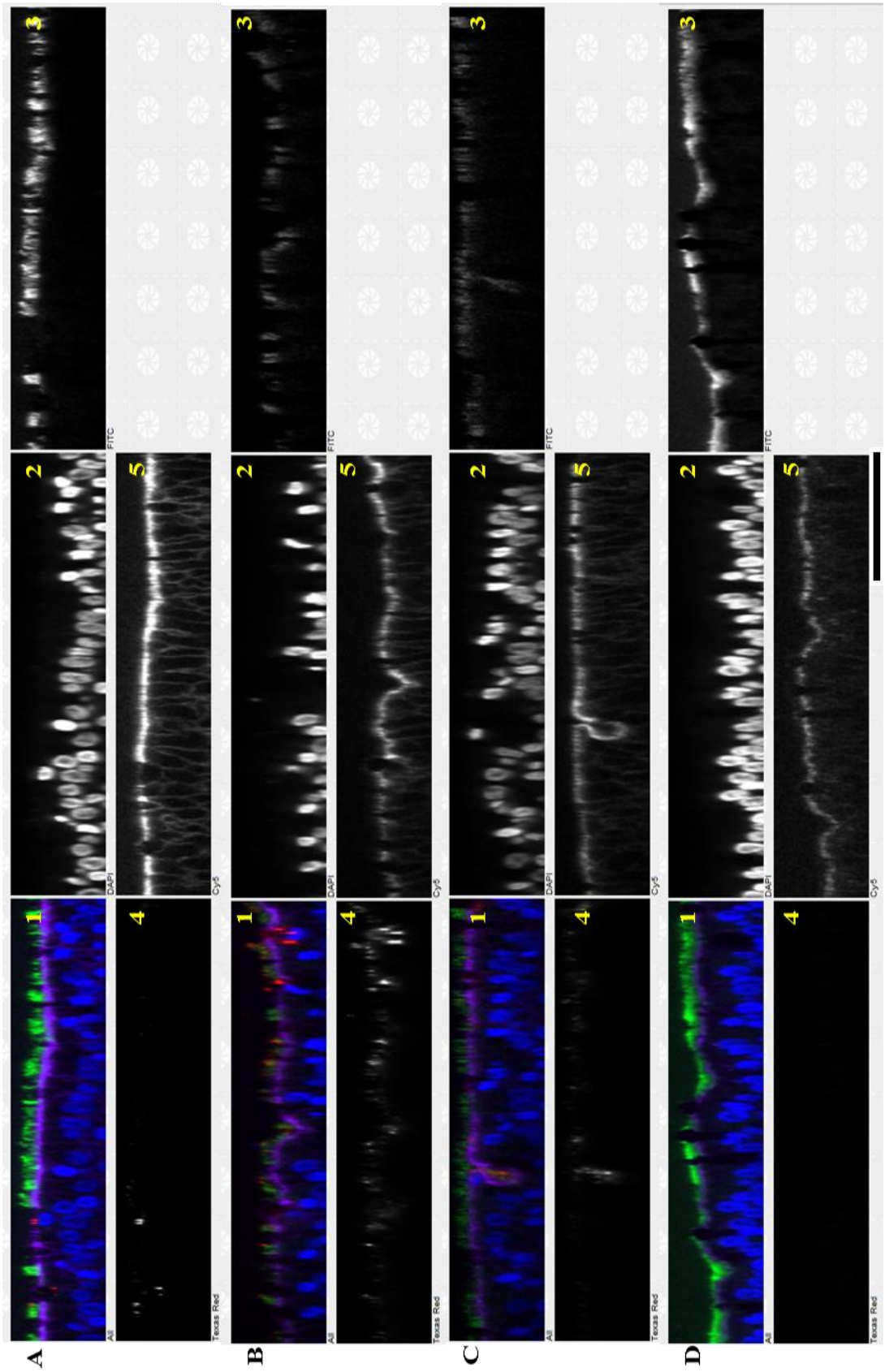
A
B
C
D
1
2
3
4
5
All
DAPI
FITC
Texas Red
Cy5

Fig. 18. Low-dose *M. pneumoniae*-infected NHBE cells at 28 days postinfection. Mycoplasma dose10^6 CCU (A-C) Cross-sections of merged (cilia, green; actin, purple; DAPI, blue; mycoplasma, red) (1), DAPI (2), cilia (3), mycoplasma (4) and actin (5) demonstrated poor cilia detection (panel 3) and prominent actin abnormality (panel 5) when compared to control (D). Color change units (CCU/100 μl). Bar = 40 μm.

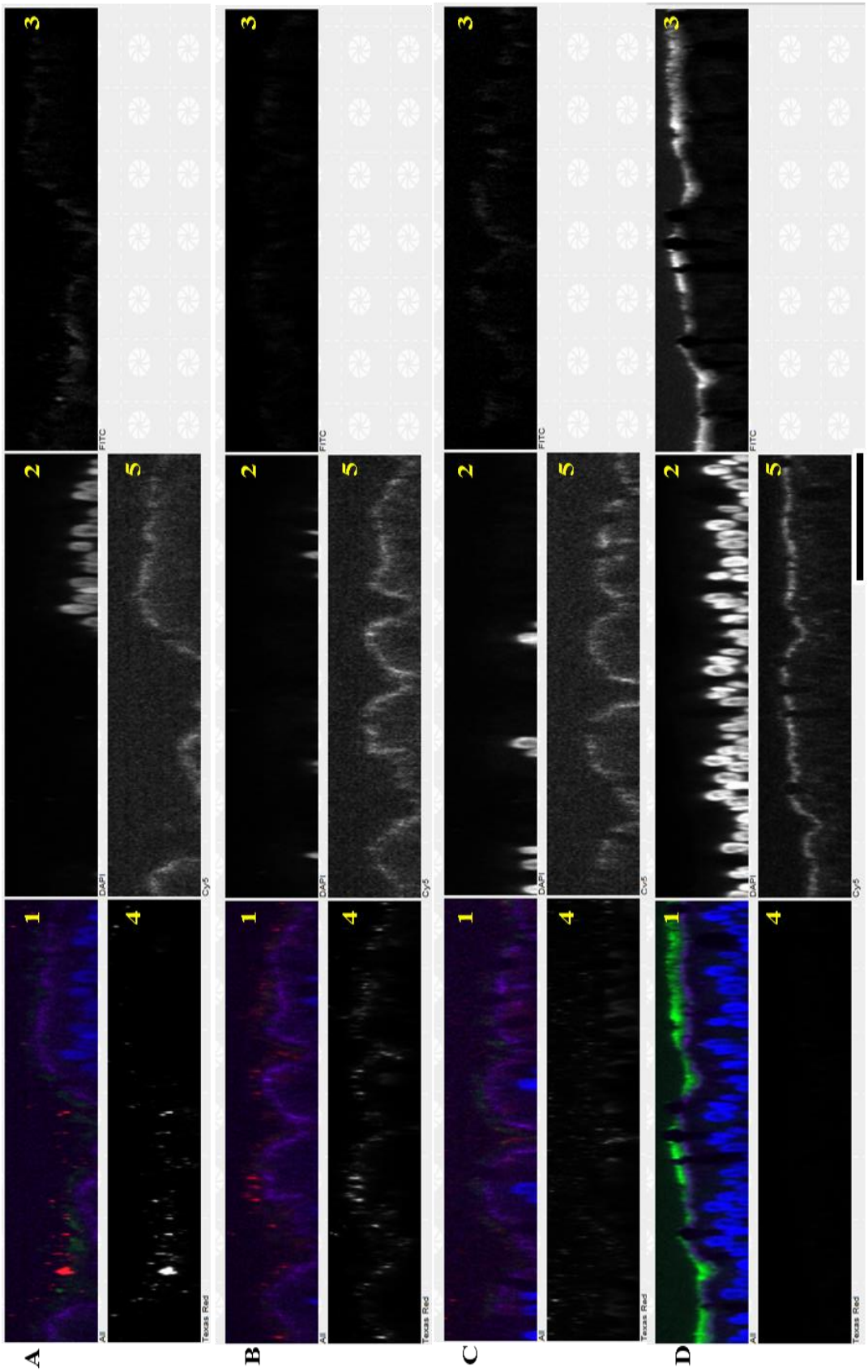
A
B
C
D
1
2
3
4
5
All
DAPI
FITC
Texas Red
Cy5

Fig. 19. High-dose *M. pneumoniae*-infected NHBE cells at 4 h postinfection. Mycoplasma dose 10^9 CCU. (A-C) Cross-sections of merged (cilia, green; actin, purple; DAPI, blue; mycoplasma, red) (1), DAPI (2), cilia (3), mycoplasma (4) and actin (5) demonstrated early evidence of mycoplasma invasion (panel 4) and cilia abnormality compared to control (panel 3). Control (D). Color change units (CCU/100 μl). Bar = 40 μm.

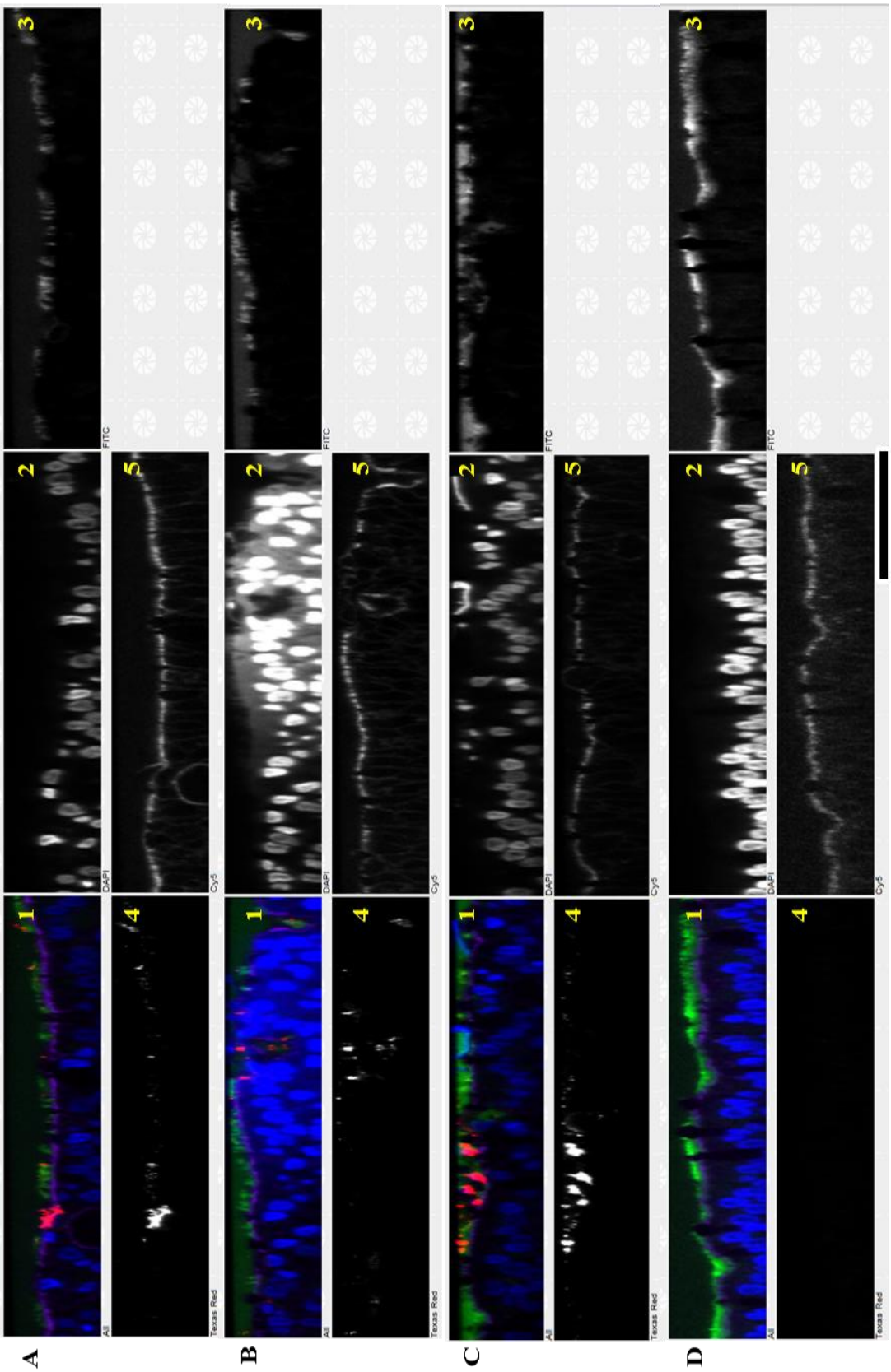
A
B
C
D
1
2
3
4
5
All
DAPI
FITC
Texas Red
Cy5

Fig. 20. High-dose *M. pneumoniae*-infected NHBE cells at 7 days postinfection. Mycoplasma dose10^9 (CCU). (A-C) Cross-sections of merged (cilia, green; actin, purple; DAPI, blue; mycoplasma, red) (1), DAPI (2), cilia (3), mycoplasma (4) and actin (5) demonstrated evidence of epithelium loss (panel 1) and cilia reorganization (panel 3). Control (D). Color change units (CCU/100 μl). Bar = 40 μm.

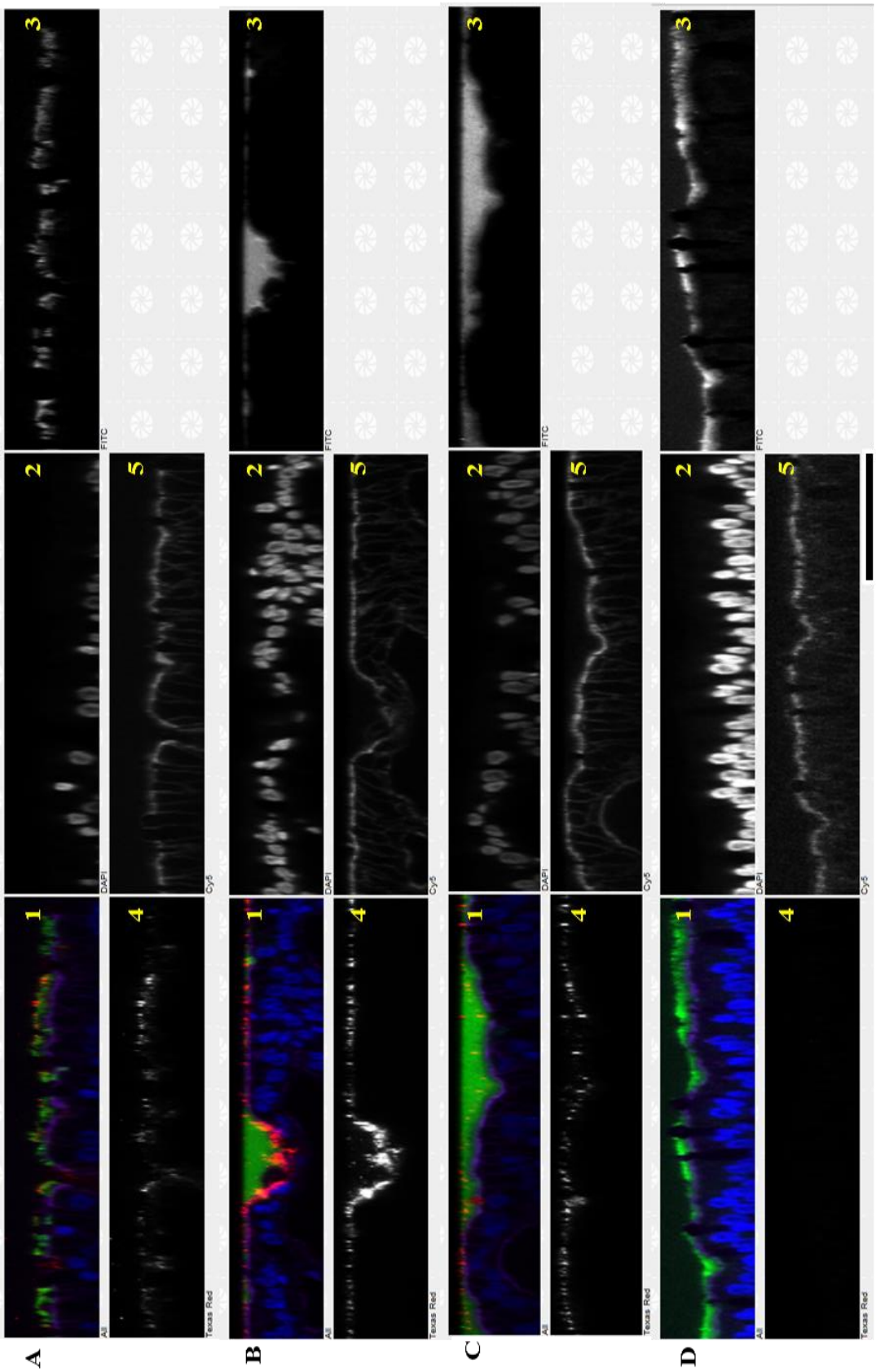
A
B
C
D
1
2
3
4
5
All
DAPI
FITC
Texas Red
Cy5

Fig. 21. High-dose *M. pneumoniae*-infected NHBE cells at 28 days postinfection. Mycoplasma dose10^9 CCU. (A-C) Cross-sections of merged (cilia, green; actin, purple; DAPI, blue; mycoplasma, red) (1), DAPI (2), cilia (3), mycoplasma (4) and actin (5) demonstrated evidence of invasion and desquamation (panel 1) with cilia reorganization (panel 3) and actin rearrangement (panel 5). Control (D). Color change units (CCU/100 μl). Bar= 40 μm.

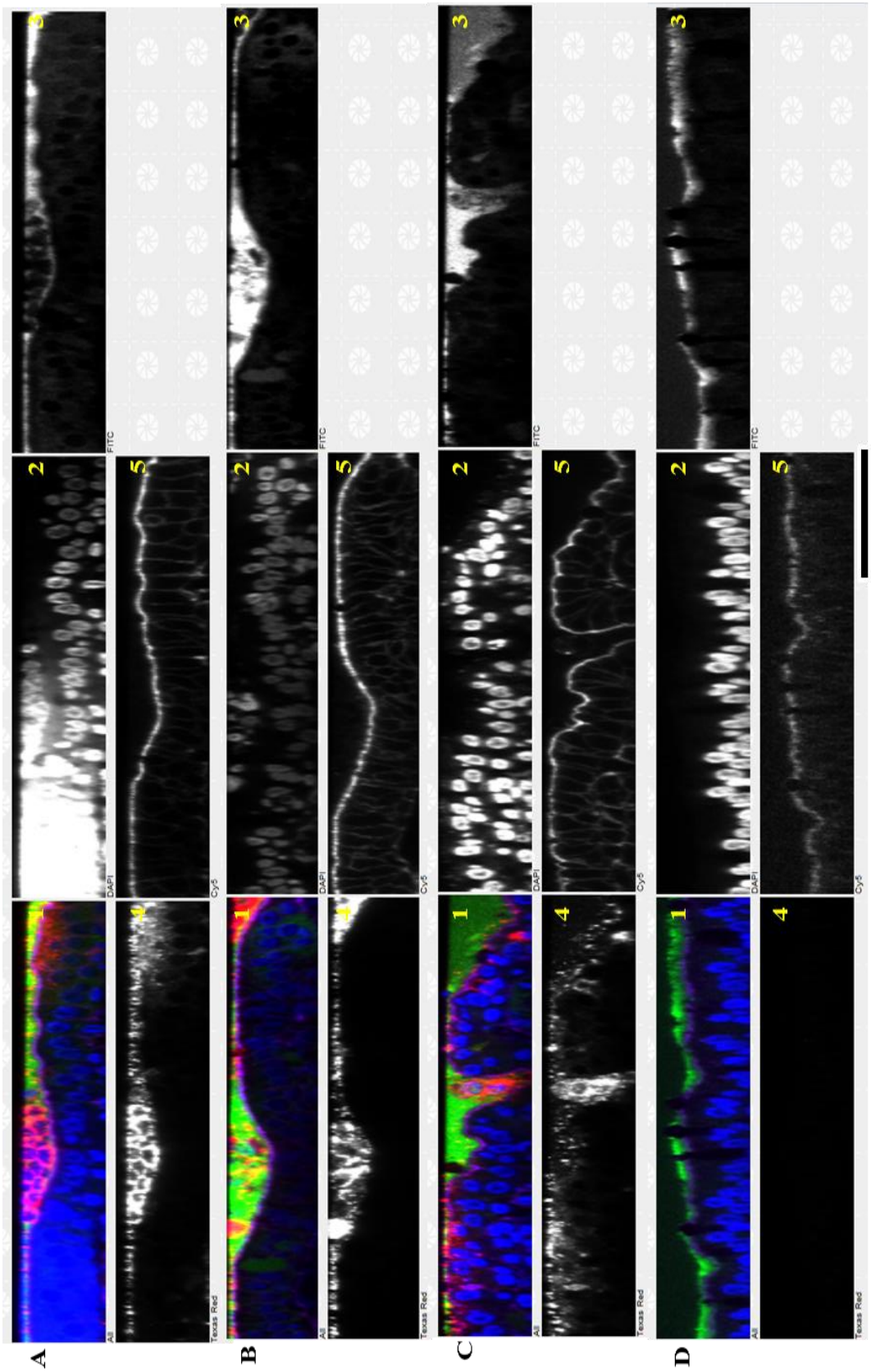
A
B
C
D
All
Texas Red
DAPI
Cy5
FITC
1
2
3
4
5

Fig. 22. *M. pneumoniae* attached to desquamated cells. Desquamated epithelium from a parallel experiment exhibited mycoplasma localization at the cell periphery and in large aggregates (white arrowheads). The panel on the left shows approximately 10 infected epithelial cells, while the panel on the right is part of an epithelial sheet of > 20 cells. NucBlue nuclear labeled cells are artificially colored such that: green= mycoplasma, blue=background of epithelium, yellow= high concentration of DNA. Note the intensity and morphology of the NHBE nuclei (yellow arrowhead) is different from that of the mycoplasma (white arrowhead). Bar= 15 μm.

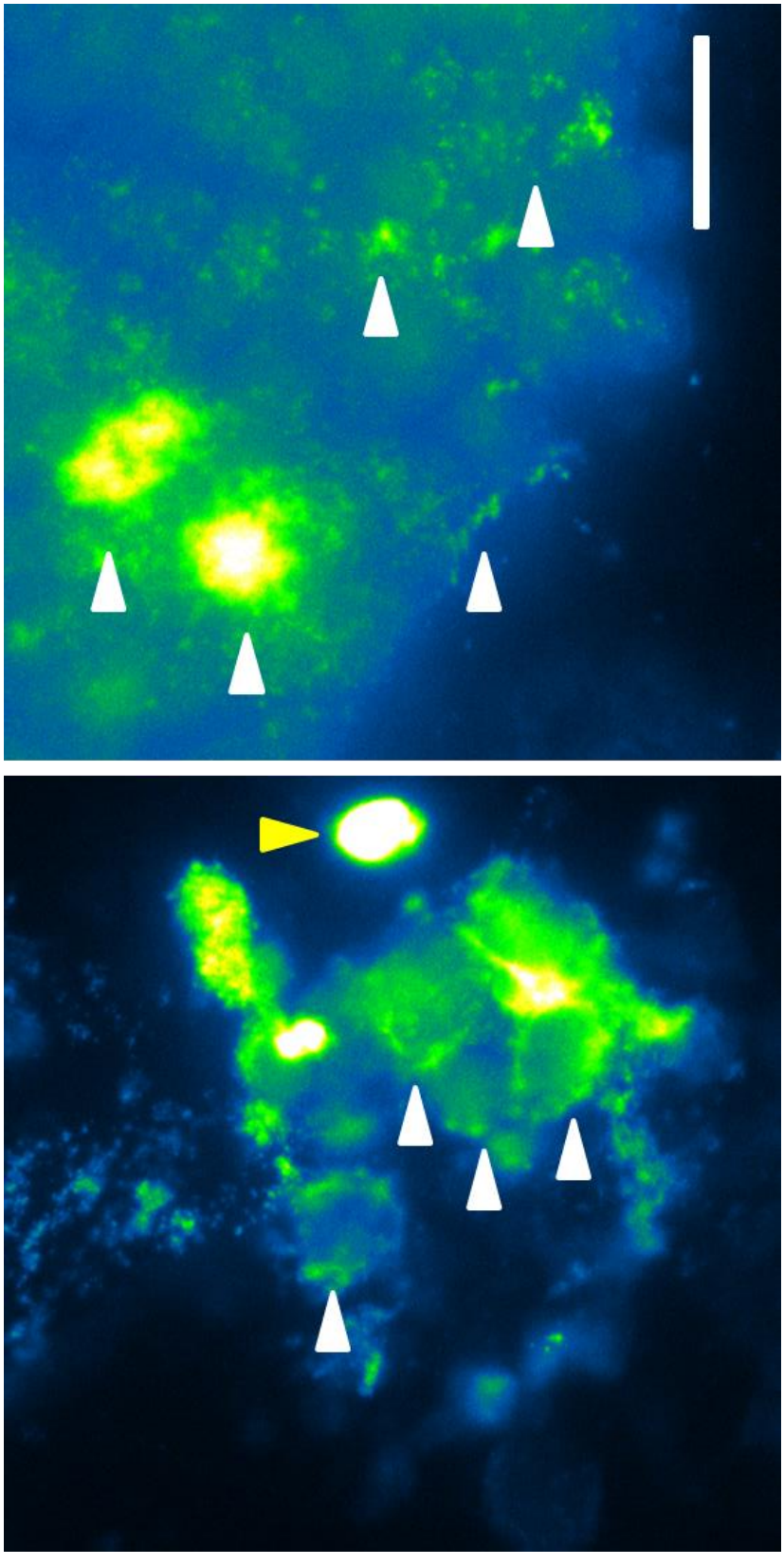

Fig. 23. Depth coding of actin in uninfected NHBE cells. Depth coding indicated that actin labeling within uninfected controls was mainly localized to the luminal region (magenta to red). The region of interest is a total of 60 μm in depth.

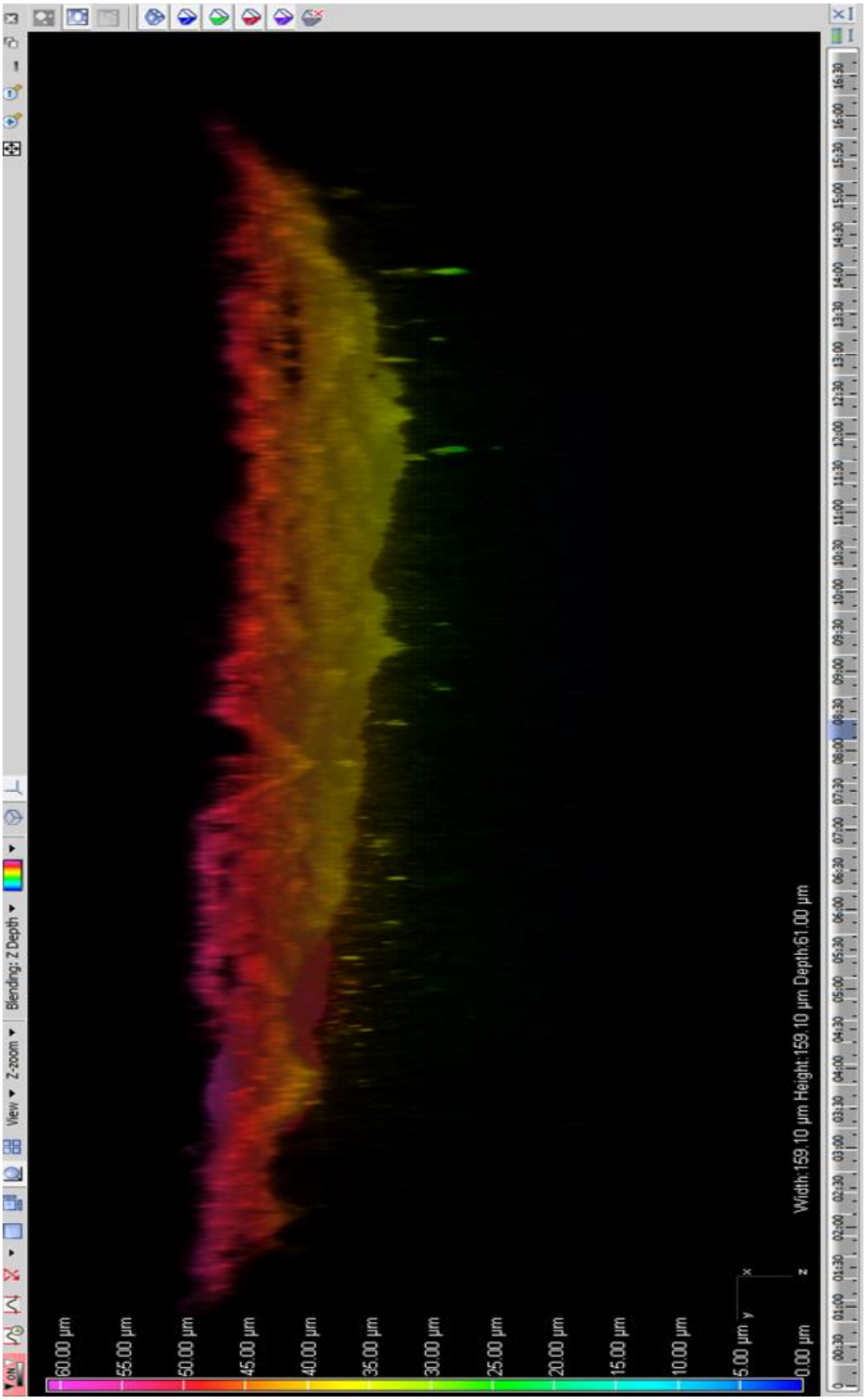
Blending: Z Depth
View
Z-zoom
60.00 µm
55.00 µm
50.00 µm
45.00 µm
40.00 µm
35.00 µm
30.00 µm
25.00 µm
20.00 µm
15.00 µm
10.00 µm
5.00 µm
0.00 µm
Width:159.10 µm Height:159.10 µm Depth:61.00 µm

Fig. 24. Depth coding of actin reorganization of mycoplasma-infected NHBE cells (low-dose). Infected NHBE cells exhibited extensive reorganization extending 15-25 μm into the monolayer (green to blue). The region of interest is a total of 60 μm in depth.

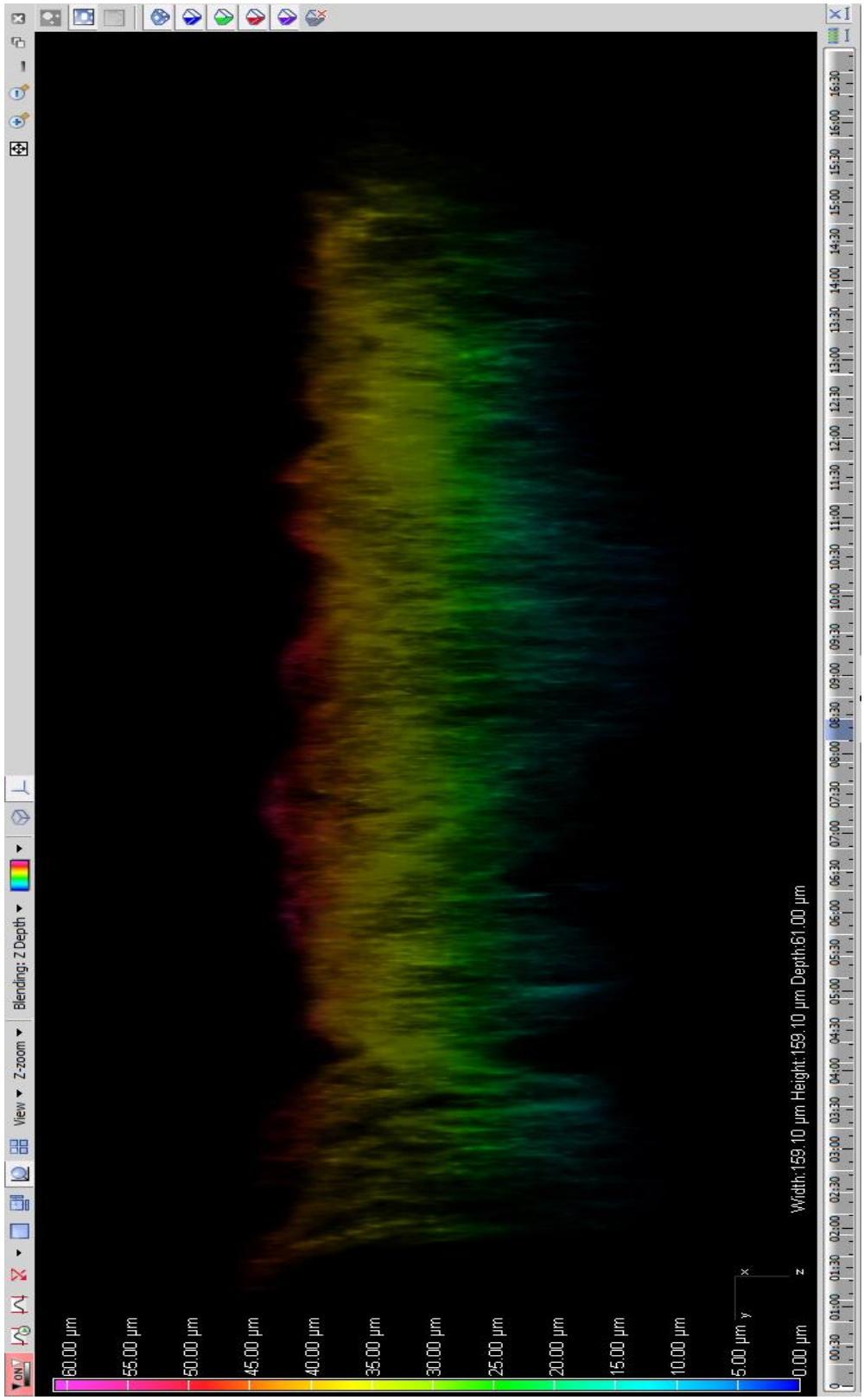
View
Z-zoom
Blending: Z Depth
60.00 µm
55.00 µm
50.00 µm
45.00 µm
40.00 µm
35.00 µm
30.00 µm
25.00 µm
20.00 µm
15.00 µm
10.00 µm
5.00 µm
0.00 µm
Width:159.10 µm Height:159.10 µm Depth:61.00 µm

Fig. 25. Depth coding of actin reorganization of mycoplasma-infected NHBE cells (high-dose). Infected NHBE cells exhibited extensive actin reorganization extending the entire 60 μm depth (magenta to blue), suggesting access to basal compartment and thickening of the monolayer (more defined yellow-blue regions). The region of interest is a total of 60 μm in depth.

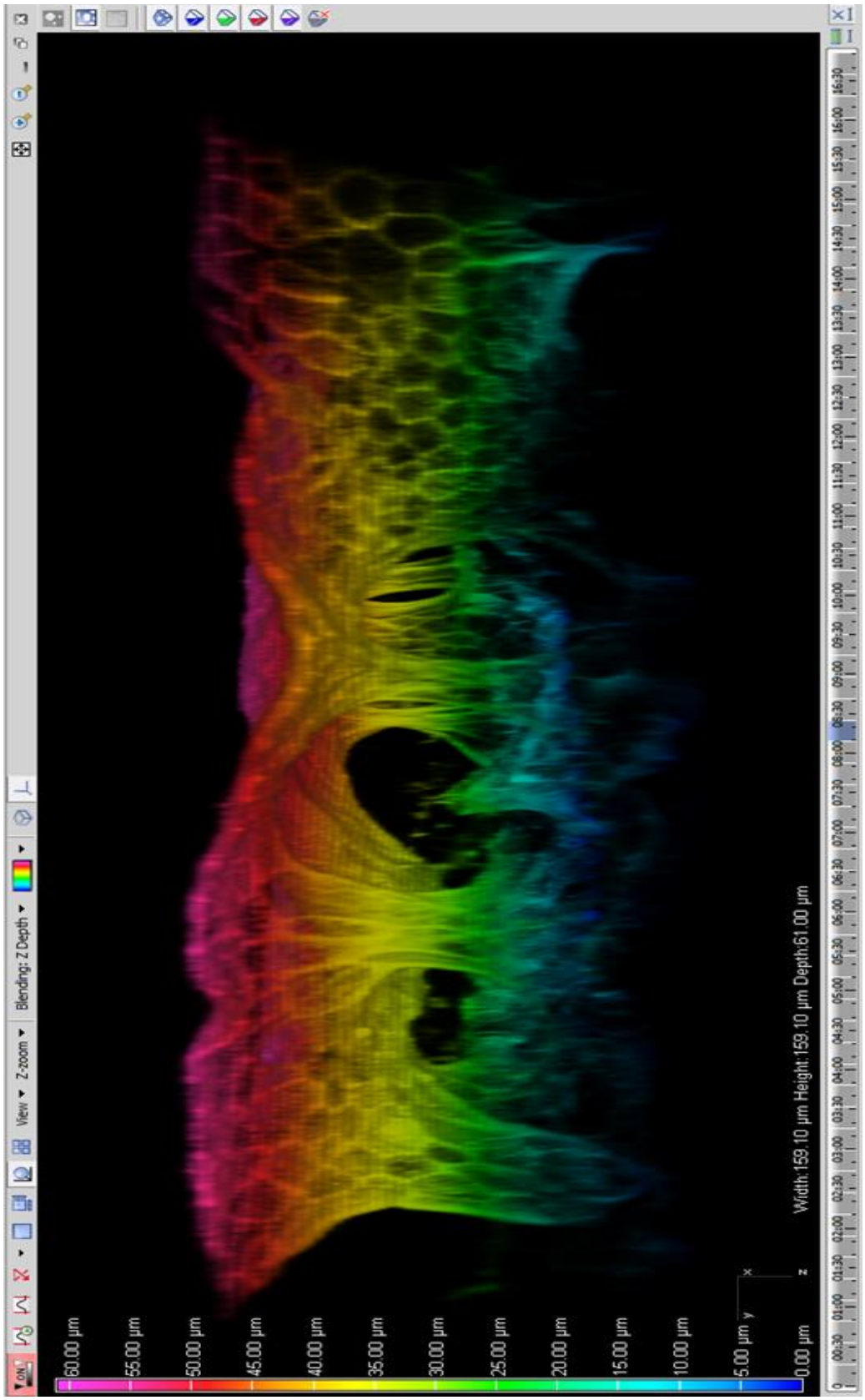
60.00 µm
55.00 µm
50.00 µm
45.00 µm
40.00 µm
35.00 µm
30.00 µm
25.00 µm
20.00 µm
15.00 µm
10.00 µm
5.00 µm
0.00 µm
Width:159.10 µm Height:159.10 µm Depth:61.00 µm
Blending: Z Depth
View
Z-zoom

Fig. 26. Macroscopic impact of *M. pneumoniae* infection. Images are representative of the typical uninfected NHBE cell epithelium at 28 days of culture (Top), which contrasted sharply with the typical mycoplasma infected NHBE cells 28 days postinfection (Bottom). Arrowheads correspond to cilia within the regions of monolayer invaginations described within the text. Regions of interest contain ~9000 apically exposed epithelial cells in each panel. Samples were labeled for cilia. Bar= 65 μm.

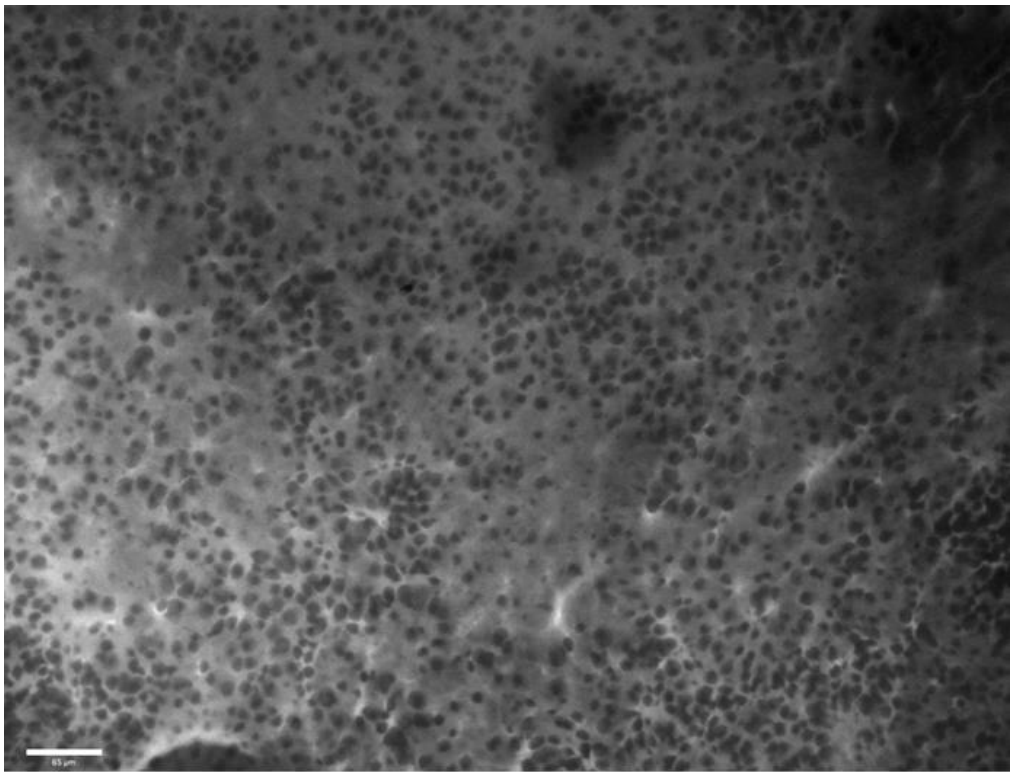

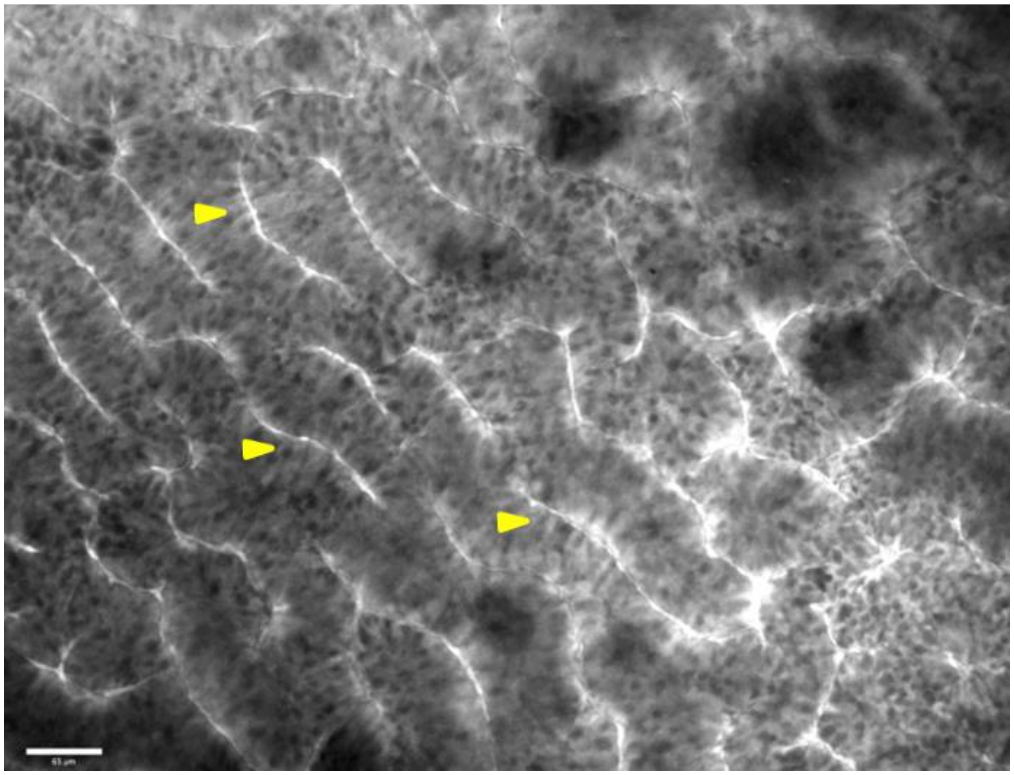

Fig. 27. E-cadherin localization in uninfected NHBE cells. Uninfected controls at 4 h (Top) and 28 days (Bottom) of culture showing the typical localization of E-cadherin (yellow arrowheads) within the pseudostratified layer. The intensity was essentially uniform in all instances for all controls, showing little variability. Both overhead and cross-sectional views (guide bar) of the region of interest are shown. E-cadherin, green; actin, purple; DAPI, blue; background, red. Bar = 20 μm.

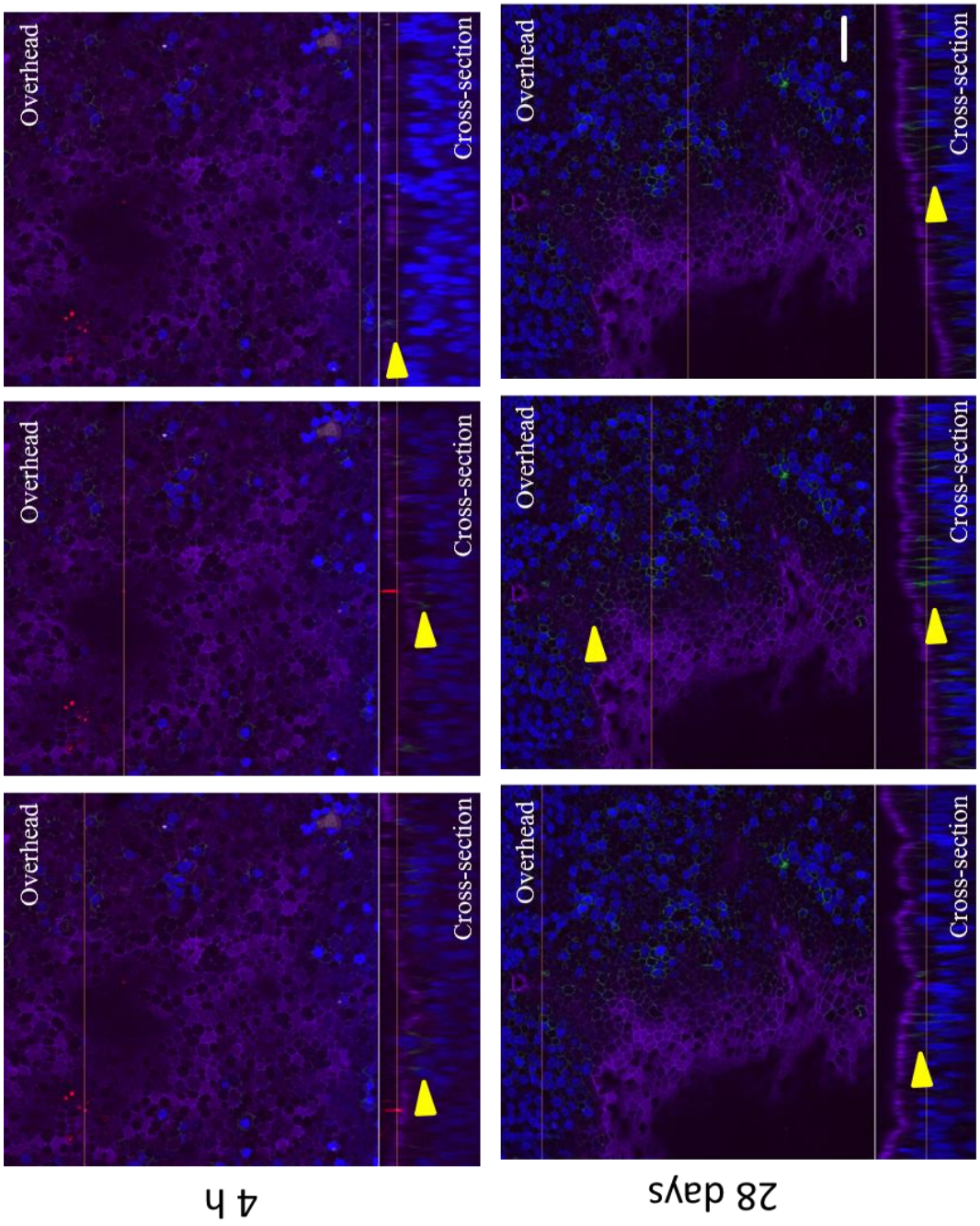
Overhead
Cross-section
Overhead
Cross-section
Overhead
Cross-section
Overhead
Cross-section
Overhead
Cross-section
Overhead
Cross-section
4 h
28 days

Fig. 28. E-cadherin localization in *M. pneumoniae*-infected NHBE cells. Mycoplasma (LOW=10^6 CCU, Top and HIGH=10^9 CCU, Bottom) infected NHBE cells at 28 days postinfection. Images show distinct detection patterns of E-cadherin associated with luminal mycoplasmas (yellow arrowheads) and invading mycoplasmas (white arrowheads). Both overhead and cross-sectional views (guide bar) of the region of interest are shown. Color change units (CCU/ 100 μl); E-cadherin, green; actin, purple; DAPI, blue; mycoplasma, red. Bar = 20 μm.

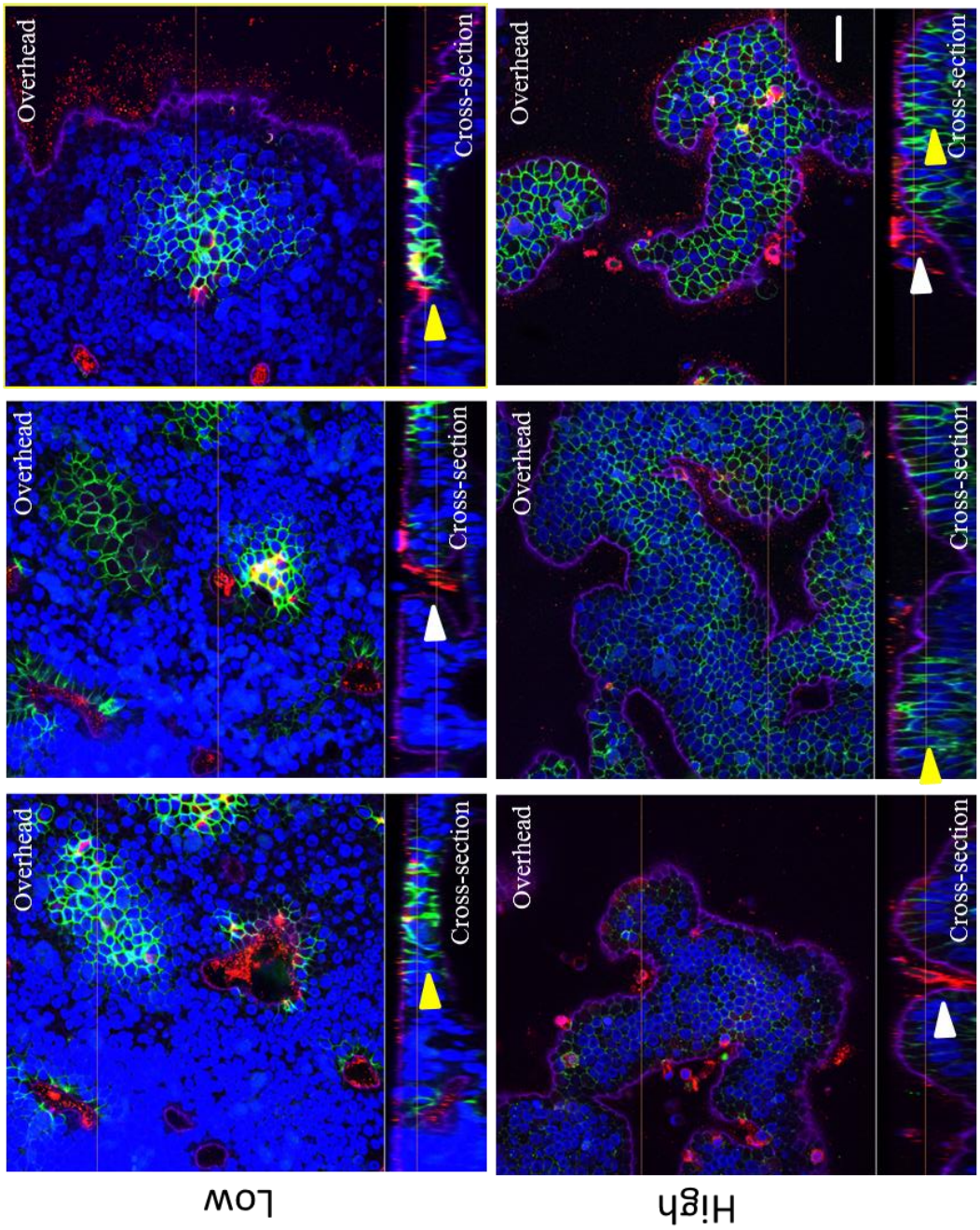
Overhead
Cross-section
Overhead
Cross-section
Overhead
Cross-section
Overhead
Cross-section
Overhead
Cross-section
Overhead
Cross-section
High
Low

Fig. 29. E-cadherin localization in low-dose *M. pneumoniae* infected NHBE cells at 28 days postinfection. Invading mycoplasmas were associated with low E-cadherin labeling (A) while high intensity labeling (B & C, yellow arrowheads) was associated with luminal mycoplasmas, suggesting that the infection was highly localized. Note that the adjacent regions in B and C have non-detectable E-cadherin. Cross-sections of merged (E-cadherin, green; actin, purple; DAPI, blue; mycoplasma, red) (1), DAPI (2), E-cadherin (3), mycoplasma (4) and actin (5). Control (D). Bar = 40 μm.

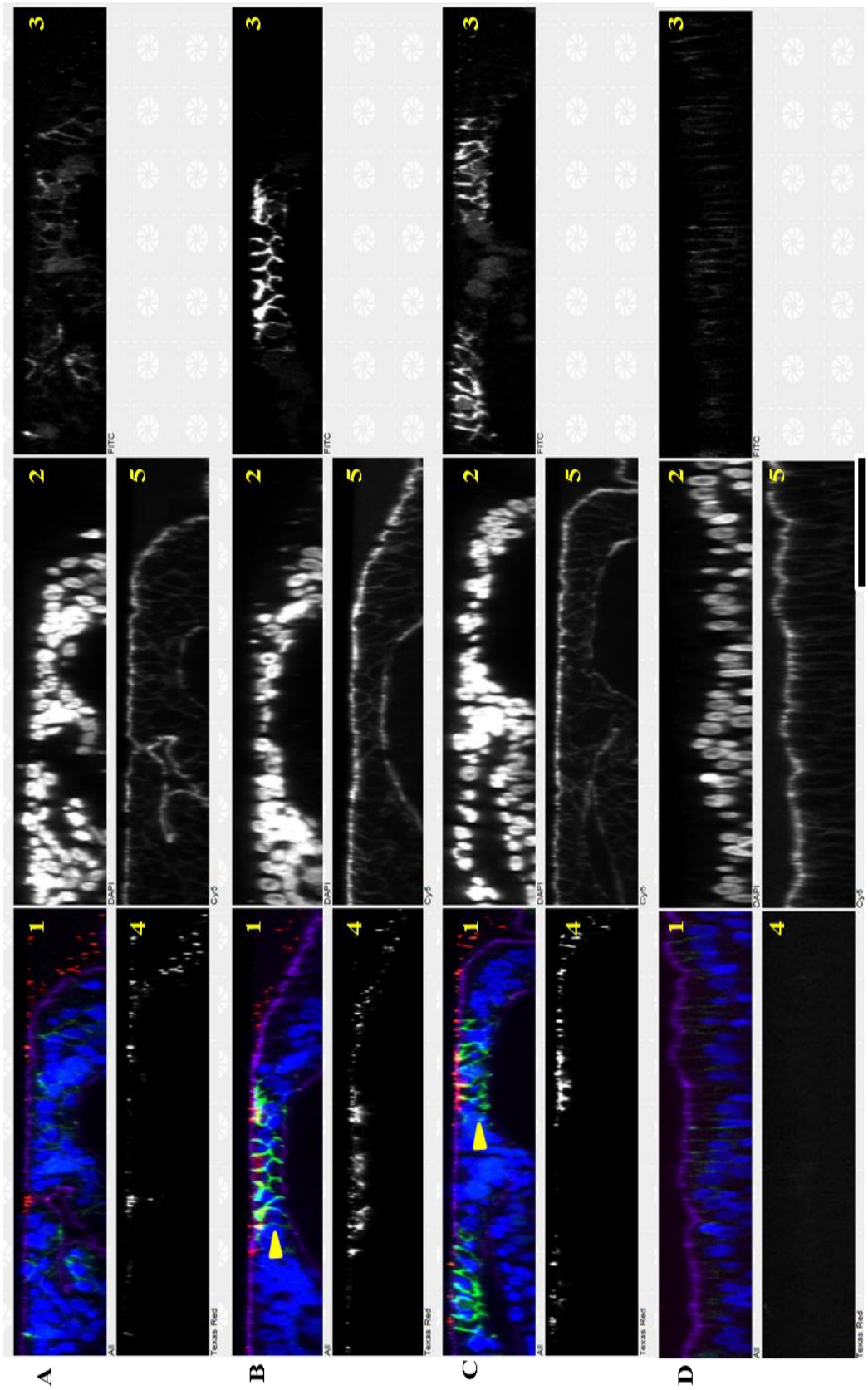
A
B
C
D
1
2
3
4
5
All
DAPI
FITC
Texas Red
Cy5

Fig. 30. E-cadherin localization in high-dose *M. pneumoniae* infected NHBE cells at 28 days postinfection. Panels show poor E-cadherin detection associated with heavily infected NHBE cells (white arrowheads), which are also associated with reorganizing actin (panel 5). Note that in panel C E-cadherin detection occupies more of the field of view when compared to control (panel 3). Cross-sections of merged (E-cadherin, green; actin, purple; DAPI, blue; mycoplasma, red) (1), DAPI (2), E-cadherin (3), mycoplasma (4) and actin (5). Control (D) Scale bar = 40 μm.

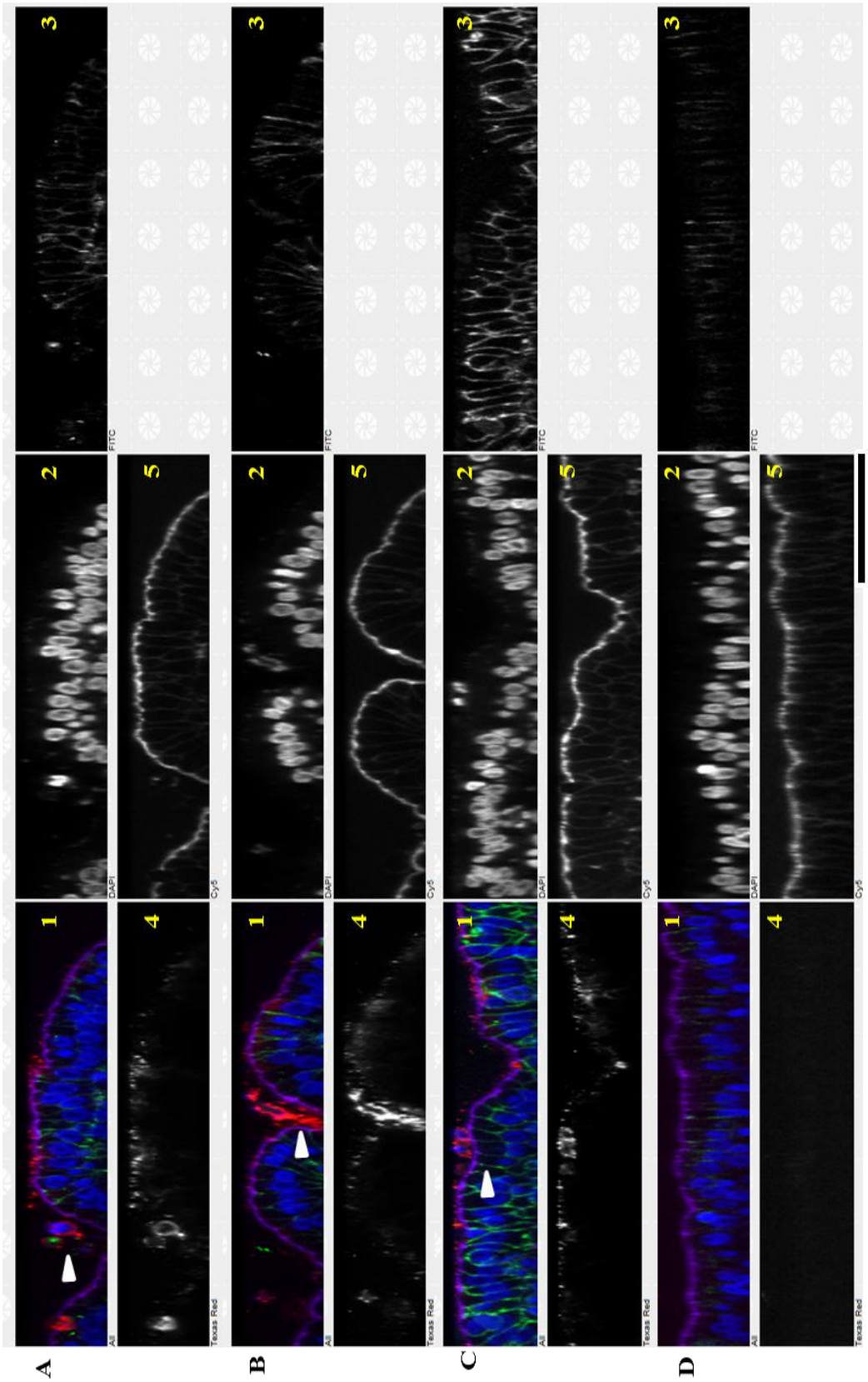
A
B
C
D
1
2
3
4
5
All
DAPI
FITC
Texas Red
Cy5

Fig. 31. ***M. pneumoniae*** **isolation.** Infected NHBE cell transwells and respective basal compartments were harvested to assay for mycoplasma recoverability during the infection. Starting infection inocula were: LOW=10^6 or HIGH=10^9 CCU in 100 µl and the results were compared accordingly. Color change units (CCU/ml) are reported as means and the 95% confidence interval. Uninfected controls had no growth.

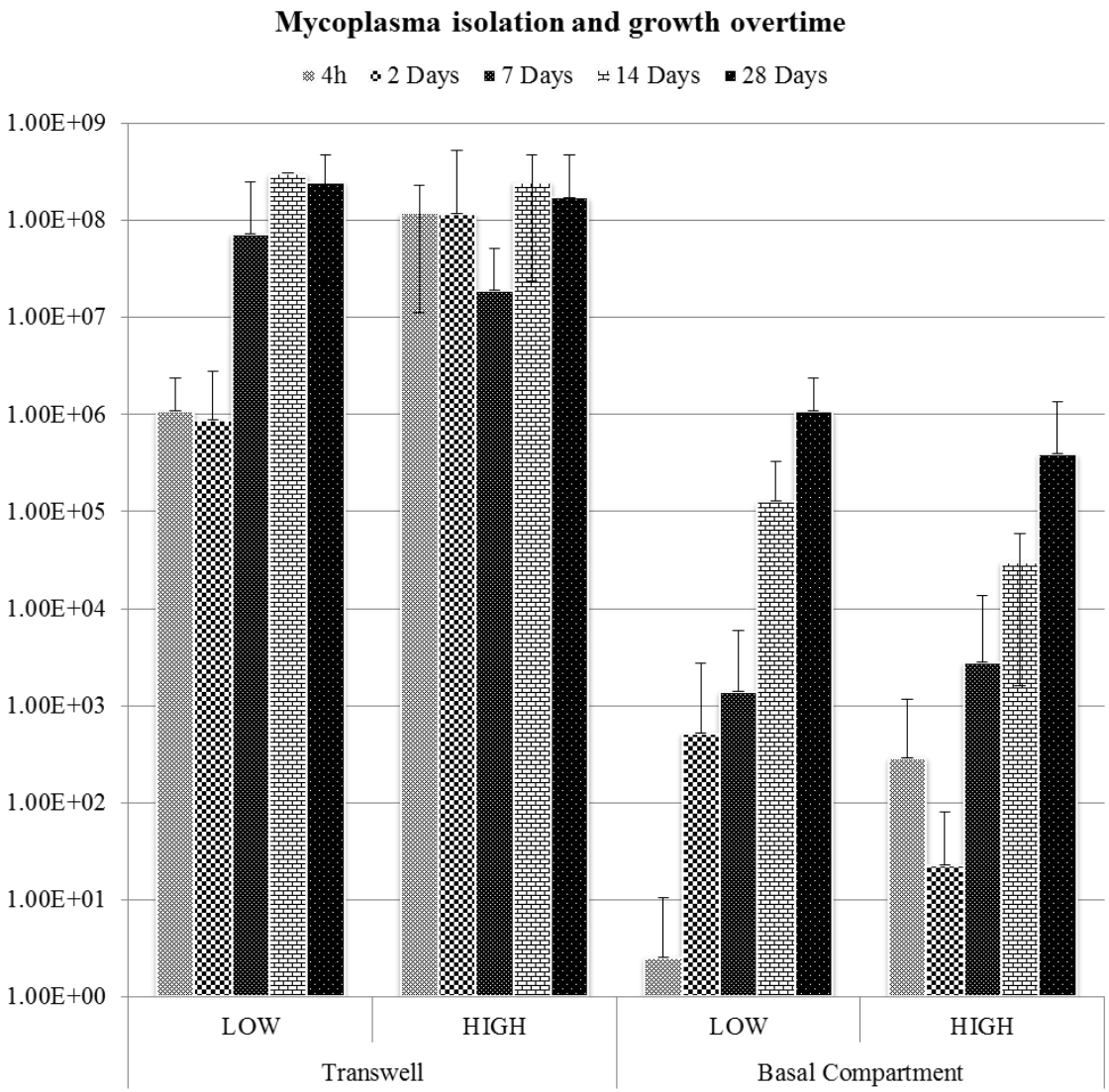
Mycoplasma isolation and growth overtime
4h
2 Days
7 Days
14 Days
28 Days
1.00E+09
1.00E+08
1.00E+07
1.00E+06
1.00E+05
1.00E+04
1.00E+03
1.00E+02
1.00E+01
1.00E+00
LOW
HIGH
LOW
HIGH
Transwell
Basal Compartment

CHAPTER 5

DISCUSSION

The *In Vitro M. pneumoniae*-NHBE Cell Model

The culmination of this dissertation is a model that describes the course of *M. pneumoniae* infection of the human conducting airway (Fig. 32). The central theme of this dissertation was that mycoplasma gliding motility was driving localization and spread. Gliding motility may not be the sole factor contributing to the *M. pneumoniae*-NHBE cell model, however it is the primary virulence factor with sufficient support from the literature, which spans decades of research (30, 54, 95, 98, 108, 183-185). With this in mind the model will be summarized.

During the localization phase (Fig. 32), successful gel-layer mucus penetration placed *M. pneumoniae* bacteria at the tips of the cilia whereby gliding became essential for increasing the likelihood of contact. *M. pneumoniae* bacteria traversed or were funneled the length of the cilia shaft and rapidly localized to the base of the cilia. *M. pneumoniae* bacteria have been observed localized at varying depths along the cilia shaft (Fig. 5, panel B). However, the nature of this interaction may be short lived and rapid since the most common manifestation of mycoplasma localization was to the base of the cilia (Fig. 5, panel A). Drawing from work on the periciliary layer (145, 170), the negative charge repulsion associated with the mucin domain oligosaccharides may create channels between beating cilium (whose mechanics may also contribute (158)) that facilitate rapid mycoplasma localization towards the base. What is compelling is that

having no cell wall may give mycoplasmas flexibility in penetrating the size-restricting periciliary layer (145). Consistent with this, *M. pneumoniae* bacterial accumulations localized between epithelial cells, suggesting lateral mycoplasma movement was partially dictated by the components of the periciliary layer (Figs. 5, 7, 8 & 11).

During the invasion and desquamation phase (Fig. 32), *M. pneumoniae* bacteria colocalized with the epithelial cell junctions (Figs. 8 & 11). Individual mycoplasmas penetrated the paracellular and basolateral surfaces, where they began to accumulate. Where the mycoplasmas took up residence within the basolateral surface appeared to be random. However, localization may be associated with specific binding partners restricted to this compartment. *M. pneumoniae* bacterial accumulation may be the result of direct movement to the basolateral surface or growth by the primary invaders. Bacterial accumulation within the basolateral surface initiated a series of events as follows: loss of cilia, desquamation, actin reorganization, thickening of the monolayer and return of cilia to dislodge the infected desquamating epithelium (Figs. 15-26, collectively). The desquamating epithelium was characteristically heavily infected with *M. pneumoniae* bacteria (Figs. 15, 21 &22), which were determined to be metabolically active and viable (data not shown). Loss of the mycoplasma-infected epithelium resulted in invaginations of the epithelial monolayer that likely contributed to reduced barrier function and mycoplasma recovery from the basal media compartment (Figs. 14, 26 & 31). It was noteworthy that while the mycoplasmas had free access to the basal media compartment, as a result of the infectious process, there was no observed flow of airway media from the basal compartment to the luminal surface (no phenol red on top). In addition, the infectious process appeared to be highly localized, such that uninfected

regions of interest, adjacent to visibly infected areas, appeared indistinguishable (morphologically) from uninfected controls (data not shown). Taken together, this suggested that *M. pneumoniae* bacterial invasion was a coordinated event and not simply a matter of NHBE cell necrosis or toxin mediated damage, which has been reported in submersion culture (43). The desquamation event was significant because, prior to this, the infected epithelium appeared to lose its cilia and become more squamous-like (Figs. 15 & 22), which resulted in a familiar colonization pattern observed in the acute exposure study (compare Figs. 8 & 22). These morphological changes to the epithelium were consistent with the observations from the acute exposure study (Fig. 2) as result of the development of the airway barrier (prior to infection).

During the invasion and reorganization phase (Fig. 32) ciliated cells appeared abnormal as a result of beta-tubulin reorganization (Fig. 15) and localized within the invaginations of the reorganizing epithelium (Fig. 26). It is likely that ciliated cells within the invaginations do not contribute to the overall mucociliary clearance. However, they may be involved in localized dislodging of the heavily infected mycoplasmas from the monolayer (Figs.19 - 22). Dislodging of the mycoplasma-desquamated epithelium appeared to reinfect the tips of adjacent ciliated cells, thus reinitiating the infection. In this case mycoplasma initiated airway reorganization directly inhibited overall clearance by altering the airway architecture and creating a mechanism for reinfection mediated by desquamated epithelium. During this process *M. pneumoniae* bacteria accessed the basolateral surface directly or indirectly as a result of the continued epithelial reorganization. In either case, these observations were supported by recovery of bacteria

from the basal media compartment (Fig. 31). The *in vitro* model of chronic exposure and reinfection likely reflect what may occur during a long-term *in vivo* infection in humans.

Evidence of the complete reconstitution of airway barrier, postinfection (Fig. 32), remained elusive. The observed looping-out of infected epithelium and the resultant invaginations suggested a return to normal barrier function (Figs. 20 & 21). There was sufficient evidence to support that with extended incubation (months) mycoplasmas would be lost to desquamation of the epithelium and invasion of the basal compartment (Figs. 22 & 31). *M. pneumoniae* bacterial infection, in this system, reached peak colonization when the epithelium was invaded, which was followed by a drop in colonization during desquamation and epithelial reorganization. Washing the epithelium every other day (instead of every 3rd day) may limit the reinfection cycle initiated by desquamating epithelium, permitting recovery and repair of the NHBE cells. Isolation of mycoplasmas from the basal compartment is a significant observation and suggests an innate capability to bypass the mucociliary barrier independent of a complete immune system.

In summary, the successful *M. pneumoniae* bacterial infection involved localization to cilia and direct invasion of the basolateral surface. Mycoplasmas present within the basolateral surface initiated loss of ciliation and desquamation of the epithelium, which stripped away the mucociliary barrier and interfered with clearance. The subsequent airway reorganization facilitated additional mycoplasma invasion of the basal media chamber (*in vitro*) and likely facilitates invasion of the basal lamina (*in vivo).* These events strongly suggest that *M. pneumoniae* bacteria are capable of bypassing the epithelial barrier of the conducting airway.

Comparison of the *M. pneumoniae*-NHBE Cell Model to Animal Models

The *M. pneumoniae*-NHBE cell model, when compared to the Hardy mouse model (118) yields some insight into the pathway of chronic airway disease. The author's report a reduced ability to detect mycoplasmas in lavage fluid via culture and PCR at 530 days (118). The *M. pneumoniae*-NHBE cell model suggests that this may reflect a transition from surface exposed mycoplasmas to localization to the basolateral compartment. Sequestration in this compartment would limit the access of the lavage fluid. As mycoplasmas localize within the basolateral compartment, detection via lavage fluid becomes less sensitive. In seven mice at 530 days postinfection, which had abnormal pathology, none had cultivatable mycoplasma (118). The *M. pneumoniae*-NHBE cell model predicts that this stage reflects where mycoplasma-induced desquamation remodels the conducting airway (Fig. 32). The inability to detect mycoplasmas at this stage is not surprising because they were cleared previously (as demonstrated by successful early detection at early timepoints (118) and are likely sequestered from lavage detection. This is an oversimplified comparison between the two systems because the NHBE cell system lacks the complexity of an animal model and it is unclear how well mouse models reflect human infection. It is noteworthy that this dissertation is the only *in vitro* human model, to date, which demonstrates *M. pneumoniae* localization, invasion and airway reorganization in primary human cells cultured in air-liquid interface.

The Significance of *M. pneumoniae* Airway Infection

The vicious circle hypothesis suggests that insults to the mucociliary apparatus increases bacterial colonization, which then leads to direct airway damage via bacterial

byproducts or indirect cell injury via the inflammatory response (138, 186). The *M. pneumoniae*-NHBE cell model agrees with this hypothesis. In fact, the mycoplasma-associated desquamated epithelium was likely responsible for maintaining the infection for such an extended period. As a result, the NHBE cells were constantly reinfected, which resulted in striking actin reorganization that not only altered the localization of cilia but appeared to thicken the airway (Figs. 24 - 26), all of which may not be that different mechanistically from *in vivo* chronic mycoplasmosis. Airway desquamation and reorganization and loss of mucociliary clearance due to infection potentially exposes the basal lamina (underlying tissues) to insults from other airway pathogens, reinfection from the same pathogen and to particulate matter (187, 188). These findings of desquamation, airway thickening and reorganization are consistent with chronic airway disease studies (189-192). *M. pneumoniae* infection is known to be associated with various extrapulmonary manifestations, which has been reviewed elsewhere (2, 193-196). The current *in vitro* NHBE cell model observation of mycoplasma invasion of the basal media compartment strongly supports *in vivo* invasion. In this context, the idea of a mild upper respiratory *M. pneumoniae* infection should be approached with caution since this in no way suggests that mycoplasmas are cleared from the host even when the airway appears normal (197).

Future Work

Future emphasis should be placed on elucidation of the mechanism of *M. pneumoniae* airway invasion. *M. pneumoniae* is known to produce both peroxide and a putative ADP-ribosylating toxin which may independently and/or collectively contribute to airway reorganization. Peroxide formation is known to alter tight junctions and

reorganize actin, which is similar to the known function of ADP-ribosylating toxins (198-200). It is also noteworthy that hydrogen peroxide may function as a signaling molecule and appears to be highly regulated in the airway (201, 202). The NHBE cell model offers the ideal backdrop for addressing the mechanism question because it is the only model that offers air-liquid interface that adequately parallels the human conducting airway.

Fig. 32. The *M. pneumoniae*-NHBE cell model. Dissertation derived model for mycoplasma infection of conducting airway cells. Immune and stromal cells are intentionally left out for clarity. Not drawn to scale.

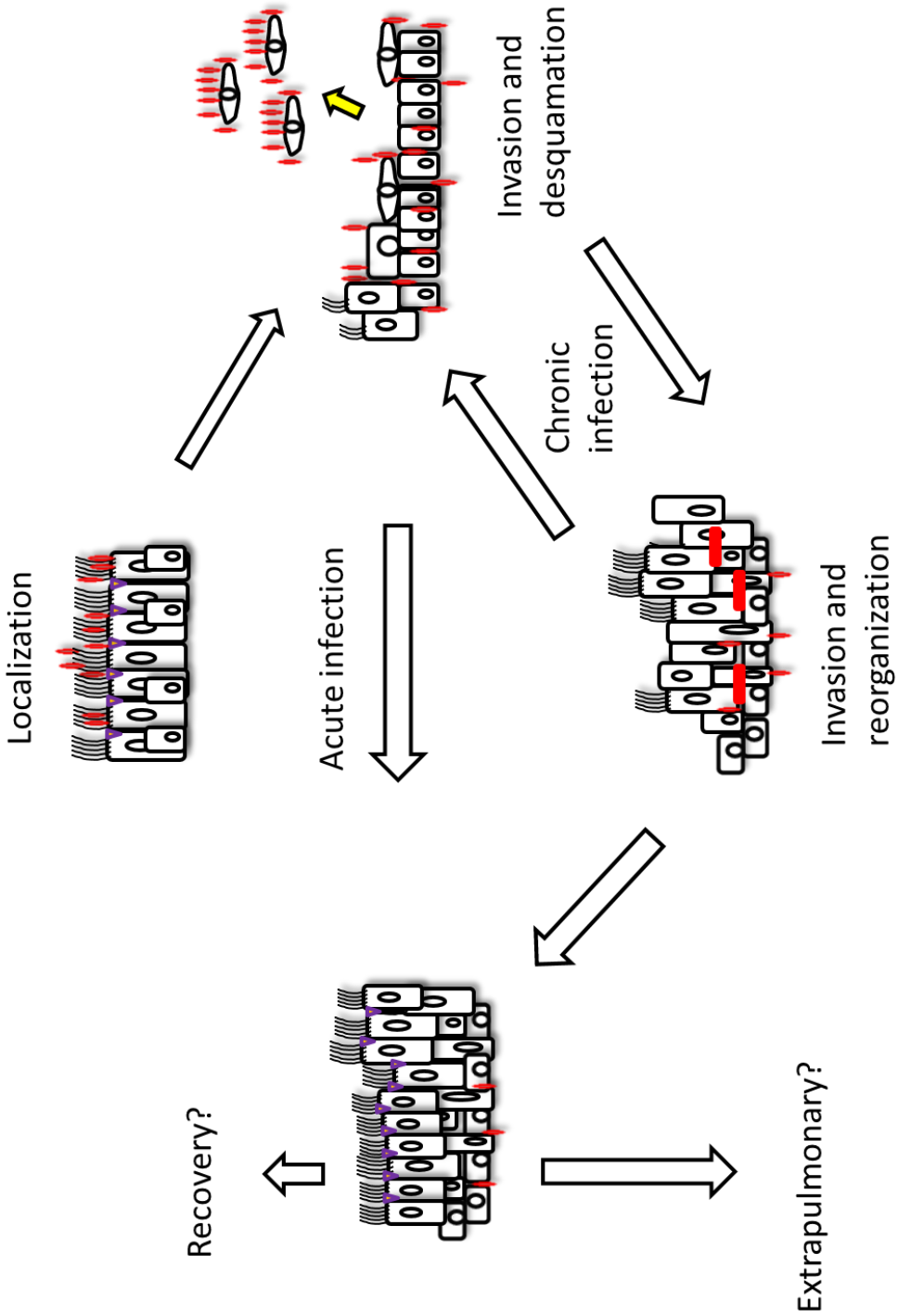
Localization
Acute infection
Invasion and desquamation
Chronic infection
Invasion and reorganization
Recovery?
Extrapulmonary?

REFERENCES

1. **Esposito S, Blasi F, Bosis S, Droghetti R, Faelli N, Lastrico A, Principi N.** 2004. Aetiology of acute pharyngitis: the role of atypical bacteria. J. Med. Microbiol. **53:**645-651.
2. **Waites KB, Talkington DF.** 2004. *Mycoplasma pneumoniae* and its role as a human pathogen. Clin. Microbiol. Rev. **17:**697-728.
3. **Clyde WA, Jr.** 1993. Clinical overview of typical *Mycoplasma pneumonia*e infections. Clin. Infect. Dis. **17 Suppl 1:**S32-36.
4. **Atkinson TP, Boppana S, Theos A, Clements LS, Xiao L, Waites K.** 2011. Stevens-Johnson syndrome in a boy with macrolide-resistant *Mycoplasma pneumonia*e pneumonia. Pediatrics **127:**e1605-1609.
5. **Dua J, Nandagudi A, Sutcliffe N.** 2012. Mycoplasma pneumoniae infection associated with urticarial vasculitis mimicking adult-onset Still's disease. Rheumatol. Int. **32:**4053-4056.
6. **Godron A, Pereyre S, Monet C, Llanas B, Harambat J.** 2013. Hemolytic uremic syndrome complicating *Mycoplasma pneumoniae* infection. Pediatr. Nephrol. **28:**2057-2060.
7. **Hanzawa F, Fuchigami T, Ishii W, Nakajima S, Kawamura Y, Endo A, Arakawa C, Kohira R, Fujita Y, Takahashi S.** 2014. A 3-year-old boy with Guillain-Barre syndrome and encephalitis associated with *Mycoplasma pneumoniae* infection. J. Infect. Chemother. **20:**134-138.

8. **Meyer Sauteur PM, Huber BM, Goetschel P.** 2012. Neuroinvasive *Mycoplasma pneumoniae* infection without intrathecal antibody response. Pediatr. Infect. Dis. J. **31:**1199-1200.

9. **Meyer Sauteur PM, Streuli JC, Iff T, Goetschel P.** 2011. *Mycoplasma pneumoniae*-associated encephalitis in childhood--nervous system disorder during or after a respiratory tract infection. Klin. Padiatr. **223:**209-213.

10. **Park SJ, Pai KS, Kim AR, Lee JH, Shin JI, Lee SY.** 2012. Fulminant and Fatal Multiple Organ Failure in a 12-Year-Old Boy With *Mycoplasma pneumoniae* Infection. Allergy Asthma Immunol. Res. **4:**55-57.

11. **Schomburg J, Vogel M.** 2012. A 12-year-old boy with severe mucositis: extrapulmonary manifestation of *Mycoplasma pneumoniae* infection. Klin. Padiatr. **224:**94-95.

12. **Spuesens EB, Fraaij PL, Visser EG, Hoogenboezem T, Hop WC, van Adrichem LN, Weber F, Moll HA, Broekman B, Berger MY, van Rijsoort-Vos T, van Belkum A, Schutten M, Pas SD, Osterhaus AD, Hartwig NG, Vink C, van Rossum AM.** 2013. Carriage of *Mycoplasma pneumoniae* in the upper respiratory tract of symptomatic and asymptomatic children: an observational study. P.L.o.S. Med **10:**e1001444.

13. **Smith-Norowitz TA, Silverberg JI, Kusonruksa M, Weaver D, Ginsburg D, Norowitz KB, Durkin HG, Hammerschlag MR, Bluth MH, Kohlhoff SA.** 2013. Asthmatic children have increased specific anti-*Mycoplasma pneumoniae* IgM but not IgG or IgE-values independent of history of respiratory tract infection. Pediatr. Infect. Dis. J. **32:**599-603.

14. **Wood PR, Hill VL, Burks ML, Peters JI, Singh H, Kannan TR, Vale S, Cagle MP, Principe MF, Baseman JB, Brooks EG.** 2013. *Mycoplasma pneumoniae* in children with acute and refractory asthma. Ann. Allergy Asthma Immunol. **110:**328-334 e321.

15. **Kraft M, Adler KB, Ingram JL, Crews AL, Atkinson TP, Cairns CB, Krause DC, Chu HW.** 2008. *Mycoplasma pneumoniae* induces airway epithelial cell expression of MUC5AC in asthma. The European respiratory journal **31:**43-46.

16. **Martin RJ, Kraft M, Chu HW, Berns EA, Cassell GH.** 2001. A link between chronic asthma and chronic infection. J. Allergy Clin. Immunol. **107:**595-601.

17. **Mufson MA, Bloom HH, Manko MA, Kingston JR, Chanock RM.** 1962. Acute respiratory diseases of viral etiology. V. Eaton agent: a review. Am. J. Public Health Nations Health **52:**925-932.

18. **Matricardi PM, Minelli E, Aït-Khaled N, Bateman ED, Baena-Cagnani C, Boland M, Buist SA, Canonica GW, Carlsen K-H, Dahl R, Fabbri LM, Fukuchi Y, Grouse L, Humbert M, Lenfant C, Malo JL, McNicholas WT, Pawankar R, Rabe KF, Simons FER, Turnbull A, Valovirta E, Van Cauwenberge P, Viegi G, Van Weel C, Wenzel S, Zhong N.** 2007. Chronic respiratory disease, p. 12-31. *In* Bousquet J, Khaltaev N (ed.), Global surveillance, prevention and control of chronic respiratory diseases: a comprehensive approach. World Health Organization, Switzerland.

19. **Staugas R, Martin AJ.** 1985. Secondary bacterial infections in children with proved *Mycoplasma pneumoniae*. Thorax **40:**546-548.

20. **Toikka P, Juven T, Virkki R, Leinonen M, Mertsola J, Ruuskanen O.** 2000. *Streptococcus pneumonia*e and *Mycoplasma pneumoniae* coinfection in community acquired pneumonia. Arch. Dis. Child. **83:**413-414.

21. **Watanabe H, Uruma T, Nakamura H, Aoshiba K.** 2014. The role of *Mycoplasma pneumonia*e infection in the initial onset and exacerbations of asthma. Allergy Asthma. Proc. **35:**204-210.

22. **Hu PC, Collier AM, Baseman JB.** 1977. Surface parasitism by *Mycoplasma pneumoniae* of respiratory epithelium. J. Exp. Med. **145:**1328-1343.

23. **Wilson MH, Collier AM.** 1976. Ultrastructural study of *Mycoplasma pneumoniae* in organ-culture. J. Bacteriol. **125:**332-339.

24. **Powell DA, Hu PC, Wilson M, Collier AM, Baseman JB.** 1976. Attachment of *Mycoplasma pneumoniae* to respiratory epithelium. Infect. Immun. **13:**959-966.

25. **Muse KE, Powell DA, Collier AM.** 1976. *Mycoplasma pneumoniae* in hamster tracheal organ culture studied by scanning electron microscopy. Infect. Immun. **13:**229-237.

26. **Collier AM, Clyde WA, Jr., Denny FW.** 1971. *Mycoplasma pneumoniae* in hamster tracheal organ culture: immunofluorescent and electron microscopic studies. Proc. Soc. Exp. Biol. Med. **136:**569-573.

27. **Collier AM, Clyde WA.** 1971. Relationships between *Mycoplasma pneumoniae* and human respiratory epithelium. Infect. Immun. **3:**694-701.

28. **Hasselbring BM, Jordan JL, Krause RW, Krause DC.** 2006. Terminal organelle development in the cell wall-less bacterium Mycoplasma pneumoniae.

Proceedings of the National Academy of Sciences of the United States of America **103:**16478-16483.

29. **Seto S, Kenri T, Tomiyama T, Miyata M.** 2005. Involvement of P1 adhesin in gliding motility of *Mycoplasma pneumoniae* as revealed by the inhibitory effects of antibody under optimized gliding conditions. J. Bacteriol. **187:**1875-1877.

30. **Hasselbring BM, Jordan JL, Krause DC.** 2005. Mutant analysis reveals a specific requirement for protein P30 in *Mycoplasma pneumoniae* gliding motility. J. Bacteriol. **187:**6281-6289.

31. **Romero-Arroyo CE, Jordan J, Peacock SJ, Willby MJ, Farmer MA, Krause DC.** 1999. *Mycoplasma pneumoniae* protein P30 is required for cytadherence and associated with proper cell development. J. Bacteriol. **181:**1079-1087.

32. **Schmidl SR, Gronau K, Hames C, Busse J, Becher D, Hecker M, Stulke J.** 2010. The stability of cytadherence proteins in *Mycoplasma pneumoniae* requires activity of the protein kinase PrkC. Infect. Immun. **78:**184-192.

33. **Page CA, Krause DC.** 2013. Protein kinase/phosphatase function correlates with gliding motility in *Mycoplasma pneumoniae*. J. Bacteriol. **195:**1750-1757.

34. **Eaton MD, Meiklejohn G, van Herick W.** 1944. Studies on the etiology of primary atypical pneumonia : a filterable agent transmissible to cotton rats, hamsters, and chick embryos. J. Exp. Med. **79:**649-668.

35. **Gabridge MG, Bright MJ, Richards HR.** 1982. Scanning electron microscopy of *Mycoplasma pneumoniae* on the membrane of individual ciliated tracheal cells. In Vitro **18:**55-62.

36. **Gabridge MG, Taylor-Robinson D, Davies HA, Dourmashkin RR.** 1979. Interaction of *Mycoplasma pneumoniae* with human lung fibroblasts: characterization of the in vitro model. Infect. Immun. **25:**446-454.

37. **Hu PC, Collier AM, Baseman JB.** 1975. Alterations in the metabolism of hamster tracheas in organ culture after infection by virulent *Mycoplasma pneumoniae*. Infect. Immun. **11:**704-710.

38. **Yang J, Hooper WC, Phillips DJ, Talkington DF.** 2004. Cytokines in *Mycoplasma pneumoniae* infections. Cytokine Growth Factor Rev. **15:**157-168.

39. **Krivan HC, Olson LD, Barile MF, Ginsburg V, Roberts DD.** 1989. Adhesion of *Mycoplasma pneumoniae* to sulfated glycolipids and inhibition by dextran sulfate. J. Biol. Chem. **264:**9283-9288.

40. **Loveless RW, Feizi T.** 1989. Sialo-oligosaccharide receptors for *Mycoplasma pneumonia*e and related oligosaccharides of poly-N-acetyllactosamine series are polarized at the cilia and apical-microvillar domains of the ciliated cells in human bronchial epithelium. Infect. Immun. **57:**1285-1289.

41. **Roberts DD, Olson LD, Barile MF, Ginsburg V, Krivan HC.** 1989. Sialic acid-dependent adhesion of *Mycoplasma pneumoniae* to purified glycoproteins. J. Biol. Chem. **264:**9289-9293.

42. **Somerson NL, Walls BE, Chanock RM.** 1965. Hemolysin of *Mycoplasma pneumoniae*: tentative identification as a peroxide. Science **150:**226-228.

43. **Kannan TR, Baseman JB.** 2006. ADP-ribosylating and vacuolating cytotoxin of *Mycoplasma pneumoniae* represents unique virulence determinant among bacterial pathogens. Proc. Natl. Acad. Sci. U. S. A. **103:**6724-6729.

44. **Cohen G, Somerson NL.** 1969. Glucose-dependent Secretion and Destruction of Hydrogen Peroxide by *Mycoplasma pneumoniae*. Journal of bacteriology **98:**547-551.

45. **Lipman RP, Clyde WA, Jr.** 1969. The interrelationship of virulence, cytadsorption, and peroxide formation in *Mycoplasma pneumoniae*. Proc. Soc. Exp. Biol. Med. **131:**1163-1167.

46. **Berg CP, Kannan TR, Klein R, Gregor M, Baseman JB, Wesselborg S, Lauber K, Stein GM.** 2009. Mycoplasma antigens as a possible trigger for the induction of antimitochondrial antibodies in primary biliary cirrhosis. Liver Int. **29:**797-809.

47. **Ben Aissa-Fennira F, Sassi A, Bouguerra A, Benammar-Elgaaied A.** 2011. Immunoregulatory role for a public IgM idiotype in the induction of autoimmune diseases in *Mycoplasma pneumoniae* infection. Immunol. Lett. **136:**130-137.

48. **Dhouib N, Guedhami H, Mellouli F, Ben Khaled M, Kaabi H, Belhassen E, Hmida S, Bejaoui M.** 2011. *Mycoplasma pneumonia*e associated with severe autoimmune hemolytic anemia in a child with homozygous beta-thalassemia. Tunis. Med. **89:**652-653.

49. **Sharma MB, Chaudhry R, Tabassum I, Ahmed NH, Sahu JK, Dhawan B, Kalra V.** 2011. The presence of *Mycoplasma pneumoniae* infection and GM1 ganglioside antibodies in Guillain-Barre syndrome. J. Infect. Dev. Ctries. **5:**459-464.

50. **Pana Z, Hatzipantelis E, Douma S, Karteridou C.** 2012. An unusual case of *Mycoplasma pneumoniae*-associated autoimmune haemolytic anaemia in a 10-year-old female child. J. Paediatr. Child Health. **48:**621-622.

51. **Reittner P, Muller NL, Heyneman L, Johkoh T, Park JS, Lee KS, Honda O, Tomiyama N.** 2000. *Mycoplasma pneumoniae* pneumonia: radiographic and high-resolution CT features in 28 patients. A.J.R. Am. J. Roentgenol. **174:**37-41.

52. **Miyashita N, Sugiu T, Kawai Y, Oda K, Yamaguchi T, Ouchi K, Kobashi Y, Oka M.** 2009. Radiographic features of *Mycoplasma pneumoniae* pneumonia: differential diagnosis and performance timing. B.M.C. Med. Imaging. **9:**7.

53. **Meakins JF.** 1943. Primary atypical pneumonia of unknown etiology. Canadian Medical Association journal **48:**333-337.

54. **Szczepanek SM, Majumder S, Sheppard ES, Liao X, Rood D, Tulman ER, Wyand S, Krause DC, Silbart LK, Geary SJ.** 2012. Vaccination of BALB/c mice with an avirulent *Mycoplasma pneumoniae* P30 mutant results in disease exacerbation upon challenge with a virulent strain. Infect. Immun. **80:**1007-1014.

55. **Gray TE, Guzman K, Davis CW, Abdullah LH, Nettesheim P.** 1996. Mucociliary differentiation of serially passaged normal human tracheobronchial epithelial cells. Am. J. Respir. Cell. Mol. Biol. **14:**104-112.

56. **Krunkosky TM, Fischer BM, Martin LD, Jones N, Akley NJ, Adler KB.** 2000. Effects of TNF-alpha on expression of ICAM-1 in human airway epithelial cells in vitro. Signaling pathways controlling surface and gene expression. Am. J. Respir. Cell. Mol. Biol. **22:**685-692.

57. **Evans CM, Koo JS.** 2009. Airway mucus: the good, the bad, the sticky. Pharmacol. Ther. **121:**332-348.

58. **Fahy JV, Dickey BF.** 2010. Airway mucus function and dysfunction. N. Engl. J. Med. **363:**2233-2247.

59. **Knowles MR, Boucher RC.** 2002. Mucus clearance as a primary innate defense mechanism for mammalian airways. J. Clin. Invest. **109:**571-577.

60. **Liu C.** 1957. Studies on primary atypical pneumonia. I. Localization, isolation, and cultivation of a virus in chick embryos. J. Exp. Med. **106:**455-466.

61. **Liu C, Eaton MD, Heyl JT.** 1959. Studies on primary atypical pneumonia. II. Observations concerning the development and immunological characteristics of antibody in patients. J. Exp. Med. **109:**545-556.

62. **Chanock RM, Rifkind D, Kravetz HM, Kinght V, Johnson KM.** 1961. Respiratory disease in volunteers infected with Eaton agent: a preliminary report. Proc. Natl. Acad. Sci. U. S. A. **47:**887-890.

63. **Marmion BP, Goodburn GM.** 1961. Effect of an organic gold salt on Eaton's primary atypical pneumonia agent and other observations. Nature **189:**247-248.

64. **Goodburn GM, Marmion BP.** 1962. A study of the properties of Eaton's primary atypical pneumonia organism. J. Gen. Microbiol. **29:**271-290.

65. **Gay FW.** 1967. Fine structure and location of the mycoplasma-like gray lung and rat pneumonia agents in infected mouse lung. J. Bacteriol. **94:**2048-2061.

66. **Chanock RM, Hayflick L, Barile MF.** 1962. Growth on artificial medium of an agent associated with atypical pneumonia and its identification as a PPLO. P. Natl. Acad. Sci. U.S.A. **48:**41-49.

67. **Brown DR.** 2010. Phylum XVI. *Tenericutes* Murray 1984a,356^{vp}, p. 567-568. *In* Krieg NR, Ludwig W, Whitman WB, Hedlund BP, Paster BJ, Staley JT, Ward N, Brown D, Parte A (ed.), Bergey's Manual of Systematic Bacteriology, 2nd ed, vol. 4. Springer, New York, N.Y.

68. **Dienes L, Weinberger HJ.** 1951. The L forms of bacteria. Bacteriol. Rev. **15:**245-288.

69. **Smith PF.** 1964. Comparative physiology of pleuropneumonia-like and L-type organisms. Bacteriol. Rev. **28:**97-125.

70. **Hayflick L, Chanock RM.** 1965. *Mycoplasma* species of man. Bacteriol. Rev. **29:**185-221.

71. **McGee ZA, Rogul M, Falkow S, Wittler RG.** 1965. The relationship of *Mycoplasma pneumoniae* (Eaton agent) to Streptococcus MG: application of genetic tests to determine relatedness of L-forms and PPLO to bacteria. Proc. Natl. Acad. Sci. U. S. A. **54:**457-461.

72. **Wolf M, Muller T, Dandekar T, Pollack JD.** 2004. Phylogeny of Firmicutes with special reference to *Mycoplasma* (*Mollicutes*) as inferred from phosphoglycerate kinase amino acid sequence data. Int. J. Syst. Evol. Microbiol. **54:**871-875.

73. **Razin S, Yogev D, Naot Y.** 1998. Molecular biology and pathogenicity of mycoplasmas. Microbiol. Mol. Biol. Rev. **62:**1094-1156.

74. **Brown DR, May M, Bradbury JM, Balish MF, Calcutt MJ, Glass JI, Tasker S, Messick JB, Johansson K-E, Neimark H.** 2010. Genus I. Mycoplasma Nowak 1929,1349 nom. cons.Jud.Comm.Opin.22,1958,166^{AL}, p. 575-613. *In*

Krieg NR, Ludwig W, Whitman WB, Hedlund BP, Paster BJ, Staley JT, Ward N, Brown D, Parte A (ed.), Bergey's Manual of Systematic Bacteriology, 2nd ed, vol. 4. Springer, New York, N.Y.

75. **Tully JG, Whitcomb RF, Clark HF, Williamson DL.** 1977. Pathogenic mycoplasmas: cultivation and vertebrate pathogenicity of a new spiroplasma. Science **195:**892-894.

76. **Gabridge MG, Singer SE, Esposito RA.** 1976. Cultivation of mycoplasmas in a modified tissue culture medium. Applied and environmental microbiology **31:**986-989.

77. **Brown DR, Whitcomb RF, Bradbury JM.** 2007. Revised minimal standards for description of new species of the class *Mollicutes* (division *Tenericutes*). Int. J. Syst. Evol. Microbiol. **57:**2703-2719.

78. **Henderson GP, Jensen GJ.** 2006. Three-dimensional structure of Mycoplasma pneumoniae's attachment organelle and a model for its role in gliding motility. Mol. Microbiol. **60:**376-385.

79. **Balish MF, Krause DC.** 2006. Mycoplasmas: a distinct cytoskeleton for wall-less bacteria. J. Mol. Microbiol. Biotechnol. **11:**244-255.

80. **Krause DC, Balish MF.** 2004. Cellular engineering in a minimal microbe: structure and assembly of the terminal organelle of *Mycoplasma pneumoniae*. Mol. Microbiol. **51:**917-924.

81. **Neimark H, Gesner M.** 2010. Is *Mycoplasma pneumoniae* adherence to erythrocytes a factor in extrapulmonary dissemination? P.L.o.S. Pathog. **6:**e1001219.

82. **Chandler DK, Collier AM, Barile MF.** 1982. Attachment of *Mycoplasma pneumoniae* to hamster tracheal organ cultures, tracheal outgrowth monolayers, human erythrocytes, and WiDr human tissue culture cells. Infect. Immun. **35:**937-942.

83. **Layh-Schmitt G, Podtelejnikov A, Mann M.** 2000. Proteins complexed to the P1 adhesin of *Mycoplasma pneumoniae*. Microbiology (Reading, England) **146 (Pt 3):**741-747.

84. **Meng KE, Pfister RM.** 1980. Intracellular structures of *Mycoplasma pneumoniae* revealed after membrane removal. J. Bacteriol. **144:**390-399.

85. **Gobel U, Speth V, Bredt W.** 1981. Filamentous structures in adherent *Mycoplasma pneumoniae* cells treated with nonionic detergents. J. Cell. Biol. **91:**537-543.

86. **Baseman JB, Cole RM, Krause DC, Leith DK.** 1982. Molecular basis for cytadsorption of *Mycoplasma pneumoniae*. J. Bacteriol. **151:**1514-1522.

87. **Gerstenecker B, Jacobs E.** 1990. Topological mapping of the P1-adhesin of *Mycoplasma pneumoniae* with adherence-inhibiting monoclonal antibodies. J. Gen. Microbiol. **136:**471-476.

88. **Feldner J, Gobel U, Bredt W.** 1982. *Mycoplasma pneumoniae* adhesin localized to tip structure by monoclonal antibody. Nature **298:**765-767.

89. **Krause DC, Baseman JB.** 1983. Inhibition of *Mycoplasma pneumoniae* hemadsorption and adherence to respiratory epithelium by antibodies to a membrane protein. Infect. Immun. **39:**1180-1186.

90. **Morrison-Plummer J, Leith DK, Baseman JB.** 1986. Biological effects of anti-lipid and anti-protein monoclonal antibodies on *Mycoplasma pneumoniae*. Infect. Immun. **53:**398-403.

91. **Krause DC, Leith DK, Wilson RM, Baseman JB.** 1982. Identification of *Mycoplasma pneumoniae* proteins associated with hemadsorption and virulence. Infect. Immun. **35:**809-817.

92. **Waldo RH, 3rd, Krause DC.** 2006. Synthesis, stability, and function of cytadhesin P1 and accessory protein B/C complex of *Mycoplasma pneumoniae*. J. Bacteriol. **188:**569-575.

93. **Baseman JB, Morrison-Plummer J, Drouillard D, Puleo-Scheppke B, Tryon VV, Holt SC.** 1987. Identification of a 32-kilodalton protein of *Mycoplasma pneumoniae* associated with hemadsorption. Isr. J. Med. Sci. **23:**474-479.

94. **Chang HY, Jordan JL, Krause DC.** 2011. Domain analysis of protein P30 in *Mycoplasma pneumoniae* cytadherence and gliding motility. J. Bacteriol. **193:**1726-1733.

95. **Chang HY, Prince OA, Sheppard ES, Krause DC.** 2011. Processing is required for a fully functional protein P30 in *Mycoplasma pneumoniae* gliding and cytadherence. J. Bacteriol. **193:**5841-5846.

96. **Dallo SF, Chavoya A, Baseman JB.** 1990. Characterization of the gene for a 30-kilodalton adhesion-related protein of *Mycoplasma pneumoniae*. Infect. Immun. **58:**4163-4165.

97. **Dallo SF, Lazzell AL, Chavoya A, Reddy SP, Baseman JB.** 1996. Biofunctional domains of the *Mycoplasma pneumoniae* P30 adhesin. Infect. Immun. **64:**2595-2601.

98. **Jordan JL, Chang HY, Balish MF, Holt LS, Bose SR, Hasselbring BM, Waldo RH, 3rd, Krunkosky TM, Krause DC.** 2007. Protein P200 is dispensable for *Mycoplasma pneumoniae* hemadsorption but not gliding motility or colonization of differentiated bronchial epithelium. Infect. Immun. **75:**518-522.

99. **Kannan TR, Provenzano D, Wright JR, Baseman JB.** 2005. Identification and characterization of human surfactant protein a binding protein of *Mycoplasma pneumoniae*. Infect. Immun. **73:**2828-2834.

100. **Wright JR.** 2005. Immunoregulatory functions of surfactant proteins. Nat. Rev. Immunol. **5:**58-68.

101. **Whitsett JA, Weaver TE.** 2002. Hydrophobic surfactant proteins in lung function and disease. N. Engl. J. Med. **347:**2141-2148.

102. **Dallo SF, Kannan TR, Blaylock MW, Baseman JB.** 2002. Elongation factor Tu and E1 beta subunit of pyruvate dehydrogenase complex act as fibronectin binding proteins in *Mycoplasma pneumoniae*. Mol. Microbiol. **46:**1041-1051.

103. **Carson JL, Collier AM, Hu SC.** 1980. Ultrastructural observations on cellular and subcellular aspects of experimental *Mycoplasma pneumoniae* disease. Infect. Immun. **29:**1117-1124.

104. **Kannan TR, Musatovova O, Balasubramanian S, Cagle M, Jordan JL, Krunkosky TM, Davis A, Hardy RD, Baseman JB.** 2010. *Mycoplasma*

pneumoniae CARDS toxin expression reveals growth phase and infection-dependent regulation. Mol. Microbiol. **76:**1127-1141.

105. **Lipman RP, Clyde WA, Jr., Denny FW.** 1969. Characteristics of virulent, attenuated, and avirulent *Mycoplasma pneumoniae* strains. J. Bacteriol. **100:**1037-1043.

106. **McBride MJ.** 2001. Bacterial gliding motility: multiple mechanisms for cell movement over surfaces. Annu. Rev. Microbiol. **55:**49-75.

107. **Miyata M.** 2010. Unique centipede mechanism of Mycoplasma gliding. Annu. Rev. Microbiol. **64:**519-537.

108. **Leith DK, Hansen EJ, Wilson RM, Krause DC, Baseman JB.** 1983. Hemadsorption and virulence are separable properties of *Mycoplasma pneumoniae*. Infect. Immun. **39:**844-850.

109. **Chapman KE, Waters CM, Miller WM.** 2002. Continuous exposure of airway epithelial cells to hydrogen peroxide: protection by KGF. J. Cell. Physiol. **192:**71-80.

110. **Boardman KC, Aryal AM, Miller WM, Waters CM.** 2004. Actin re-distribution in response to hydrogen peroxide in airway epithelial cells. J. Cell. Physiol. **199:**57-66.

111. **Halbedel S, Hames C, Stulke J.** 2007. Regulation of carbon metabolism in the mollicutes and its relation to virulence. J. Mol. Microbiol. Biotechnol. **12:**147-154.

112. **Mogensen TH.** 2009. Pathogen recognition and inflammatory signaling in innate immune defenses. Clin. Microbiol. Rev. **22:**240-273, Table of Contents.

113. **Into T, Dohkan J, Inomata M, Nakashima M, Shibata K, Matsushita K.** 2007. Synthesis and characterization of a dipalmitoylated lipopeptide derived from paralogous lipoproteins of *Mycoplasma pneumoniae*. Infect. Immun. **75:**2253-2259.

114. **Shimizu T, Kida Y, Kuwano K.** 2005. A dipalmitoylated lipoprotein from Mycoplasma pneumoniae activates NF-kappa B through TLR1, TLR2, and TLR6. Journal of immunology **175:**4641-4646.

115. **Shimizu T, Kida Y, Kuwano K.** 2007. Triacylated lipoproteins derived from *Mycoplasma pneumoniae* activate nuclear factor-kappaB through toll-like receptors 1 and 2. Immunology **121:**473-483.

116. **Medina JL, Coalson JJ, Brooks EG, Winter VT, Chaparro A, Principe MF, Kannan TR, Baseman JB, Dube PH.** 2012. *Mycoplasma pneumoniae* CARDS toxin induces pulmonary eosinophilic and lymphocytic inflammation. Am. J. Respir. Cell. Mol. Biol. **46:**815-822.

117. **Hardy RD, Coalson JJ, Peters J, Chaparro A, Techasaensiri C, Cantwell AM, Kannan TR, Baseman JB, Dube PH.** 2009. Analysis of pulmonary inflammation and function in the mouse and baboon after exposure to *Mycoplasma pneumoniae* CARDS toxin. P.L.o.S. One **4:**e7562.

118. **Hardy RD, Jafri HS, Olsen K, Hatfield J, Iglehart J, Rogers BB, Patel P, Cassell G, McCracken GH, Ramilo O.** 2002. *Mycoplasma pneumoniae* induces chronic respiratory infection, airway hyperreactivity, and pulmonary inflammation: a murine model of infection-associated chronic reactive airway disease. Infect. Immun. **70:**649-654.

119. **Liu X, Jiang Y, Chen X, Li J, Shi D, Xin D.** 2014. Drug resistance mechanisms of *Mycoplasma pneumoniae* to macrolide antibiotics. Biomed. Res. Int. **2014:**320801.

120. **Baseman JB, Lange M, Criscimagna NL, Giron JA, Thomas CA.** 1995. Interplay between mycoplasmas and host target cells. Microb. Pathog. **19:**105-116.

121. **Dallo SF, Baseman JB.** 2000. Intracellular DNA replication and long-term survival of pathogenic mycoplasmas. Microb. Pathog. **29:**301-309.

122. **Meseguer MA, Alvarez A, Rejas MT, Sanchez C, Perez-Diaz JC, Baquero F.** 2003. *Mycoplasma pneumoniae*: a reduced-genome intracellular bacterial pathogen. Infect. Genet. Evol. **3:**47-55.

123. **Yavlovich A, Tarshis M, Rottem S.** 2004. Internalization and intracellular survival of *Mycoplasma pneumoniae* by non-phagocytic cells. F.E.M.S. Microbiol. Lett. **233:**241-246.

124. **Masters JR.** 2002. HeLa cells 50 years on: the good, the bad and the ugly. Nat. Rev. Cancer **2:**315-319.

125. **Moore AE, Sabachewsky L, Toolan HW.** 1955. Culture characteristics of four permanent lines of human cancer cells. Cancer Res. **15:**598-602.

126. **Andreev J, Borovsky Z, Rosenshine I, Rottem S.** 1995. Invasion of HeLa cells by Mycoplasma penetrans and the induction of tyrosine phosphorylation of a 145-kDa host cell protein. F.E.M.S. Microbiol. Lett. **132:**189-194.

127. **Crosby LM, Waters CM.** 2010. Epithelial repair mechanisms in the lung. Am. J. Physiol. Lung Cell. Mol. Physiol. **298:**L715-731.

128. **Plotkowski MC, de Bentzmann S, Pereira SH, Zahm JM, Bajolet-Laudinat O, Roger P, Puchelle E.** 1999. *Pseudomonas aeruginosa* internalization by human epithelial respiratory cells depends on cell differentiation, polarity, and junctional complex integrity. Am. J. Respir. Cell. Mol. Biol. **20:**880-890.

129. **de Bentzmann S, Plotkowski C, Puchelle E.** 1996. Receptors in the *Pseudomonas aeruginosa* adherence to injured and repairing airway epithelium. Am. J. Respir. Crit. Care Med. **154:**S155-162.

130. **Chanock RM, Mufson MA, Bloom HH, James WD, Fox HH, Kingston JR.** 1961. Eaton agent pneumonia. J.A.M.A. **175:**213-220.

131. **Martinez MA, Ruiz M, Zunino E, Luchsinger V, Avendano LF.** 2008. Detection of *Mycoplasma pneumoniae* in adult community-acquired pneumonia by PCR and serology. J. Med. Microbiol. **57:**1491-1495.

132. **Qu J, Gu L, Wu J, Dong J, Pu Z, Gao Y, Hu M, Zhang Y, Gao F, Cao B, Wang C.** 2013. Accuracy of IgM antibody testing, FQ-PCR and culture in laboratory diagnosis of acute infection by *Mycoplasma pneumoniae* in adults and adolescents with community-acquired pneumonia. B.M.C. Infect. Dis. **13:**172.

133. **Qu J, Yu X, Liu Y, Yin Y, Gu L, Cao B, Wang C.** 2013. Specific multilocus variable-number tandem-repeat analysis genotypes of *Mycoplasma pneumoniae* are associated with diseases severity and macrolide susceptibility. P.L.o.S. One **8:**e82174.

134. **Hennigan SL, Driskell JD, Dluhy RA, Zhao Y, Tripp RA, Waites KB, Krause DC.** 2010. Detection of *Mycoplasma pneumoniae* in simulated and true clinical

throat swab specimens by nanorod array-surface-enhanced Raman spectroscopy. P.L.o.S. One **5:**e13633.

135. **Feizi T, Taylor-Robinson D.** 1967. Cold agglutinin anti-I and *Mycoplasma pneumoniae*. Immunology **13:**405-409.

136. **Cohn L, Elias JA, Chupp GL.** 2004. Asthma: mechanisms of disease persistence and progression. Annu. Rev. Immunol. **22:**789-815.

137. **Holgate ST.** 2011. The sentinel role of the airway epithelium in asthma pathogenesis. Immunol. Rev. **242:**205-219.

138. **Sethi S, Murphy TF.** 2001. Bacterial infection in chronic obstructive pulmonary disease in 2000: a state-of-the-art review. Clin. Microbiol. Rev. **14:**336-363.

139. **Pezzulo AA, Tang XX, Hoegger MJ, Alaiwa MH, Ramachandran S, Moninger TO, Karp PH, Wohlford-Lenane CL, Haagsman HP, van Eijk M, Banfi B, Horswill AR, Stoltz DA, McCray PB, Jr., Welsh MJ, Zabner J.** 2012. Reduced airway surface pH impairs bacterial killing in the porcine cystic fibrosis lung. Nature **487:**109-113.

140. **Stoltz DA, Meyerholz DK, Pezzulo AA, Ramachandran S, Rogan MP, Davis GJ, Hanfland RA, Wohlford-Lenane C, Dohrn CL, Bartlett JA, Nelson GAt, Chang EH, Taft PJ, Ludwig PS, Estin M, Hornick EE, Launspach JL, Samuel M, Rokhlina T, Karp PH, Ostedgaard LS, Uc A, Starner TD, Horswill AR, Brogden KA, Prather RS, Richter SS, Shilyansky J, McCray PB, Jr., Zabner J, Welsh MJ.** 2010. Cystic fibrosis pigs develop lung disease and exhibit defective bacterial eradication at birth. Science translational medicine **2:**29ra31.

141. **Fonseca-Aten M, Rios AM, Mejias A, Chavez-Bueno S, Katz K, Gomez AM, Ramilo O, McCracken GH, Hardy RD.** 2006. Treatment of experimental chronic pulmonary mycoplasmosis. International journal of antimicrobial agents **28:**253-258.

142. **Braga VM, Pemberton LF, Duhig T, Gendler SJ.** 1992. Spatial and temporal expression of an epithelial mucin, Muc-1, during mouse development. Development **115:**427-437.

143. **Buisine MP, Devisme L, Copin MC, Durand-Reville M, Gosselin B, Aubert JP, Porchet N.** 1999. Developmental mucin gene expression in the human respiratory tract. Am. J. Respir. Cell. Mol. Biol. **20:**209-218.

144. **Singh PK, Hollingsworth MA.** 2006. Cell surface-associated mucins in signal transduction. Trends. Cell. Biol. **16:**467-476.

145. **Button B, Cai LH, Ehre C, Kesimer M, Hill DB, Sheehan JK, Boucher RC, Rubinstein M.** 2012. A periciliary brush promotes the lung health by separating the mucus layer from airway epithelia. Science **337:**937-941.

146. **Hattrup CL, Gendler SJ.** 2008. Structure and function of the cell surface (tethered) mucins. Annu. Rev. Physiol. **70:**431-457.

147. **Kasai T, Nakane D, Ishida H, Ando H, Kiso M, Miyata M.** 2013. Role of binding in *Mycoplasma mobile* and *Mycoplasma pneumoniae* gliding analyzed through inhibition by synthesized sialylated compounds. J. Bacteriol. **195:**429-435.

148. **Thornton DJ, Rousseau K, McGuckin MA.** 2008. Structure and function of the polymeric mucins in airways mucus. Annu. Rev. Physiol. **70:**459-486.

149. **Quraishi MS, Jones NS, Mason J.** 1998. The rheology of nasal mucus: a review. Clin. Otolaryngol. Allied Sci. **23:**403-413.

150. **Lai SK, Wang YY, Wirtz D, Hanes J.** 2009. Micro- and macrorheology of mucus. Adv. Drug Deliv. Rev. **61:**86-100.

151. **Matsui H, Randell SH, Peretti SW, Davis CW, Boucher RC.** 1998. Coordinated clearance of periciliary liquid and mucus from airway surfaces. J. Clin. Invest. **102:**1125-1131.

152. **Shai Y.** 1999. Mechanism of the binding, insertion and destabilization of phospholipid bilayer membranes by alpha-helical antimicrobial and cell non-selective membrane-lytic peptides. Biochim. Biophys. Acta. **1462:**55-70.

153. **Steiner H.** 1982. Secondary structure of the cecropins: antibacterial peptides from the moth *Hyalophora cecropia*. F.E.B.S. Lett. **137:**283-287.

154. **Zasloff M.** 2002. Antimicrobial peptides of multicellular organisms. Nature **415:**389-395.

155. **Antoniades I, Stylianou P, Skourides PA.** 2014. Making the connection: ciliary adhesion complexes anchor basal bodies to the actin cytoskeleton. Dev. Cell. **28:**70-80.

156. **Braiman A, Priel Z.** 2008. Efficient mucociliary transport relies on efficient regulation of ciliary beating. Respir. Physiol. Neurobiol. **163:**202-207.

157. **Salathe M.** 2007. Regulation of mammalian ciliary beating. Annu. Rev. Physiol. **69:**401-422.

158. **Chilvers MA, O'Callaghan C.** 2000. Analysis of ciliary beat pattern and beat frequency using digital high speed imaging: comparison with the photomultiplier and photodiode methods. Thorax **55:**314-317.

159. **Godfrey RW.** 1997. Human airway epithelial tight junctions. Microscopy research and technique **38:**488-499.

160. **Schneeberger EE, Lynch RD.** 2004. The tight junction: a multifunctional complex. Am. J. Physiol. Cell Physiol. **286:**C1213-1228.

161. **Niessen CM.** 2007. Tight junctions/adherens junctions: basic structure and function. J. Invest. Dermatol. **127:**2525-2532.

162. **van Meer G, Simons K.** 1986. The function of tight junctions in maintaining differences in lipid composition between the apical and the basolateral cell surface domains of MDCK cells. E.M.B.O. J. **5:**1455-1464.

163. **Claude P.** 1978. Morphological factors influencing transepithelial permeability: a model for the resistance of the zonula occludens. J. Membr. Biol. **39:**219-232.

164. **Claude P, Goodenough DA.** 1973. Fracture faces of zonulae occludentes from "tight" and "leaky" epithelia. J. Cell. Biol. **58:**390-400.

165. **Schamberger AC, Mise N, Jia J, Genoyer E, Yildirim AO, Meiners S, Eickelberg O.** 2013. Cigarette Smoke-Induced Disruption of Bronchial Epithelial Tight Junctions is Prevented by Transforming Growth Factor-Beta. Am. J. Respir. Cell. Mol. Biol.

166. **Mura S, Hillaireau H, Nicolas J, Kerdine-Romer S, Le Droumaguet B, Delomenie C, Nicolas V, Pallardy M, Tsapis N, Fattal E.** 2011. Biodegradable nanoparticles meet the bronchial airway barrier: how surface properties affect

their interaction with mucus and epithelial cells. Biomacromolecules **12:**4136-4143.

167. **Kastner PE, Casset A, Pons F.** 2011. Formaldehyde interferes with airway epithelium integrity and functions in a dose- and time-dependent manner. Toxicol. Lett. **200:**109-116.

168. **Forti E, Salovaara S, Cetin Y, Bulgheroni A, Tessadri R, Jennings P, Pfaller W, Prieto P.** 2011. In vitro evaluation of the toxicity induced by nickel soluble and particulate forms in human airway epithelial cells. Toxicol. In Vitro **25:**454-461.

169. **Grainger CI, Greenwell LL, Lockley DJ, Martin GP, Forbes B.** 2006. Culture of Calu-3 cells at the air interface provides a representative model of the airway epithelial barrier. Pharm. Res. **23:**1482-1490.

170. **Kesimer M, Ehre C, Burns KA, Davis CW, Sheehan JK, Pickles RJ.** 2013. Molecular organization of the mucins and glycocalyx underlying mucus transport over mucosal surfaces of the airways. Mucosal Immunol. **6:**379-392.

171. **Krunkosky TM, Jordan JL, Chambers E, Krause DC.** 2007. *Mycoplasma pneumoniae* host-pathogen studies in an air-liquid culture of differentiated human airway epithelial cells. Microb. Pathog. **42:**98-103.

172. **Jun CD, Carman CV, Redick SD, Shimaoka M, Erickson HP, Springer TA.** 2001. Ultrastructure and function of dimeric, soluble intercellular adhesion molecule-1 (ICAM-1). J. Biol. Chem. **276:**29019-29027.

173. **Simmons WL, Daubenspeck JM, Osborne JD, Balish MF, Waites KB, Dybvig K.** 2013. Type 1 and type 2 strains of *Mycoplasma pneumoniae* form different biofilms. Microbiology (Reading, England) **159:**737-747.

174. **Hedreyda CT, Krause DC.** 1995. Identification of a possible cytadherence regulatory locus in *Mycoplasma pneumoniae*. Infect. Immun. **63:**3479-3483.

175. **Dajani AS, Clyde WA, Jr., Denny FW.** 1965. Experimental Infection with *Mycoplasma pneumoniae* (Eaton's Agent). J. Exp. Med. **121:**1071-1086.

176. **Stemke GW, Robertson JA.** 1982. Comparison of two methods for enumeration of mycoplasmas. J. Clin. Microbiol. **16:**959-961.

177. **Kannan TR, Coalson JJ, Cagle M, Musatovova O, Hardy RD, Baseman JB.** 2011. Synthesis and distribution of CARDS toxin during *Mycoplasma pneumoniae* infection in a murine model. J. Infect. Dis. **204:**1596-1604.

178. **Schneider CA, Rasband WS, Eliceiri KW.** 2012. NIH Image to ImageJ: 25 years of image analysis. Nat. Methods **9:**671-675.

179. **Forteza RM, Casalino-Matsuda SM, Falcon NS, Valencia Gattas M, Monzon ME.** 2012. Hyaluronan and layilin mediate loss of airway epithelial barrier function induced by cigarette smoke by decreasing E-cadherin. J. Biol. Chem. **287:**42288-42298.

180. **Hong KU, Reynolds SD, Watkins S, Fuchs E, Stripp BR.** 2004. In vivo differentiation potential of tracheal basal cells: evidence for multipotent and unipotent subpopulations. Am J Physiol Lung Cell Mol Physiol **286:**L643-649.

181. **Hong KU, Reynolds SD, Watkins S, Fuchs E, Stripp BR.** 2004. Basal cells are a multipotent progenitor capable of renewing the bronchial epithelium. Am. J. Pathol. **164:**577-588.

182. **LeDizet M, Beck JC, Finkbeiner WE.** 1998. Differential regulation of centrin genes during ciliogenesis in human tracheal epithelial cells. Am. J. Physiol. **275:**L1145-1156.

183. **Prince OA, Krunkosky TM, Krause DC.** 2014. *In vitro* spatial and temporal analysis of *Mycoplasma pneumoniae* colonization of human airway epithelium. Infect. Immun. **82:**579-586.

184. **Hasselbring BM, Page CA, Sheppard ES, Krause DC.** 2006. Transposon mutagenesis identifies genes associated with *Mycoplasma pneumoniae* gliding motility. J. Bacteriol. **188:**6335-6345.

185. **Radestock U, Bredt W.** 1977. Motility of *Mycoplasma pneumoniae*. J. Bacteriol. **129:**1495-1501.

186. **Cole P.** 1989. Host-microbe relationships in chronic respiratory infection. Respiration; international review of thoracic diseases **55 Suppl 1:**5-8.

187. **Ye Q, Xu XJ, Shao WX, Pan YX, Chen XJ.** 2014. *Mycoplasma pneumoniae* Infection in Children Is a Risk Factor for Developing Allergic Diseases. TheScientificWorldJournal **2014:**986527.

188. **Chu HW, Honour JM, Rawlinson CA, Harbeck RJ, Martin RJ.** 2003. Effects of respiratory *Mycoplasma pneumoniae* infection on allergen-induced bronchial hyperresponsiveness and lung inflammation in mice. Infect. Immun. **71:**1520-1526.

189. **Beasley R, Roche WR, Roberts JA, Holgate ST.** 1989. Cellular events in the bronchi in mild asthma and after bronchial provocation. Am. Rev. Respir. Dis. **139:**806-817.

190. **Chetta A, Foresi A, Del Donno M, Consigli GF, Bertorelli G, Pesci A, Barbee RA, Olivieri D.** 1996. Bronchial responsiveness to distilled water and methacholine and its relationship to inflammation and remodeling of the airways in asthma. Am. J. Respir. Crit. Care Med. **153:**910-917.

191. **Boulet LP, Laviolette M, Turcotte H, Cartier A, Dugas M, Malo JL, Boutet M.** 1997. Bronchial subepithelial fibrosis correlates with airway responsiveness to methacholine. Chest **112:**45-52.

192. **Chetta A, Foresi A, Del Donno M, Bertorelli G, Pesci A, Olivieri D.** 1997. Airways remodeling is a distinctive feature of asthma and is related to severity of disease. Chest **111:**852-857.

193. **Waites KB, Balish MF, Atkinson TP.** 2008. New insights into the pathogenesis and detection of *Mycoplasma pneumoniae* infections. Future. Microbiol. **3:**635-648.

194. **Narita M.** 2009. Pathogenesis of neurologic manifestations of *Mycoplasma pneumoniae* infection. Pediatric neurology **41:**159-166.

195. **Weng W-C, Peng SS-F, Wang S-B, Chou Y-T, Lee W-T.** 2009. *Mycoplasma pneumoniae*–Associated Transverse Myelitis and Rhabdomyolysis. Pediatric neurology **40:**128-130.

196. **Tsiodras S, Kelesidis I, Kelesidis T, Stamboulis E, Giamarellou H.** 2005. Central nervous system manifestations of *Mycoplasma pneumoniae* infections. Journal of Infection **51:**343-354.

197. **Spuesens EB, Fraaij PL, Visser EG, Hoogenboezem T, Hop WC, van Adrichem LN, Weber F, Moll HA, Broekman B, Berger MY, van Rijsoort-Vos T, van Belkum A, Schutten M, Pas SD, Osterhaus AD, Hartwig NG, Vink C, van Rossum AM.** 2013. Carriage of *Mycoplasma pneumoniae* in the upper respiratory tract of symptomatic and asymptomatic children: an observational study. P.L.o.S. Med. **10:**e1001444.

198. **Zhu D, Tan KS, Zhang X, Sun AY, Sun GY, Lee JC.** 2005. Hydrogen peroxide alters membrane and cytoskeleton properties and increases intercellular connections in astrocytes. J. Cell. Sci. **118:**3695-3703.

199. **Barth H, Aktories K.** 2011. New insights into the mode of action of the actin ADP-ribosylating virulence factors Salmonella enterica SpvB and Clostridium botulinum C2 toxin. Eur. J. Cell. Biol. **90:**944-950.

200. **Lee HS, Namkoong K, Kim DH, Kim KJ, Cheong YH, Kim SS, Lee WB, Kim KY.** 2004. Hydrogen peroxide-induced alterations of tight junction proteins in bovine brain microvascular endothelial cells. Microvasc. Res. **68:**231-238.

201. **Bienert GP, Schjoerring JK, Jahn TP.** 2006. Membrane transport of hydrogen peroxide. Biochim. Biophys. Acta. **1758:**994-1003.

202. **Fischer H.** 2009. Mechanisms and function of DUOX in epithelia of the lung. Antioxid. Redox. Signal. **11:**2453-2465.